THE UNIVERSITY *of* EDINBURGH

Solitary Waves in Focussing and Defocussing Nonlinear, Nonlocal Optical Media

John Michael Larratt MacNeil

Doctor of Philosophy
University of Edinburgh
May 19, 2016

Declaration

I declare that this thesis was composed solely by myself, that it has not been submitted, in whole or in part, in any previous application for a degree, and that the work contained therein is my own, except where explicitly stated otherwise in the text.

(*John Michael Larratt MacNeil*)

To my family.

Abstract

Nonlinear, nonlocal optical media has emerged as an ideal setting for experimentally observing and studying spatial optical solitary waves which otherwise cannot occur in Kerr media. Of particular interest is the eventual application to all-optical circuits. However, there is considerable work left to do on the theoretical end before this is a possibility. In this thesis we consider three problems. The first is how to solve the governing equations for optical beam propagation in the particular medium of the nematic liquid crystal (NLC), which is used as a prototypical example, exactly and approximately. In this respect we provide the first known, explicit solutions to the model as well as a comprehensive assessment on how to use variational, or modulation theory, in this context. This leads to the discovery of a novel form of bistability in the system, which shows there are two stable solitary wave solutions for a fixed power or L^2 norm. We then consider how to approximate solutions for optical solitary waves propagating in a more general class of nonlocal nonlinear media using asymptotic methods. This is a long open problem and is resolved in the form of a simple to implement method with excellent accuracy and general applicability to previously intractable models. We conclude with the discovery and characterization of an instability mechanism in a coupled, defocussing nonlinear Schrödinger system. We show there is no stable, coupled, localized solution. This result is compared with the more well-studied bright solitary wave system and physical and mathematical explanations are offered.

Lay Summary

One of the more fascinating areas of physics is optics. It underlies research spanning the areas of basic physics, chemistry, electrical engineering, computer graphics, and much more. A basic question one asks when studying optics is "what happens when light hits this material". An amazing example is light impinging on liquid crystals. Liquid crystals are a material which microscopically look like oriented rods which do not have a spatial order. A good analogy is people facing a screen, but are not sitting in an organized arrangement like in a theater, rather they are free to stand where they like.

Liquid crystals offer a multitude of exciting technological applications as best demonstrated by the success of the LCD display. However, the underpinning mathematics of light in liquid crystals is still not well understood. In fact, liquid crystals are not alone in this respect. The same underlying equations (known as nonlocal, nonlinear) equations pose challenges for other areas of physics as well. This thesis makes progress on the mathematical tools used to study such equations.

Acknowledgements

I want to first and foremost thank my supervisor Prof. Noel Smyth for everything he has done for me over the past 4 years. Without his bottomless knowledge, constant encouragement, and sincere effort in helping me to succeed, this thesis would certainly not be possible. I was very, very lucky to have studied under such a great teacher. It has been an absolute privilege and an experience I will never forget.

I would also like to extend a big thank you to other scientists in the nematicon community who made this possible. To Prof. Gaetano Assanto, who has such a deep intuition for nonlinear optics that I can only hope some if it rubs off. And, additionally, for the thorough education on eating delicious Italian food properly. Best meals I have ever had in my life. To Prof. Tim Minzoni for the considerable encouragement in pursuing my ideas and the amazing time I spent in Mexico City.

This thesis would also be sorely incomplete without thanking some of the many friends I made in Edinburgh. The reason my time in Edinburgh was so special was thanks to them. In no particular order, big shout out to the boys Dr. Kevin Hughes, Dr. John Pearson, Bill de Jong, Spencer McElhinney, Nigel Smith, Court Howlett-Ben, Jordan Tekenos-Levy, Sam Zdatny and Jono Cottingham. Thanks for everything.

Finally, I'm very thankful for the support of my family to whom this thesis is dedicated. This work, and everything else I have done, would not be possible without them. To my parents, Diana and John, my brother James, my sister Laura, and cousin Geordie. Thank you so much.

Contents

Chapter 1

Introduction

1.1 Solitary Waves and Solitons

This thesis is dedicated to the study of solitary waves arising in nonlinear, nonlocal optical media. For the purposes of an introduction, there is no universally accepted definition of a solitary wave, nor is there one for such waves in nonlocal optical media. However, the rich history of the first subject and the considerable recent interest in the second allows us to have a reasonably clear picture. In describing solitary waves, a natural departure point is their discovery. This took place at Edinburgh's own Union Canal by John Scott Russell and is described in his "Report on Waves" in 1844 [1]. The central finding from this work is

> *I was observing the motion of a boat which was rapidly drawn along a narrow channel by a pair of horses, when the boat suddenly stopped - not so the mass of water in the channel which it had put in motion; it accumulated round the prow of the vessel in a state of violent agitation, then suddenly leaving it behind, rolled forward with great velocity, assuming the form of a large solitary elevation, a rounded, smooth and well-defined heap of water, which continued its course along the channel apparently without change of form or diminution of speed. I followed it on horseback, and overtook it still rolling on at a rate of some eight or nine miles an hour, preserving its original figure some thirty feet long and a foot to a foot and a half in height. Its height gradually diminished, and after a chase of one or two miles I lost it in the windings of the channel. Such, in the month of August 1834, was my first chance interview with that singular and beautiful phenomenon which I*

have called the Wave of Translation.

Russell's "Wave of Translation" was remarkable mainly in the respect that it was not oscillatory. The expectation of the time was that *all* waves are oscillatory. Furthermore, the wave retained its form over an astonishingly large distance. This suggests it was robust enough to withstand the perturbations inflicted by the naturally imperfect canal floor. All these novel features led to considerable scepticism from the scientific community of the time, including G.G. Stokes. The specific criticism was the lack of an acceptable theory detailing the possibility of such a phenomenon. Such a theory was first given by Boussinesq in 1871 [2] and later, in 1895, rediscovered by Korteweg and de Vries [3, 4]. Korteweg and de Vries demonstrated that travelling waves of their now widely studied model, the KdV equation, of weakly nonlinear long waves, admitting exactly solvable wavetrain solutions using Jacobi elliptic functions [4]. In the limit of an infinite period, this Jacobi elliptic function approaches the solitary wave described by Russell. This was hugely important as there was now a sound connection between oscillatory waves and the solitary wave of Russell. The phenomenon now had a solid theoretical basis.

The word "soliton" for the same solitary wave described by Russell came from the physics community. Kruskal and Zabusky [5] showed using numerical simulations in the 1960's that, perhaps more amazingly than their shape retention, solitary wave solutions of the KdV equation interact cleanly. By interacting cleanly, we mean the solitary waves retain their shape after interacting with other solitary waves, leaving *no measurable evidence that the interaction even occurred*, apart from a phase shift. This gave birth to the term "soliton" to reflect the particle like interaction of the waves and the term was adopted almost immediately.

Shortly after this work, the initial value problem for the KdV on the line was solved by Gardener, Greene, Kruskal and Miura [6] using what is now known as the "inverse scattering transform" or IST. This was significant as, prior to this discovery, there were no general methods for solving nonlinear partial differential equations of any significance. The IST changed this and with it emerged the field of "integrable" systems with solitons at its focal point. Note that, in this thesis, we will use the term "integrable" to mean the equation is exactly solvable using the IST. Since then, the terms "solitons" and "solitary waves" have been used more or less interchangeably in the physics community to describe solutions to nonlinear wave equations which are

1. localised, with an enduring and persistent shape, like Russell's "smooth, well-defined heap of water", and

2. interact cleanly, like Kruskal's solitons.

As the field developed, this became a rather restrictive definition. There are many examples of solutions of nonlinear wave equations which we title solitons that are not necessarily steady, such as "breathers" or other periodic "gap solitons" [7, 8] or are not a well-defined lump, such as vortex solitons [9], or are instable to perturbations, such as the vector dark solitary waves considered in this work [10,11,12]. Furthermore, many of them do not interact cleanly as for Zabusky and Kruskal's solitons, leaving a wake of radiation behind or spiralling around one another with considerable effect on their initial profile. Clean interaction appears to be a quality restricted to integrable equations, which comprise a relatively small subset of those that admit solitary wave solutions. In this work, we focus exclusively on localized solutions which may not interact cleanly and thus adopt the formal term solitary wave as distinct from the term soliton, which is the more common terminology in applied mathematics communities. In particular, there will be two different flavors, the first being bright solitary waves, which arise in self-focussing media, and the second will be dark solitary waves, which arise in defocussing media. The difference between these two will now be described.

1.2 Focussing and Defocussing Nonlinear Optics

Understanding bright and dark solitary waves as they arise in focussing and defocussing media brings us to optics. The idea is simple and is best illustrated through the canonical nonlinear wave equation in optics, the nonlinear Schrödinger (NLS) equation, which is

$$i\partial_z\psi + \frac{1}{2}\partial_x^2\psi + |\psi|^2\psi = 0. \tag{1.1}$$

The first two terms alone comprise the free Schrödinger operator from quantum mechanics and the last term is a nonlinearity arising from, typically, a weakly nonlinear medium response to the beam which depends on the intensity $|\psi|^2$ termed the "Kerr" nonlinearity [11]. The NLS equation is such a widely studied equation, in so many different branches of physics, that it has been termed a "universal equation" [11]. In general, it arises for a weakly nonlinear wave packet which has wave numbers grouped around a central value with the nonlinear interaction depending on the intensity $|\psi|^2$ [4].

It is an integrable system, as shown by Zakharov and Shabat [13] and possesses *bright* solitary wave solutions similar to those described by Russell for the KdV or Boussinesq equations. In particular, one can verify the soliton solution

$$\psi = a\,\mathrm{sech}(ax)e^{i\frac{a^2}{2}z}, \tag{1.2}$$

where a is an arbitrary parameter. Notice, in particular, that the intensity $|\psi|$ is invariant in z. Furthermore, it is not periodic, but localized and monotonically decaying in x, thus fitting with our picture of a solitary wave solution. Note, there are, of course, periodic solutions in the form of Jacobi elliptic functions as there were for the KdV equation. To give it more physical meaning, we will take the z direction to be the propagation direction of an optical beam, such that the nonlinear medium is contained in $z \in (0, \infty)$, x is a spatial variable and ψ is the envelope of our wave packet. One interpretation of the soliton solution (1.2) is that it is the result of a balance between *dispersive* effects ($\partial_x^2\psi$) and self-steepening, or *self-focussing* effects ($|\psi|^2\psi$) [4,11]. The dispersive effects are attributed to the free Schrödinger portion of the equation. Indeed, a classic result on Schrödinger equations is that solutions of

$$i\partial_z u + \nabla^2 u = 0, \quad x \in \mathbb{R}^n, \tag{1.3}$$

$$u(x, 0) = f(x), \tag{1.4}$$

satisfy the estimate

$$||u||_{L^\infty(\mathbb{R}^n)} \leq \frac{1}{(2\pi z)^{n/2}}||f||_{L^1(\mathbb{R}^n)}. \tag{1.5}$$

The fact then that localized solutions exist to the NLS equation can be attributed to the nonlinearity counteracting this tendency to decay. Thus the term self-focussing, as the beam focusses itself in the material without the aid of external tools such as a lens. In effect, it creates its own *wave-guide* and thus the term "self-guided" waves are also used in the engineering community.

De-focussing media has a fundamentally different effect on optical beams. The idea is best illustrated through the mathematics followed by a physical discussion. The canonical model is the *de-focussing* nonlinear Schrödinger equation, which is

$$i\partial_z\psi + \frac{1}{2}\partial_x^2\psi - |\psi|^2\psi = 0. \tag{1.6}$$

The only difference between the two equations (1.1) and (1.6) is the sign of the nonlinearity and both are integrable. However, the conditions as $x \to \pm\infty$ differ significantly and reflect the difference in the physics. For focussing media, we required that $\psi \to 0$ as $|x| \to \infty$. In the case of dark solitary waves we are looking for localized solutions which are "carried" by a continuous wave. That is, we impose

$$\psi \to U_0^{\pm} e^{-iU_0^2 z}, \quad x \to \pm\infty, \tag{1.7}$$

where, the constants U_0^+ and U_0^- are real and are related by

$$U_0^+ = U_0 > 0, \quad U_0^- = -U_0, \tag{1.8}$$

so that U_0^2 in the boundary condition (1.7) is defined by

$$U_0^2 = (U_0^+)^2 = (U_0^-)^2, \tag{1.9}$$

In particular, for U_0 as defined above, a localized solitary wave solution of the defocussing NLS equation (1.6) is given by

$$\psi = [B \tanh(B(x - Az)) + iA]\, e^{-iU_0^2 z}, \tag{1.10}$$

$$A^2 + B^2 = U_0^2. \tag{1.11}$$

The second condition leaves a sole free parameter, either A or B. One can now see by taking the modulus of this soliton solution that we have a localized dark notch that approaches its bright "carrier wave" as $x \to \pm\infty$. In essence, an analogous effect as the self-focussing case has occurred. The dispersive term has forced the bright portion out of the center, while the defocussing nonlinearity arrests this at a particular point, creating a stable localized soliton. This is something of a mirror image to what occurs in focussing media. Thus, we term this to be a *de-focussing* nonlinear media.

1.3 Nonlocal Media and Nematicons

The motivation for studying nonlocal optical media lies in a subtle, but classical result on the NLS equation in dimensions higher than one. In particular, there exists a critical power (L^2 norm) of the initial condition such that, above this power, solutions

blow-up (approach an infinite L^∞ norm) in finite time [11], which is sometimes called "catastrophic collapse". Below this value, they decay to radiation. This blow-up of solutions for the NLS equation for more than one dimension means that it is an inadequate model for dimensions higher than one. Furthermore, it implies that weakly nonlinear media with a "Kerr", or cubic, nonlinearity resulting in the NLS equation, are not suitable for observing spatial optical solitary waves. Alternative materials with a fundamentally different nonlinear response are needed, which, in general, may lead to governing equations which are no longer integrable. In a series of papers devoted to experimentally producing spatial optical solitary waves, Assanto et al. [14,15,16,17] studied the possibility of launching an optical beam into a cell filled with a nematic liquid crystal (NLC). Note that NLC and nematicons will be discussed thoroughly in Chapter 2. The theoretical motivation was that the governing equations had a fundamentally different nonlinearity from the Kerr response of the NLS equation (1.1). The nonlinear response balanced diffraction for low intensity beams and was given by a convolution. For example, a central system of this thesis is the "nematicon equations"

$$i\partial_z u + \frac{1}{2}\nabla^2 u + 2\theta u = 0, \tag{1.12}$$

$$\nu\nabla^2\theta - 2q\theta + 2|u|^2 = 0. \tag{1.13}$$

Solving for θ explicitly using a Green's function gives a convolution nonlinearity in $|u|^2$ in the NLS type equation (1.12). In general, the nematicon system belongs to a broader class of solitary wave equations which are of the general form of the *nonlocal*, nonlinear Schrödinger equation

$$i\partial_z u + \frac{1}{2}\nabla^2 u + 2\left(K * |u|^2\right)u = 0. \tag{1.14}$$

Here $*$ denotes a convolution in the spatial variable, so that

$$K * |u|^2 = \int_\Omega K(x,s)|u(s,z)|^2 ds, \tag{1.15}$$

for K some kernel, restrictions on which we discuss in Chapter 2. The *nonlocal* nonlinearity in the nematicon equations, and for a broad array of other NLS-type equations, has the ability to arrest catastrophic collapse. Solitary wave solutions can then exist and can be observed experimentally. Furthermore, (1.14) is a significantly more general equation, reducing to the NLS equation for a Dirac delta kernel $K = \delta(x-s)$ and includes the nematicon equations for a Helmholtz kernel, as well as a wide variety of

other physical phenomena described in depth in Chapter 2. A crucial aspect is that equation (1.14) is no longer integrable, that is, the solution of the initial value problem can no longer be found using the IST.

The main physical system in this thesis is solitary waves in nematic liquid crystals, sometimes called nematicons [18,19], which we use as a prototypical example for solitary waves in focussing and defocussing nonlinear, nonlocal optical media [14]. There are several well founded reasons for this. The first is how simply observable they are [15, 18, 19]. As discussed in this thesis, the so-called nematicon equations apply to a broad spectrum of physical phenomena such as model systems in quantum gravity [20, 21], plasma physics [22], mathematical biology [23] and fluid mechanics [24, 25]. By exploiting this equivalence, one can now directly observe effects in plasma physics or astrophysics that are otherwise unobservable in a laboratory setting. Further, the nematicon set up is relatively inexpensive and fits on a table top [18, 19]. The second is their flexibility. NLC's can be tuned to have a weak nonlocality, which means the nematicon equations (1.12) and (1.13) approach the NLS equation in the limit of $\nu \ll 1$, as well as a strong nonlocality ($\nu \gg 1$), to produce stable solitary waves. Furthermore, one can study defocussing effects by adding an azo-dye to the nematic so that it becomes a defocussing medium [26]. One can also study stronger nonlinear effects in more complex models for both the focussing and defocussing cases, as discussed in Chapter 2. The third reason is technological relevance. There is strong potential for an engineering application in using nematicons as "bits" of information and NLC's as the basis for an all-optical circuit. This promises, potentially, faster and more flexible computing, as well as many other possibilities [15, 17, 27, 28, 29, 30, 31] . Finally, and crucially, the mathematics of nematicons and their related phenomena are in their infancy when compared with more well understood universal and integrable models such as the NLS or KdV equations, with much left to explore and study. As such, nematicons are given a special prominence in this thesis, with us detailing the derivation of the equations in Chapter 2 and studying them throughout Chapters 3, 4 and 5.

1.4 Outline of the Thesis

In this thesis we study three problems in solitary waves in focussing and defocussing nonlinear, nonlocal optical media using nematicons as a prototypical example. The work is organized as follows.

In Chapter 2 we provide a thorough background to nematicons, including a physical background and derivation of the governing equations, as well as analytical and numerical methodologies used in their study. The general principles and approximation techniques of nonlinear optics, as well as basic physical background on nematic liquid crystals, is reviewed. The governing equations are introduced in this way and applications to other areas of physics are discussed. Background is also given on analytical methods, such as the variational method, and attempts at perturbation methods being used in the context of nematicons. We finish the Chapter by detailing the numerical methods that will be used in the succeeding three chapters.

In Chapter 3 we present the first known explicit solutions of the nematicon equations, derive variational approximations to the nematicon solutions and study effects of linearization in the modelling. The exact solution is introduced by construction, rather than by direct substitution as in previous attempts [32] and results for both (1+1) dimensional and (2+1) dimensional solitary waves are presented. This raises questions on which ansatz should used in the widely used variational method and an extensive comparison of four different, commonly used ansatzë is done. The relative accuracy when compared with numerical solutions for differing asymptotic regimes is discussed extensively. We then study the effect of linearization in the modelling and compare, numerically, solutions of the nematicon and pre-tilted nematicon equations. This leads to the discovery of a novel form of optical bistability in nonlocal, nonlinear media.

In the fourth Chapter, we describe a general and universal method for approximating solitary waves in nonlinear, nonlocal focussing media. The approach is the first of its kind in terms of range of applicability, accuracy, ease of implementation and asymptotic arguments. We derive approximate solutions for solitary waves for four different models, three of which were previously analytically intractable, the fourth being the nematicon equations, which are studied in both (1+1) and (2+1) dimensions. These are then compared extensively with numerical solutions and the error, as well as limitations of the method, are discussed.

In Chapter 5 we present the discovery of a novel instability mechanism for coupled nonlinear dark solitary waves in defocussing media. The model under consideration is that of two coupled nonlinear Schrödinger equations with differing diffraction coefficients. A novel, nonlinear type of instability for differing diffraction coefficients is found and analyzed thoroughly, in particular why it does not arise in the case of focussing media, which are more widely studied and would explain why the phenomenon has gone

undetected in the literature. Explicit asymptotic behaviour is found at leading order and first order for small differences in the diffraction coefficients. Numerical simulations are given for large differences in the diffraction coefficients.

Chapter 6 contains a summary of the thesis, including a summary of the key contributions to the area, as well as discussing future work.

Chapter 2

Background

The area of theoretical nonlinear optics can be broadly summarized as deriving and analyzing simplified models of the interaction between light and matter. Light is generally treated as a wave with Maxwell's equations governing its dynamics. Included in Maxwell's equations is a refractive index term which, in nonlinear materials, depends on the electric or magnetic field itself. Thus a material or medium response equation is needed to close the system. If one wished to faithfully reproduce the physics of a beam propagating in an NLC, the medium response would be governed by a high dimensional molecular system with a distinct equation of motion (as of yet, still under research) for each molecule in the sample under consideration. Even with the significant advances in modern computing, this type of problem is far from being computationally tractable. As an example, consider that the modelling and computation of NLC dynamics alone, in the absence of an electromagnetic field, is in and of itself, a large and healthy area of research. However, this issue of computational intractability is not a new one in nonlinear optics. The field has developed considerably by deriving asymptotic approximations of Maxwell's equations and the material response to arrive at a simplified model. Our problem of nematicons is an intriguing one as the modelling must also navigate the difficulties of liquid crystal motion by isolating the most pertinent optical effects. Fortunately, the modelling was done by Peccianti et al. [15] and is reviewed, with thorough explanations of the background physics, in section 2.1. Additionally, basic mathematical facts of the model, such as the variational formulation, existence, uniqueness, and stability have been established in [33], and are presented in section 2.2.

Most of the applied mathematics outside of modelling in nonlinear optics is dedicated to the analysis of the derived models. The nematicon equations presented in

section 2.1 form a so called nonlinear, highly nonlocal system that is in some limits closely related to the NLS equation, and in others very distinct. In contrast to the generalized NLS equation, with an algebraic or rational nonlinearity, where one has a variety of analytic methods for its analysis, there are comparably less methods for handling the nonlocal NLS equation. One of the more robust methods is the variational method, used widely in nonlinear optics and with deep connections to multiple scales, which is reviewed in section 2.3 and analyzed in depth in Chapter 3. Interestingly, even with the presence of a natural small parameter in the governing equations, few satisfying asymptotic methods for the analysis of "highly nonlocal" equations are available. Isolated, model specific methods have been developed and successfully applied, and these are also reviewed in section 2.3 to provide background for a unified method developed in Chapter 4. Finally, we conclude this chapter by presenting the numerical methods used throughout the thesis, which act as a benchmark by which to the measure the accuracy of approximate methods, in section 2.4.

2.1 Governing Equations

In discussing the origins of the nematicon model it is useful to give some physical background on liquid crystals. Liquid crystals are a type of soft matter known as a thermotropic fluid, that is, a fluid whose "phase" depends on the temperature. The nematic phase is characterized by ellipsoid-shaped molecules, called nematics, which macroscopically move as a fluid and share properties with a crystalline lattice. In more detail, NLC's have no particular spatial order and the molecules are free to flow, making their motion appear macroscopically as a fluid. Long range directional or orientational order is maintained, which gives it the optical properties of a crystal. The orientation of the NLC is locally quantified by the "director", a vector measuring bulk average direction of the major axis of the molecules. Physically, the director is governed by intermolecular forces between the molecules. Fortunately, the changes induced by lasers occur on substantially larger scales than the intermolecular distance, allowing a continuum limit to be used.

NLC's are also a dielectric medium, so applying an electric or magnetic field to them induces a dipole, a nonuniform charge distribution along the crystal. The chemical reason for this dipole is the presence of benzene rings in the nematics. A dipole applies a torque to the crystal which can rotate them. This reorientational effect, quantified by

the director, is the main nonlinear effect considered in this thesis as it mathematically manifests in the form of a convolution. It is worth noting this intentionally neglects a host of other possible nonlinear optical effects arising from a laser impinging on an NLC. These include temperature fluctuations, velocity or flow effects with a non-trivial viscosity, changes in the elasticity properties and even the presence of pockets of different phases of liquid crystals such as the rigid smectic phase. It is considerable advances in the engineering of experimental apparatuses that allow us to consider reorientation alone.

The manner in which molecules in an NLC can reorient themselves is also a nonlinear process. That is, nematics can align themselves in interesting ways when viewed as local groups. They can splay, a configuration you can see by spreading your fingers and imagining each to be a nematic; bend, whereby the nematics organize themselves like cars navigating a turn; and twist, in the same way as threads in a rope. The degree to which an NLC prefers to splay, bend or twist is a material property encapsulated in the elasticity constants K_i, $i \in \{1, 2, 3\}$. In the models considered in this thesis, one major assumption regarding NLC's is these elastic constants are equal, an assumption supported by numerous numerical simulations and experiments.

Understanding the nature and simple dynamics of NLC's, we turn to electromagnetic waves propagating through them. The departure point for modelling of beams is Maxwell's equations. The then standard assumptions are a time harmonic wave and proportionality of the magnetic and electric fields, which reduces the system to the "fully nonlinear Maxwell's equation for the electric field" [34]. This is a vector, nonlinear, elliptic equation and a standard asymptotic tool for reducing it to a more manageable form is the Slowly Varying Envelope Approximation (SVEA for brevity) [14]. The idea is simple. For an incident plane wave the *envelope* of the wave varies on a scale that is much longer than the wavelength. Note in particular, this can be made rigorous. [35]. Nematicons persist and retain they're shape on the millimeter scale which is vastly larger than the wavelength of a standard laser is $3 \sim 5\mu m$, thus are safely in the realm of the SVEA. A further assumption has to do with the anisotropy (dependence of the director on wavenumber and polarization), which we take to be weak. While weak anisotropy does not necessarily hold, this reduces the vector Maxwell equation to a scalar equation and does not compromise much accuracy when compared to models with stronger anisotropy [34]. The remaining electric field component is that in the *extraordinary* direction, that is, the dispersive beam, and the term "electric field" will

be used to describe this component.

In summary, the major assumptions of the nematicon models are as follows

- The major nonlinear effect is reorientational as encapsulated by the director. Flow, thermal effects, and changes in elasticity and viscosity are neglected.
- The elastic constants governing splay, bend and twist in the NLC are considered equal.
- The refractive index depends weakly on the wavenumber and polarization of the beam.
- The SVEA holds.

We now formally pose the problem. Consider a linearly polarized beam of finite width launched into a planar NLC waveguide contained between two glass plates. Attached to each plate is an electrode creating a background static voltage across the cell acting in the same direction as the polarization of the electric field.The presence of this background voltage will be explained in a moment. The beam is taken to propagate in the Z direction and the X direction is taken in the direction of its electric field, with the Y direction completing the coordinate system. The coordinates are taken to be centered in the middle of the rectangular cell domain Ω, given by $\Omega = (-L_x, L_x) \times (-L_y, L_y)$. The director is taken to be (X, Z) plane and remains and rotates in this plane. We intentionally neglect the "walk-off" effect, whereby the beam doesn't travel in a straight line, as this amounts to a reorientation of these coordinates. A schematic of the physical system is given in Fig. 2.1.

The governing equations for the extraordinary beam and the director are as follows [18]

$$2ik\frac{\partial E}{\partial Z} + \nabla^2_{XY} E + k_0^2 \varepsilon_a \left(\sin^2\phi - \sin^2\theta_0\right) E = 0, \tag{2.1}$$

$$4K\nabla^2_{XY}\phi + 2\Delta\epsilon_{RF} E_S^2 \sin(2\phi) + \varepsilon_0 \varepsilon_a \sin(2\phi)|E|^2 = 0, \tag{2.2}$$

where E is the slowly varying envelope of the beam's electric field and ϕ is the total mean director rotation induced by both the applied voltage and optical beam. The total mean angle is then decomposed as $\phi = \theta + \theta_0$ where θ is the rotation induced by the beam, or "optical rotation", and θ_0 is the pre-tilt induced by the background electric field. The boundary conditions are simple homogeneous Dirichlet along the edge of

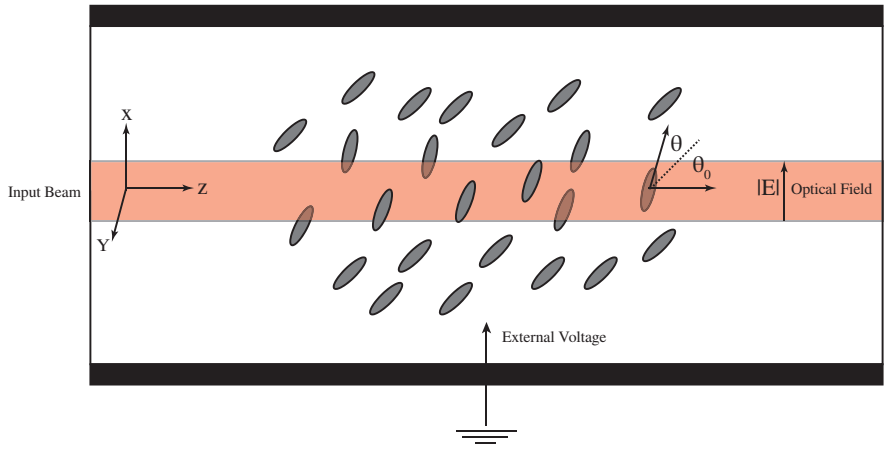

Figure 2.1: Schematic of a nematic on propagating in an NLC waveguide. Note the angle θ is intentionally exaggerated for illustration.

the rectangle, which we denote henceforth by Γ. In general boundary conditions are not always Dirichlet. The nematics can take an arbitrary angle for cell walls that are rubbed but for our consideration, we take un-rubbed walls which impose a type of no-slip condition at the boundary. θ_0 represents the director in the absence of any applied electric field and depends on the boundary conditions as explained shortly. k is the wavenumber of the beam in the NLC, considered a constant material property, and k_0 is the input wavenumber of the beam in free space. The constants ε_a and ε_0 are the birefringence and permittivity of free space. Birefringence is an optical property of a material and occurs when the refractive index is dependent on the polarization and direction of propagation of the electromagnetic wave. Permittivity is a measure of how much a medium is affected by, and how much it affects, an electric field in its presence and is related to the refractive index. K is the Frank constant measuring the elasticity of splay, bend and twist, assumed equal. The remaining parameters E_S and $\Delta\epsilon_{RF}$ denote the strength of the static/low frequency anisotropy induced by the electrodes.

For convienience we re-scale (2.1) and (2.2) and consider the non-dimensional equations

$$i\frac{\partial u}{\partial z} + \frac{1}{2}\nabla^2 u - \cos(2\phi)u = 0, \tag{2.3}$$

$$\nu\nabla^2\phi + \sin(2\phi)\left(2|u|^2 + \alpha\right) = 0, \tag{2.4}$$

where $x = C_1 X$, $y = C_1 Y$ where $C_1 = k_0\sqrt{\varepsilon_a}/2$, $z = k_0^2\varepsilon_a Z/4$ and

$$E = u(x, y, z)\exp\left(ik_0^2\varepsilon_a\left(1/2 - \sin^2(\theta_R)\right)z\right). \tag{2.5}$$

The remaining parameters, ν and α, are related to the former parameters by

$$\alpha = \frac{4\Delta\epsilon_{RF}E_S^2}{\varepsilon_a\varepsilon_0}, \quad \nu = \frac{4Kk_0}{\sqrt{\varepsilon_a}\varepsilon_0}. \tag{2.6}$$

Returning to the model for a moment, one may now reasonably ask why a set of electrodes inducing a pre-tilt to the NLC is necessary. The answer has to do with a phenomenon of NLC's known as the Fréedericksz threshold. For NLC's initially orthogonal to the electric field of an optical beam, the Fréedericksz threshold states there exists a minimum optical electric field to overcome elastic forces and induce a rotation in the molecules [36]. If the molecules are pre-tilted at an angle θ_0 in the (x, z) plane, this threshold is reduced, and in fact is zero if the molecules are rotated by $\theta_0 = \pi/4$. In principle, this pre-tilt is not needed if the optical beam has sufficient power. However, if the optical beam has too much power, thermal effects can raise the temperature of the liquid crystal above the level at which the nematic state can exist. Thus the pre-tilt is an elegant means of overcoming the Fréedericksz threshold while maintaining the nematic phase. In general, a uniform pre-tilt of $\theta_0 = \pi/4$ across the entire NLC cell is not simply achieved. To see this, consider (2.3) and (2.4), in the absence of an optical beam $u = 0$ and solely in the presence of the static electric field. The director obeys the nonlinear PDE

$$\nu\nabla^2\theta_0 + \alpha\sin(2\theta_0) = 0, \quad \theta_0 = 0 \text{ for } \mathbf{x} \in \Gamma \tag{2.7}$$

where, recall, Γ denotes the boundary of the rectangular domain and we have used θ_0 to stress this is for the pre-tilt. In one dimension, one may recognize this equation as that of a nonlinear oscillator from the classical pendulum problem [37]. In general, the solution to the equation (2.7) is non-constant ($\theta_0 \neq \pi/4$ as needed), and non-trivial, given in terms of elliptic functions [38]. The engineering tactic is then to choose α by varying the background electric field, such that θ_0 is taken to be slowly varying w.r.t. x and y and close to $\pi/4$ within the center of the cell. In general this will depend on the size of the cell, as well as boundary conditions. For cell size of 75 μm and beam widths of $3\mu m$, this approximation compares well with experiment [18].

A slowly varying background pre-tilt not only aids in the experimental observation of nematicons, but allows us to simplify (2.3) and (2.4) by expanding around the pre-tiled field. Decomposing the director by $\phi = \theta + \theta_0$, where θ is the rotation induced by

the beam and θ_0 is the pre-tilt, the director equation (2.4) becomes

$$\nu\nabla^2\theta_0 + \nu\nabla^2\theta + \alpha\sin(2\theta_0)\cos(2\theta) + \alpha\cos(2\theta_0)\sin(2\theta) + 2|u|^2\sin(2\theta_0)\cos(2\theta) + 2|u|^2\cos(2\theta_0)\sin(2\theta) = 0. \tag{2.8}$$

We now use (2.7) so that $\nu\nabla^2\theta_0 = -\alpha\sin(2\theta_0)$ giving, after some rearrangements

$$\nu\nabla^2\theta + \alpha\cos(2\theta_0)\sin(2\theta) + 2|u|^2\sin(2\theta_0)\cos(2\theta) - \alpha(1-\cos(2\theta))\sin(2\theta_0) + 2|u|^2\cos(2\theta_0)\sin(2\theta) = 0. \tag{2.9}$$

Here, a heuristic balance argument is used to reduce this to a more manageable form. As mentioned, θ_0 is assumed to be slowly varying and thus can be taken to be a constant $\theta_0 > \pi/4$, as $\theta_0 < \pi/4$ leaves the beam subject to the Fréedericksz threshold and $\theta = \pi/4$ is generally unobtainable in practice. Furthermore, milliwatt beams are used and high values of ν lead to small values of the optical rotation θ [18]. We then assume the following [18]

$$\alpha\cos(2\theta_0)\sin(2\theta) \gg \alpha(1-\cos(2\theta))\sin(2\theta_0), \tag{2.10}$$

$$2|u|^2\sin(2\theta_0)\cos(2\theta) \gg 2|u|^2\cos(2\theta_0)\sin(2\theta). \tag{2.11}$$

Which leads to the system

$$\nu\nabla^2\theta + \alpha\cos(2\theta_0)\sin(2\theta) + 2|u|^2\sin(2\theta_0)\cos(2\theta) = 0. \tag{2.12}$$

Finally, noting taking θ_0 close to $\pi/4$ makes $\sin(2\theta_0) \sim 1$ and we absorb $\cos(2\theta_0)$ by defining $q = -\cos(2\theta_0)\alpha$ to arrive at

$$\nu\nabla^2\theta - q\sin(2\theta) + 2\cos(2\theta)|u|^2 = 0. \tag{2.13}$$

The same arguments simplify the beam equation (2.3). Omitting the details, we have

$$i\partial_z u + \frac{1}{2}\nabla^2 u + \sin(2\theta)u = 0. \tag{2.14}$$

One can further simplify equations (2.13) and (2.14) by expanding the trigonometric

terms in small θ to obtain

$$i\partial_z u + \frac{1}{2}\nabla^2 u + 2\theta u = 0, \tag{2.15}$$

$$\nu\nabla^2\theta - 2q\theta + 2|u|^2 = 0. \tag{2.16}$$

The final two models, (2.14), (2.13) and (2.15), (2.16), are generally posed on a infinite domain as the beam width is small (3 μm) relative to the cell width (75μm) and the profiles sought are cylindrically symmetric, as discussed in the next section.

Any one of the introduced models so far could be considered the "nematicon equations". The term has been used in [14], for (2.1) and (2.2). The term "Full nematicon" system has been used in [39] for (2.14) and (2.13). The most simplified system (2.15) and (2.16) has also been called the "nematicon equations", while being an approximation. As we will be considering all models, we offer something of a dictionary so as to avoid ambiguity and confusion. The title of *full nematicon equations* will be used to describe the re-scaled system (2.3) and (2.4). This is the most general description of nematicon behaviour outside of a full numerical study with coupling to Maxwell's equations. The title of *pre-tilted nematicon equations* will be used to describe the system (2.14) and (2.13). While the original system is also, as mentioned, subject to a static electric field inducing a pre-tilt, we arrive at the pre-tilted nematicon equations because of this simplification thus the title. Finally, when we refer to *the* nematicon equations, we are referring to (2.15) and (2.16). The models and their assumptions are summarized in the following table.

Title	Equations	Assumptions
Full nematicon	$i\frac{\partial u}{\partial z} + \nabla^2 u - \cos(2\phi)u = 0$ $\nu\nabla^2\phi + \sin(2\phi)\left(2\lvert u\rvert^2 + \alpha\right) = 0$	N/A
Pre-tilted nematicon	$i\partial_z u + \frac{1}{2}\nabla^2 u + \sin(2\theta)u = 0$ $\nu\nabla^2\theta - q\sin(2\theta) + 2\cos(2\theta)\lvert u\rvert^2 = 0$	$\nabla^2\theta_0 \ll 1$, $\theta_0 \sim \pi/4$.
Nematicon	$i\partial_z u + \frac{1}{2}\nabla^2 u + 2\theta u = 0$ $\nu\nabla^2\theta - 2q\theta + 2\lvert u\rvert^2 = 0$	$\theta \ll 1$ and $\nu \gg 1$.

The nematicon equations are interesting mathematically in their own right owing to their universality and are a focal point of this thesis. By universality, we mean

applicability across a broad range of physical applications. There are examples in other areas of nonlinear optics. One is optical solitary waves in thermal nonlinear media [40] whose refractive index changes are driven by thermal fluctuations, such as lead glasses [41, 42, 43]. Similar equations apply to optical beams in photorefractive crystals [44,45]. The exact same system as the nematicon equations arises when two beams are launched into a χ^2 media (that is, a medium whose permittivity is proportional to the square of the electric field), also called "quadratic solitons" [14,32]. Another interesting connection is with the Schrödinger-Newton equations from the theory of quantum gravitation [46] proposed as a model to investigate the role of a classical gravitational field in wave function collapse. The system consists of the standard Schrödinger equation coupled to a Newtonian graviational potential. While posed in three dimensions rather than two, this equation is the same as the nematicon equations when there is no pre-tilt. A system similar to the nematicon equations also arises in α models of fluid turbulence [24,25], which are attractive owing to their global regularity as proved by Leray [24]. It will also be shown in this thesis that they are further related to those for reaction-diffusion fronts governed by Fisher's equation [23] and those for a self-gravitating gas in astrophysics [47]. If the NLS is considered a canonical, universal example of weakly nonlinear, narrow banded waves, then the nematicon system is a canonical example of nonlinear, highly nonlocal waves.

2.2 Basic Mathematical Properties and Solitary Waves

Given a particular set of models, one interesting direction of study in nonlinear optics are its basic properties. In addition to existence and uniqueness of the initial value problem, nonlinear wave equations have proven to be a thoroughly rich area in the analysis of PDE's [48]. Of interest in this thesis are properties such as the existence of a ground state (equivalent to the existence of a solitary wave), stability proper ties of these ground states when used as initial conditions in the initial value problem, and the existence of power thresholds. Fortunately, all of these basic questions have been answered conclusively for the nematicon equations in [33], which we summarize here without proofs. We comment that the properties for the pre-tilted, as well as the full nematicon equations, remain open and lie outside the scope of this work.

Consider the nematicon equation's (2.15) and (2.16) in (2+1) dimensions. In sim-

plifying the analysis, θ is solved for using a Greens function, giving

$$\theta = \frac{2}{\nu} \int_{\mathbb{R}^2} K_0 \left(\sqrt{\tfrac{2q}{\nu}} \, |x - s| \right) |u|^2(s) ds \tag{2.17}$$

where K_0 is the modified Bessel function of zeroth order. For brevity, we write θ as $\theta = G\left(|u|^2\right)$, thus we have the single integro-differential equation for u

$$i\partial_z u + \frac{1}{2}\nabla^2 u + 2G(|u|^2)u = 0. \tag{2.18}$$

All analysis results now refer to the single equation (2.18) which, of course, is completely equivalent to the nematicon equations.

We begin by reviewing the results for ground states as this is the realm of solutions that are of the highest interest in this thesis, solitary waves. Seeking a solitary wave solution by substituting $u = u(\mathbf{x})e^{i\sigma z}$ for $u(\mathbf{x})$ real-valued into (2.18), we have the nonlinear eigenvalue problem

$$\frac{1}{2}\nabla^2 u - \sigma u + 2G(u^2)u = 0 \tag{2.19}$$

posed for $\mathbf{x} \in \mathbb{R}^2$ with the requirement that $u \to 0$ as $|\mathbf{x}| \to \infty$. The main result is summarized as follows,

> *For some $\sigma_0 > 0$ and for all $\sigma > \sigma_0$, we have the existence of at least one solution $u \in C^2(\mathbb{R}^2)$ to (2.19) which is strictly positive, can be taken to be cylindrically symmetric, and is orbitally stable.*

The proof relies on direct methods in the calculus of variations, in particular, finding solutions which minimize the Hamiltonian (energy)

$$H = \int_{\mathbb{R}^2} \frac{1}{4}|\nabla u|^2 - G(|u|^2)|u|^2 dx \tag{2.20}$$

subject to the constraint that u has a non-zero power, defined by

$$P = \int_{\mathbb{R}^2} |u|^2 dx, \tag{2.21}$$

both of which, are conserved quantities. There are a couple of important remarks regarding this result. First, that the solitary wave solutions are known to be cylindrically symmetric is a particularly nice property as it allows us to reduce the dimension of the

system in seeking stationary solutions without loss of generality. Second, the quantity σ_0, in terms of q and ν, is unknown and states that there exists a *power threshold* for the formation of nematicons, whereby this is a minimum power needed so that the solution remains stationary and propagates noiselessly, without decaying. In general, one can also show, using solitary waves as initial conditions such that they have sufficiently small L^2 norm, the solution of the initial value problem decays in the L^4 norm. This is also something observed experimentally but difficult to relate to the solitary wave threshold analytically. Third, that these solutions are a minimizing sequence of a constrained optimization problem leads naturally to numerical methods introduced in section 2.4.

The most crucial attribute of these solitary wave solutions is that they are *orbitally stable*. This is a particularly desirable quality of solitary waves as physically it translates into a statement about their robustness in the presence of noise. Orbital stability is also known as fully nonlinear stability or Lyapunov stability. Formally this means the following. Denote a solitary wave solution parametrized by σ as u_σ. Now consider an initial condition for the IVP (2.18) that is the sum of a solitary wave and a pertubation, denoted by $u_0 = u_\sigma + \delta$. Denote the solution of the IVP for initial condition u_0 as u_e (which, as a quick aside, exists and is bounded for all time). Then for any $\delta > 0$, there exists a $\varepsilon(\delta) > 0$ such that if

$$||u_0 - u_\sigma|| < \delta, \tag{2.22}$$

then for all $z > 0$

$$||u_e - u_\sigma|| < \varepsilon(\delta) \tag{2.23}$$

for a given norm $||\cdot||$ that is usually determined in the course of the analysis [49]. Essentially, this states that if the initial data is near a solitary wave, then the solution stays near this solitary wave for all time. It is relatively uncommon to have such a strong and conclusive result regarding nonlinear stability, a phenomenon which is generally studied numerically. Furthermore, it is a distinguishing feature from solutions of the NLS equation in more than one spatial dimension, which experience either decay below a certain threshold, or blow up in the L^∞ norm at some finite value in z for higher dimensions. Orbital stability implies that the nematicon convolution nonlinearity is sufficiently strong to support solitary waves in higher dimensions, even in the presence of noise. The fact that it also describes a physical system in which this happens is fascinating.

2.3 Analytic Methods

Having the necessary existence results, we turn our attention to methods used in the approximation of the solution of the nematicon equations, which we call analytic methods. In comparison to integrable systems such as the NLS equation, in which the initial value problem can be solved via the inverse scattering transform, relatively few analytic methods are available for deriving solutions of the nematicon equations. In lieu of an exact inversion transform, various approximate, asymptotic and semi-analytic methods have been put forth in order to study the models, namely the nematicon equations. To date, there are no methods known capable of analyzing the full nematicon or pre-tilted nematicon equations. Most of this thesis is concerned with addressing fundamental questions surrounding existing analytic methods, as well as developing novel asymptotic methods for the study of nematicons. In this section, we review these methods starting with the variational method, certainly the most widely used in the nematicon context [39, 50, 51, 52, 53, 54, 55], and then discuss the current state of semi-analytical and asymptotic methods. The variational method is crucial for the study presented in Chapter 3 and the semi-analytical/asymptotic methods form the basis for the method presented in Chapter 4.

2.3.1 The Variational Method

The variational method is a widely used, straightforward approximate technique employed in optics [56] since its first appearance in Anderson [57]. The main steps are outlined as follows

1. Derive a Lagrangian for the system of interest.
2. Substitute an appropriate ansatz into this Lagrangian and take the average over the domain of interest [4].
3. Take variations with respect to each of the ansatz's parameters in the averaged Lagrangian [4].

The first two steps are those employed in the classical approximate method of the calculus of variations, the Rayleigh-Ritz method. The third step can trace its origins to the principle of stationary action and has been widely used in perturbative methods for nonlinear dispersive waves [4]. Whitham [4] developed a very influential theory for the

analysis of slowly varying wavetrains based on averaged Lagrangians, called modulation theory. To illustrate the method in some generality, consider the functional

$$I[u] = \int_{\Omega \times [z_0, z_f]} L(u, u_z, \nabla u)\, dxdz,$$

where L is the Lagrangian density of the system, $\Omega \subset \mathbb{R}^n$ is some open, bounded spatial region and z_0 to z_f defines the trajectory of propagation. We search for u to minimize I, which is equivalent to solving the resulting Euler-Lagrange equations, or the original PDE. We now substitute an "appropriate" ansatz. The appropriate ansatz is generally a known elementary, or sufficiently simple function of the spatial variable, depending on N parameters which we denote $p_i(z)$ for $i = 1, \ldots, N$, depending on the propagation variable z. Having substituted the chosen ansatz, the spatial integral, or the averaged Lagrangian $\mathcal{L} = \int_\Omega L(u, u_z, \nabla u)dx$ [4] can now be computed. This leaves a functional being integrated over the trajectory now depending on the ansatz parameters $p_i(z)$, i.e. $I[u]$ becomes

$$I[p_1, .., p_N] = \int_{z_0}^{z_f} \mathcal{L}(p_1, .., p_N, p_1', ..., p_N')\, dz. \tag{2.24}$$

The principle of stationary action is now invoked, leading to the system of Euler-Lagrange equations which determine p_i, also known as the modulation equations [4], given by

$$\frac{\partial}{\partial z}\frac{\partial \mathcal{L}}{\partial p_i'} - \frac{\partial L}{\partial p_i} = 0 \tag{2.25}$$

for $i = 1, \ldots, N$.

The variational method is, effectively, the approximate Rayleigh-Ritz method applied to partial differential equations. However, there are some further simplifications. In the Rayleigh-Ritz method, a truncated orthonormal basis of L^2 is substituted into the Lagrangian and the coefficients are determined from solving the resulting minimization problem [58]. If one has more experience with such solutions, a sufficiently close ansatz is used to lead to a simpler, approximate system, the modulation equations. Indeed, for the correct choice of ansatz, the variational method collapses into classical multiple scales and is capable of finding exact solutions [4].

This leads us to what constitutes an "appropriate" ansatz and how can one be found. There is no rigorous mathematical approach to answering this question, just a guiding principle.

The ansatz should be sufficiently representative of the exact solution without

depending on too many parameters.

Generally, the "sufficiently close" portion comes from experience with numerical solutions and the physics of the particular problem. The "too many parameters" portion is one of simple practicality. Too many parameters can overcomplicate the modulation system, simply to the point where the method fails to offer insight outside of what can be obtained from numerical solutions. Furthermore, too many parameters can be construed as over-fitting.

This question of an appropriate ansatz is something explored in depth in Chapter 3. With the introduction of an exact solution of the nematicon equations, questions are raised as to which of the existing and previously unexplored ansätze should be used in the variational method. This is studied and treated extensively.

2.3.2 The Snyder-Mitchell Method

Much of the experimental work on nematicons and other nonlocal spatial optical solitary waves was motivated by a popular paper by Snyder and Mitchell [59]. The work looked to introduce so-called "accessible solitons", which are defined as solitary waves that can be approximated via *linear* equations, usually those resulting in elementary quantum mechanics. In this way, analysis of solitary waves becomes simple and avoids the inverse scattering transform. The idea is best explained by working through it.

We consider the evolution of an extraordinary beam propagating through a nonlinear medium as before under the SVEA. The governing equation, using our notation, is the following Schrödinger equation

$$2ik\frac{\partial u}{\partial Z} + \nabla_{XY}^2 u + k_0^2(n^2 - n_0^2)u = 0, \tag{2.26}$$

where all values are as before but we recall them briefly. The slowly varying envelope is u, k is the wavenumber in the medium, k_0 the initial wave number, n_0 the refractive index in the absence of a beam, and n is the, possibly nonlinear, total refractive index. The coordinates in this circumstance are the same as before. This is a general equation where we note that taking the $n^2 = n_0^2 + \chi|\psi|^2$, and after some scaling, recovers the NLS equation and similarly $n^2 = n_0^2 + \sin^2(\phi) - \sin^2(\theta_0)$ where ϕ obeys (2.2) recovers the unscaled nematicon system given by (2.1) and (2.2). The idea, and hope, of Snyder Mitchell was to study nonlinear optics without having to resort to the "mathematically abstruse" inverse scattering transform. This idea is not unique to their paper.

Anderson [57] originally introduced the variational method to avoid the IST. Kath and Smyth's [60] extended variational method was designed to shed more analytical light onto the role of radiation in pulse propagation, as the fundamental mechanisms are lost in the IST approach. However, Snyder and Mitchell approached the problem from a completely different perspective. Rather than the *mathematics* itself being the problem, it was the *physical models*, namely the NLS and other integrable systems, being considered that were making soliton theory "inaccessible". The idea is then to theoretically engineer a medium in which the mathematics of solitary waves is simple.

This theoretical engineering was done through a thought experiment. If a material is sufficiently nonlocal in the sense that its response expands considerably beyond that of the beam, then one can think of observing beams in nonlocal materials as "viewing distant point-sources through badly blurred lenses." This suggests the solitary wave can treated as a point source from the perspective of the nonlocal medium. That is, if ρ is the characteristic radius of the beam and $\mathcal{R}$ is the characteristic radius of the response, then $\rho \ll \mathcal{R}$. For such a material (assuming one exists) only a local approximation of the response is needed as this is the portion which "feels" the beam. Mathematically, this suggests the nonlinear refractive index can be approximated by the Taylor series

$$n^2 = n_0^2 - \alpha(P)R^2, \tag{2.27}$$

R is the radial coordinate from the center of the initial beam and α depends on the power and is considered a material constant. Note the first derivative of the refractive index is assumed to be zero, in analogy with the curvature of a lens being essentially flat at the center when viewed closely. Furthermore, perfect lenses should be well rounded near the center of their axes, thus the portion of the lens that the beam feels should be axisymmetric or radially symmetric (otherwise there would be some defect). The coordinate system is then taken to be a cylindrical one with the Z axis oriented through the axis of the lens and R the distance from the Z axis $R = \sqrt{X^2 + Y^2}$. Combining these ideas and substituting them into the Schrödinger equation above we get

$$2ik\frac{\partial u}{\partial Z} + \nabla_{XY}^2 u - k^2\alpha(P)R^2 u = 0, \tag{2.28}$$

which is the classical quantum harmonic oscillator (QHM for brevity), one of the most basic, exactly solvable models from quantum mechanics [59]. After rescaling by $\mathbf{x} =$

$\sqrt{k}X$ (thus $r = \sqrt{x^2 + y^2}$) and $z = 1/(2n_0)Z$, $u = \tilde{u}(x, z)$ (and ignoring the tilde), we have

$$i\frac{\partial u}{\partial z} + \nabla_\perp^2 u - \alpha(P)r^2 u = 0, \tag{2.29}$$

with solitary wave solution given by the Gaussian profile ground state

$$u = a \exp\left(-\frac{\sqrt{\alpha}}{2}r^2 - i2\sqrt{\alpha}z\right). \tag{2.30}$$

The nonlinear dependence of the amplitude on the width comes the definition of $\alpha(P)$. For example, in the case of a "Kerr" type nonlocality, $\alpha = \chi P$, then using the definition of power (2.21), we have

$$\alpha = 2\pi\chi a^2 \int_0^\infty r \exp\left(-\sqrt{\alpha}r^2\right) dr, \tag{2.31}$$

which after integrating gives the amplitude dependence on the material $a = \sqrt{\frac{\alpha^{3/2}}{\pi\chi^2}}$, giving the complete solitary wave solution as

$$u = \sqrt{\frac{\alpha^{3/2}}{\pi\chi^2}} \exp\left(-\frac{\sqrt{\alpha}}{4}r^2 - i2\sqrt{\alpha}z\right). \tag{2.32}$$

The generality of this method should be fairly clear. Given a nonlocal, NLS type equation, one can find approximate solutions provided a Taylor series is available.

The approach, however, is not without it's limitations and in general is unreliable for physical systems. A glaring demonstration of this is the fact that Snyder and Mitchells solitary waves interact cleanly, like solitons, which is not observed in physically derived models of nonlocal optical media. Without going into detail, solitary waves in nonlocal media *do not* interact cleanly, producing a large amount of radiation and exhibiting considerably more complex behaviour than the Snyder-Mitchell approach would suggest [50, 52]. Furthermore, and most relevantly to this work, the approach isn't quantitatively reliable when deriving solitary wave solutions of the physically realistic systems that it has been applied to. This includes photorefractive materials mentioned, diffusive or thermal media and nematicons [18, 61]. Part of this has to do with the fact that the "degree of nonlocality" given by $\gamma = \frac{\rho}{R}$, that is the ratio of the characteristic width of the beam ρ and the characteristic width of the response, is simply not low enough in physical systems. Engineering materials or systems in which this is a possibility has proven to be particularly difficult. Shen [62], contested it

was an undertaking well worthwhile, but with the large applicability of these nonlocal systems, the author is of the differing opinion that a sufficiently simple approximation which produces accurate results is more worthwhile. This is discussed in more detail in Chapter 4.

2.3.3 Further Perturbative Methods

Given the quantitative unreliability of the Snyder-Mitchell approach for physically realistic systems various avenues have been taken to improve upon it. In this section we review those that rely on asymptotic arguments. In general, many different perturbative and semi-analytic methods have been developed and tailored to the particular physical system of interest [19, 32, 63, 64]. We review those which have a wider degree of applicability. Immediately, there are two clear avenues to do so. The first is a higher order Snyder-Mitchell method, i.e. retaining more terms in the Taylor series by arguing the quadratic term is sufficiently unrepresentative to capture the "lens" experiment in the absence of infinite nonlocality. Another interesting alternative is to approximate the material response by its Green's function, implicitly assuming the beam to be close to the Dirac delta function.

The first approach arose from an interesting criticism of the Snyder-Mitchell approximation which was its *lack* of applicability. This appears to be a confusion in the literature which we go through as it has remained persistent and is considered the motivation for developing alternative methods. The criticism is that the Snyder-Mitchell approach does not cover integral kernels that are discontinuous near $x = 0$. To illustrate, consider the nematicon equations in (1+1) dimension and seek a solitary wave solution of the form $u = \tilde{u}e^{i\sigma z}$. Solving for θ using a Greens' function, we have the integro-differential equation

$$\frac{1}{2}\frac{d^2}{dx^2}u - \sigma u + \sqrt{\frac{2\nu}{q}}\int_{-\infty}^{\infty} \exp\left(-\sqrt{\frac{2q}{\nu}}|x-s|\right) u^2(s)ds = 0. \tag{2.33}$$

The argument is then, at least in the physics literature, since

$$R(x) = \sqrt{\frac{2}{q\nu}}\exp\left(-\sqrt{\frac{2q}{\nu}}|x|\right) \tag{2.34}$$

is not continuously differentiable at $x = 0$, thus we cannot expand $R(x)$ by $R(x) = R(0) + R''(0)x^2$, the Snyder-Mitchell model no longer applies and alternative pertur-

bative methods are needed [64]. The situation, by this logic not in reality, is much worse for higher dimensional kernels where the Green's function is usually singular at the origin thus $R(0) = \infty$, such as the Helmholtz or Laplacian kernels. The confusion appears to lie in the word *response*, where the authors in [64, 65] interpret Snyder and Mitchell's use of the word to mean the kernel $R(x)$ as the response function, when in reality they are referring to the material response. The discontinuity or singularity of the Green's function is, of course, a non-issue. θ is as regular as u^2, as verified by interchanging the order of the convolution, alternatively a Taylor series can be found by a direct power series substitution for u^2 and θ into the differential equation

$$\nu \frac{d^2}{dx^2}\theta - 2q\theta = -2u^2.$$

Nonetheless, to avoid these discontinuities, researchers have turned to studying smooth model kernels such as a Gaussian $R(x) = a\exp\left(-b|x|^2\right)$ [64] as toy models, with no obvious connection to any physical models. Furthermore, this "lack of applicabilty" has been used by Guo in a series of papers [64, 65] to justify developing an alternative approach by expanding θ in a higher order Taylor series. We illustrate this method for clarity. Consider the model

$$\frac{1}{2}\frac{d^2}{dx^2}u - \sigma u + \int_{-\infty}^{\infty} R(x-\xi)u^2(\xi)d\xi u = 0. \tag{2.35}$$

By defining $V(x) = \int_{-\infty}^{\infty} R(x-\xi)u^2(\xi)d\xi$, an expansion of the form

$$V = V_0 + \alpha x^2 + \beta x^4, \tag{2.36}$$

is assumed. The resulting equation

$$\frac{1}{2}\frac{d^2}{dx^2}u - \sigma u + V(x)u = 0, \tag{2.37}$$

can then be solved explicitly and the notation has the form

$$u = ae^{-bx^2}\left(1 + cx^2 + dx^4 + ex^6 + fx^8\right), \tag{2.38}$$

where a, b, c, d, e, f have relatively complicated dependence on α and β and are determined by direct substitution. The material parameters, α, β are in turn solved by

directly substituting u into the definition of V. This is completely equivalent to the differential equation formulation and the Snyder-Mitchell approach that was mentioned. This has the benefit of, perhaps clearly, being an improvement quantitatively over the Snyder-Mitchell for non-infinite nonlocality. In general, the term "asymptotic method" appears to be loosely used for this approach, justifying their approach by saying the consecutive coefficients of the polynomial c, d, e and f get smaller and smaller. In reality, it is more likely due to the fact that this is a truncated Hermite function series, an orthonormal basis of L^2 which converges super-algebraically to smooth elements of the space [66]. No conclusive regularity result exists for nonlocal solitons past second order continuity [33]. However, rapid convergence of pseudo-spectral methods applied to the problem suggests they are smooth [50].

Apart from misunderstandings, Nikolov et al. [63] proposed an alternative method based on a different view of the nonlocal response. The idea is that, rather than use a local approximation of the response, use a more global one. We demonstrate this in detail.

Consider (2.35) again with a modified Helmholtz kernel $R = (2\alpha)^{-1}\exp(-|x|/\alpha)$. Then the approach, for the nonlocal limit $\alpha \gg 1$, is to assume

$$\int_{-\infty}^{\infty} R(x-\xi)u^2(\xi)d\xi \sim R(x)\int_{-\infty}^{\infty} u^2(\xi)d\xi = R(x)P, \tag{2.39}$$

giving the linear equation for u

$$\frac{1}{2}\frac{d^2}{dx^2}u - \sigma u + R(x)Pu = 0. \tag{2.40}$$

No obvious reasoning is available from the work of Nikolov et al. [63] although we presume the "expansion" is done in the ξ variable near $\xi = 0$ and the first term is retained. More importantly, and this argument appears to have been overlooked, this has the same implicit assumption as Snyder and Mitchell that the material response sees the beam as a point source. Thus it is a more faithful mathematical representation of the "blurry lens" thought experiment. However, the elegance of the QHM analogy is now lost. Interestingly, this equation can be solved exactly with the aid of Bessel functions. To do so, without loss of generality, divide the domain and consider $x \geq 0$, then impose that $u'(0) = 0$ and that $u(-x) = u(x)$. Then using the change of variable

$t = \exp(-x/(2\alpha))$ and shifting σ by $\sigma = \frac{\tilde{\sigma}}{8\alpha^2}$ and dropping the tilde we have

$$t^2 \frac{d^2}{dt^2} u + t \frac{d}{dt} u + \left(4\alpha P t^2 - \sigma\right) u = 0, \tag{2.41}$$

which can be solved explicitly with Bessel functions of the first kind. Returning to the original variables, the solution is

$$u = A_1 J_{\sqrt{\sigma}} \left(2\sqrt{\alpha P} \exp(-x/(2\alpha))\right), \tag{2.42}$$

where A_1 is an arbitrary constant found from imposing a maximum at the origin. The central idea of this is an interesting and rather natural interpretation of the Snyder-Mitchell approach, however, suffers from many of the same drawbacks due to the same underlying assumptions as pointed out in [67]. In particular, the method suffers quantitatively for physically realistic values of α and in the higher order modes that it predicts. Furthermore, the applicability appears to be restricted to the (1+1) nematicon case where the resulting linear Schrödinger equation is exactly solvable. In higher dimensions or differing contexts, this nice property is lost.

We comment there is one more semi-analytical method, due to Sukhorukov [32], which is a very accurate semi-analytic method for (1+1) dimensional solitons. In general, the accuracy is impressive, however, there is no asymptotic arguments employed in this method. It relies heavily on the availability of an isolated exact solution, and the fact that the local limit reproduces the NLS. While accurate for (1+1) dimensions, it lacks extensibility in the spirit of the above approaches. Thus we mention it for reference but omit its presentation.

2.4 Numerical Methods

While our goals are predominantly analytical, verification with numerical solutions is a necessity to determine the accuracy of the approximate and variational solutions. Fortunately, due to scientific interest, technological demand and industrial interest in solitary waves in optics, there has been a wealth of numerical methods specifically designed for their computation [68,69]. We employ two widely used methods for differing purposes.

The first is the Imaginary Time Evolution Method or ITEM, a long known idea that is perhaps the simplest possible method for computing ground states solitary waves to

implement [68]. The ITEM method replaces the propagation distance in NLS-type equations, z, with iz (thus imaginary time) and iterates the equation forward, while rescaling with respect to the power or amplitude of interest. Recall from section 2.2 solitary waves are the minimum of the Hamiltonian with a fixed non-zero power. Thus this iteration has long been known to constitute a minimizing sequence [68, 70]. The second is the family of Newton Methods. Using the Newton-Kantorovich theorem, one can construct another convergent sequence to a solution provided the initial guess is close enough. The advantage of the ITEM is that the solutions it computes are linearly stable, otherwise it does not converge. The advantage of the Newton Method is its speed and ability to compute unstable solutions as well. Furthermore, we use a variant of the Newton Method, the modified Newton Method in Chapter 4. Both of these methods are reviewed in this section and illustrated by an application to one of the nematicon equations.

2.4.1 Imaginary Time Evolution Method

While still used in practice, the ITEM is known for relatively slow computation times due to the small z steps required for it to converge [68]. Successful acceleration techniques have been achieved by choosing the steepest descent direction for the sequence in an appropriately defined Sobolev space, allowing larger z steps to be taken [68, 70]. However, Louis et al. [71] recently showed for the linearized nonlocal system no advantage was gained as the acceleration did not offset the time needed to compute the director equation. While Newton methods [69] have been shown to be considerably faster than both the ITEM and its accelerations for generalized NLS equations [69, 71], the ITEM saves some time in computing linear stability as otherwise the method will not converge, avoiding a potentially large eigenvalue computation at the end of a Newton computation. Furthermore, with the constant advancement of computing power, the slowness of the ITEM is more than tolerable given its ease of implementation.

To illustrate the ITEM in detail, we describe its application to the pre-tilted nematicon equations in (1+1) as the extension to the simpler nematicon system and higher dimensions should be clear. The preliminaries are as follows. We look to compute solitary waves of the form $E = u(x)e^{i\sigma z}$, σ a propagation constant, and $\theta(x, z) = \theta(x)$

for (2.13) and (2.14), with a fixed power

$$P = \int_{-\infty}^{\infty} u(x)^2 dx, \tag{2.43}$$

of the solitary wave. The spatial discretization is taken to be a uniform grid of $N+1$ segments of length h ranging from $-L$ to L, where L is appropriately large so that the solitary wave is $\mathcal{O}(10^{-12})$ towards the ends of the computational domain. Denoting the nth iterate of u at the point $-L+jh$ for $j = 1, \ldots, N+1$ as u_j^n and similarly for θ_j^n and using the shorthand

$$\delta_h^2 u^n = \frac{1}{h^2}(u_{j+1}^n - 2u_j^n + u_{j-1}^n) \tag{2.44}$$

for the standard central difference operator, the ITEM algorithm as applied to (2.13) and (2.14) is

$$\tilde{u_j}^n = u_j^n + \Delta z\Big(\frac{1}{2}\delta_h^2 u^n + \sin(2\theta_j^n)u_j^n\Big), \tag{2.45}$$

$$u^{n+1} = \sqrt{\frac{P}{<\tilde{u}^n, \tilde{u}^n>}}\tilde{u}^n, \tag{2.46}$$

where $<\cdot,\cdot>$ denotes the standard inner product on L^2 and $j = 2, \ldots, N$. All integrals, including the inner product just mentioned, are computed using the trapezoidal rule. The first step, equation (2.45), integrates (2.15) forward in imaginary time using a standard forward Euler, while the second step, equation (2.46) normalizes the power. The initial iterate is taken to be an approximate solution (usually one sufficiently close from the variation method or other approximations) and the boundary conditions are $\theta(L) = \theta(-L) = u(L) = u(-L) = 0$ as L is chosen to be sufficiently large to apply artificial boundary conditions [66]. The final step in the algorithm is to obtain θ^{n+1} at each iteration by solving (2.16) for a given u^{n+1}. This was done by solving

$$\nu\nabla^2\theta - 2q\theta = -2q\theta + q\sin(2\theta) - 2\cos(2\theta)u^2 \tag{2.47}$$

using a regular Picard iteration. It was found from experience that iterating (2.47) in the nonlocal limit, rather than (2.16), vastly improved convergence as the linear $2q\theta$ term on the LHS lessens the difficulty of the $q\sin(2\theta)$ nonlinear term for large ν. For an idea as to the speed of this scheme, for most runs at each iteration one to two Picard

iterations were needed to make the norm of (2.16) below 10^{-10}. This is essentially due to the fact that u^{n+1} is a small perturbation away from u^n. If $u(x)e^{i\sigma z}$ and $\theta(x)$ comprise a linearly stable solution of (2.13) and (2.14) with a power P, then u and θ are the limit of the sequence defined by (2.45), (2.46) and (2.47) [68]. The propagation constant σ can then be found using

$$\sigma = \frac{1}{P} < L(u,\theta), u >, \quad L(u,\theta) = \frac{1}{2}\nabla^2 u + \sin(2\theta)u. \tag{2.48}$$

In some circumstances, it is more interesting to seek solitary wave solutions with a given amplitude rather than power. In this case the ITEM is adapted simply by replacing the normalizing step (2.46) with

$$u^{n+1} = \frac{A}{||v^n||_\infty} v^n, \tag{2.49}$$

where A is the amplitude of interest and the norm $||\cdot||_\infty$ returns the maximum value of its input.

In most computations the numerical values used were $h = 0.1$ and $\Delta z = 0.001$, with a stopping condition of $||u^{n+1} - u^n||_2 \leq 10^{-10}$, where $||\cdot||_2$ is the Euclidean norm. This choice gives an acceptable amount of spatial accuracy without exacting large computation times and agrees with previous numerical studies of computing solitary waves [68, 69, 71]. This measure of error may change from Chapter to Chapter but any changes will be made explicitly when necessary.

2.4.2 Newton Methods

One of the most successful methods for computing solutions of nonlinear partial differential equations is the so-called Newton-Kantorovich method [72, 73]. Given the many players and the amount of time that has passed in the development of Newton's method, the historical details of exactly who used it for what purpose is murky (note all historical comments we refer to reference [74]). Certainly, Newton used the method for transcendental equations, although most records indicate he only applied it to polynomials, and the method we employ here is nearly exactly that used by him. The power and, although the figure was not known, order of convergence was noted immediately. Independently, Simpson noted the extension to systems of nonlinear equations, but the largest leap in the development of the method was Kantorovich, who extended the

applicability of Newtons method to Banach spaces. The so-called Newton-Kantorovich theorem then provides precise details on when a nonlinear functional equation admits a zero, sitting at a rare intersection of a pure mathematics, nonlinear functional analysis result, with a direct numerical method for partial differential equations. The analysis is in and of itself interesting as it offers an alternative to Banach's fixed point theorem in proving the existence and uniqueness of a solution, and a means of constructing it. However the bounds involved can be difficult (if not impossible) and thus numerical trial and error is generally the means of determining whether or not the method applies. The application of the Newton method to solitary wave computation was popularized by Yang [69], pointing out the vast gains in computation time over the ITEM and accelerated ITEM, mostly for scalar equations. While there are potential problems, all the same ones possible with Newton's method for a function of real numbers, the method is particularly powerful. Notably, it is capable of computing unstable solutions the ITEM is incapable of computing [69, 75].

In this work, we are interested in using two types of Newton's method, namely the classic Newton's method and the *modified* Newton's method. The modified Newton's method has a lower order of convergence, yet performs considerably faster for a strong initial guess for reasons detailed later [76]. To introduce both, we illustrate how to apply Newton's method to the nematicon equations, from which the extensions to other nonlinear equations and the modified Newton's method should be clear. We omit a detailed proof of convergence in a Banach space, but refer the reader to a standard paper for a self-contained account [72] and to the books [58, 76]

Consider computing a solitary wave solution of the nematicon equations by substituting $u = \tilde{u}(x)e^{-i\sigma z}$ into 2.15 and 2.16. Dropping the tilde as before we obtain

$$\frac{1}{2}\nabla^2 u - \sigma u + 2\theta u = 0, \tag{2.50}$$

$$\nabla^2\theta - 2q\varepsilon\theta + 2\varepsilon u^2 = 0, \tag{2.51}$$

where we have written $\varepsilon = \frac{1}{\nu}$ as most values of ν under consideration will be large as it is in the experimental arrangement [14, 18, 77]. We re-cast this is a nonlinear functional equation by defining the operator

$$F(u,\theta) = \begin{pmatrix} \frac{1}{2}\nabla^2 u - \sigma u + 2\theta u \\ \nabla^2\theta - 2q\varepsilon\theta + 2\varepsilon u^2 \end{pmatrix} \tag{2.52}$$

and searching for u^*, θ^* such that $F(u^*, \theta^*) = 0$. The idea is now to linearize around a given, known, guess which we denote u^n, θ^n. Substituting $u = u^n + \delta_u$ and $\theta = \theta^n + \delta_\theta$, where δ_u and δ_θ are considered small, into F we have

$$F(u,\theta) = F(u^n,\theta^n) + \mathcal{L}_{(u^n,\theta^n)}(\delta_u,\delta_\theta) + \mathcal{O}(||\delta||^2) \tag{2.53}$$

$$= F(u^n,\theta^n) + \begin{pmatrix} \frac{1}{2}\nabla^2 - \sigma + 2\theta^n & 2u^n \\ 2\varepsilon\left(u^n\right)^2 & \nabla^2 - 2q\varepsilon \end{pmatrix} \begin{pmatrix} \delta_u \\ \delta_\theta \end{pmatrix} + \mathcal{O}(||\delta||^2), \tag{2.54}$$

where we have used the notation $\mathcal{L}_{(u^n,\theta^n)}(\delta_u,\delta_\theta)$ to read as: the linearized operator (equivalently, the Fréchet derivative or Jacobian) around a given iterate (u^n, θ^n) as applied to $(\delta_u, \delta_\theta)$. The Newton-Kantorovich method is then defined by the sequence (using $\mathbf{u}^n = (u^n, \theta^n)$ for brevity)

$$\mathbf{u}^{n+1} = \mathbf{u}^n - \mathcal{L}^{-1}_{\mathbf{u}^n} F\mathbf{u}^n, \tag{2.55}$$

where $\mathcal{L}^{-1}_{\mathbf{u}^n} F\mathbf{u}^n$ is the solution of the linear equation $\mathcal{L}_{(u^n,\theta^n)}\delta\mathbf{u}^n = -F(u^n,\theta^n)$, with $\delta\mathbf{u}^n$ the unknown. The Kantorovich theorem states, that, under certain constraints on the initial guess $\mathbf{u}^0$ and $\mathcal{L}_{\mathbf{u}^0}$, this sequence converges to a zero of the nonlinear functional equation F. Remarkably, up until this point, there is no discretization in this method. The entire setting is a Banach space and thus, provided one can invert the linearized operator at each step, one can compute an exact solution of the nonlinear PDE. Unfortunately, there is no such general method for solving systems of linear PDE's explicitly, and thus some numerical discretization must be introduced. In this thesis we use centered finite differences as described in the previous section and details are given in the chapters as it is needed.

An interesting observation that doesn't appear to be as widely used in the numerical analysis community is that the iteration

$$\mathbf{u}^{n+1} = \mathbf{u}^n - \mathcal{L}^{-1}_{\mathbf{u}^0} F\mathbf{u}^n, \tag{2.56}$$

where $\mathcal{L}^{-1}_{\mathbf{u}^0}$ denotes the inverse Fréchet derivative of F around only the *first* guess, also converges to a solution of $F = 0$ and is called the modified Newton's method [76]. Naturally this iteration is considerably simpler than the Newton iteration from both an analysis and an implementation stand point. The cost is stricter restrictions on how close an initial iterate needs to be, as well as only linear order of convergence

rather than quadratic. This loss of convergence and robustness to initial guesses is more than made up for in computation time. One no longer has to keep constructing and decomposing a linear operator. An LU decomposition of the discretization of $\mathcal{L}_{\mathbf{u}^0}$ can be stored and inverted rapidly.

2.4.3 Time dependent Method

In Chapter 3, Section 3.5.3, stability to radially symmetric perturbations of steady profiles computed using the Newton iteration was checked by solving the full z dependent problem (3.4) and (3.5) using a fourth order Runge-Kutta (RK4) z-step. The spatial discretization and boundary conditions are the same as those described in the steady case for the ITEM and Newton iterations. We use the notation

$$u_j^k = u(r_j = j\Delta r, z_k = k\Delta z),$$
$$\theta_j^k = \theta(r_j = j\Delta r, z_k = k\Delta z),$$

for $j = 1, \ldots, N_x$, $k = 1, \ldots, N_z$ and the shorthand for the centred finite difference discretization to the cylindrically symmetric Laplacian applied to an arbitrary function g is

$$\delta^2_{\Delta r}(g) = \frac{g_{j+1} - 2g_j + g_{j-1}}{(\Delta r)^2} + \frac{g_{j+1} - g_{j-1}}{2(j-1)(\Delta r)^2}.$$

Applying a centred finite difference spatial discretion to (3.4) and (3.5), the resulting ode's can be solved using the RK4 scheme as follows. Defining

$$f(u_{j,k}, \theta_{j,k}) = i\delta^2_{\Delta r} u^k + 2i\theta_j^k u_j^k, \tag{2.57}$$

the scheme steps to $z = (k+1)\Delta z$ as follows

$$u_j^{k+1} = u_j^k + \frac{\Delta z}{6}\Big(a_j^k + 2b_j^k + 2c_j^k + d_j^k\Big), \tag{2.58}$$

where

$$a_j^k = f\Big(u_j^k, \theta_j^k\Big), \quad b_j^k = f\Big(u_j^k + \frac{\Delta z a_j^k}{2}, \theta^k_{j,(1)}\Big),$$
$$c_j^k = f\Big(u_j^k + \frac{\Delta z b_j^k}{2}, \theta^k_{j,(2)}\Big), \quad d_j^k = f\Big(u_j^k + \Delta z b_j^k, \theta^k_{j,(3)}\Big).$$

The additional subscripts on θ in the definitions of b_j^k, c_j^k and d_j^k reflect the solution to the θ equation (3.5) at each stage of the RK4 scheme. For example, in the computation of b_j^k, the θ needed at this stage is the solution of

$$\nu\delta_{\Delta r}^2\theta_j^k - 2q\theta_j^k = -2|u_j^k + \frac{\Delta z a_j^k}{2}|^2,$$

which we denote by $\theta_{j,(1)}^k$. The same principle holds in the computation of c_j^k and d_j^k. In all computations a large domain, $[0, 700]$ was used, with $\Delta r = 0.1$ and $\Delta z = 0.01$.

Chapter 3

Exact Solutions and Variational Approximations of Nematicons

3.1 Motivation

Nematicons have been studied intensively in recent years, as outlined in the Chapter 2. However, one may notice a number of rather subtle holes that are in need of answering. A core question one could ask is with regards to the guiding principle of the variational method, that is, asking that the trial function used to approximate a nematicon be sufficiently close without being too complicated. As it stands, there is a a reasonably long list of ansätze that fit this criterion. There was the approximation developed by Snyder and Mitchell [59], the director being approximated by a quadratic, the electric field by a Gaussian; by Guo [19], the director being a higher order polynomial, the electric field a Gauss-Hermite function series; and by Nikolov [63], the director being approximated by a Green's function, the field a Bessel function depending nonlinearly on x. More commonly, researchers use the Gaussian for its ease of use and the NLS soliton due to its relation to the local limit. One would expect in the limit $\nu \to \infty$ that the profile approaches a Gaussian in some sense [67], as predicted by Snyder and Mitchell (although a rigorous proof remains absent) whereas, at the opposite limit $\nu \to 0$, it is known the solution approaches the NLS soliton [78]. A grey area arises for ν large, but not so large. In this case, the Snyder-Mitchell approximation breaks down, as shown by previous studies [61], and the NLS soliton is no longer valid as the Laplacian in (2.16) becomes non-negligible. This is the territory where a variational approximation is known to perform well. However, any one of the mentioned approximations (Gaussian,

NLS type) is a candidate as an ansatz. A thorough comparative study as to which of these approximations should be employed is lacking.

Interestingly, such a study has not been undertaken and in particular, there is little work on the steady state solutions for nematicons. This is partially due to the fact that, historically, the variational method was developed for the study of the dynamics of solitary wave propagation. The method was introduced in optics by Anderson [57] who, looking to avoid the Inverse Scattering Transform, wanted to study the propagation of input Gaussian beams into an optical fiber. Initial optical beams with a Gaussian profile are relevant as these are a first approximation to the profiles produced by a standard laser. While one can, to an impressive extent, generate a profile of desired shape in optics, the amount of lenses needed to do so can be cumbersome and thus studying a simple Gaussian input is desirable. Anderson then studied the evolution of a Gaussian input by taking it as an ansatz in the variational method and evolving the parameters as outlined in the previous chapter. One issue was analytically handling radiative losses. This is not a new problem in optics, being a numerical issue as well [79], and was handled by Anderson by adding a "chirp" to the Gaussian profile, that is the solitary wave has a linear plane wave type term associated with it. This certainly helped in terms of comparison with numerical solutions. However, it was Kath and Smyth [60] who answered the question of radiative losses in the NLS equation more conclusively. In that work, perturbations around the NLS soliton were considered and thus the trial function was the NLS soliton itself with coefficients allowed to vary in z. Radiation in the vicinity of the pulse was then treated as a shelf, based on numerical simulations, and loss could be computed by enforcing conservation of mass onto the radiating soliton. Apart from historical development, steady-state studies have been largely ignored due to the rich array of dynamical physical phenomena nematicons demonstrate. In particular, collisons between nematicons [80], as well as attractive or repulsive effects between beams [50], or refraction when encountering a change in the medium etc. [54] are all scenarios in defining distinct differences in behaviour when compared to algebraic or rational nonlinearities [18]. Thus, exhaustive theoretical efforts have been expended to find novel and rich dynamical physical phenomenon. As such, steady state solutions, until this thesis, have gone largely unstudied in the community.

While dynamical phenomenon are interesting in their own right, the fundamental steady state phenomenon of nonlocal nonlinearities, bistability, has lain unapproached. Bistability is a quality of an optical system that has various definitions, but all require

that there exists at least two stable steady states (thus *bi*-stability). In early studies of the phenomenon, two steady states were accompanied by a third, unstable state [81]. The presence of this gives rise to a hysteresis loop, whereby one can switch from one stable "branch" to another by varying the optical properties. In a seminal paper by Kaplan [82], the notion was extended to solitons governed by a generalized (algebraic or rational) NLS equation, where two solitons could exist for the same wave number (σ in (2.19), or as introduced in the next section) with a different power. The importance of this phenomena is its potential application as a mechanism for all-optical switching. Choosing one steady state as "on" and the other steady state as "off", bistability provides the theoretical underpinnings for an optical transistor [81]. We should comment that, in fairness, realization of this nematicon all optical circuit is a long way off. Considerable advancements in materials science are needed to reduce the response time of liquid crystals, something one can see in the form of lag, or "ghosting", when viewing an LCD screen. However, any chance of employing light over electronics in the advancement of computing is a pursuit well worth undertaking. One rather fiendish aspect of bistability is it is not a problem to crack, but a property for one to discover. The tools used to study the system, such as which ansatz to use in the variational method, must then be precise enough to capture such a phenomenon, further making the case for a comparative study. Furthermore, the jump from the pre-tilted nematicon equations to the nematicon equations must also be examined carefully so as not to lose any phenomena that could have technological implications.

In this chapter, we study exact solutions and variational solutions of nematicons. Isolated, exact nematicon solutions will be found in both $(1+1)$ and $(2+1)$ dimensions. In $(1+1)$ dimensions the exact solution is similar to the soliton solution of the KdV equation [4]. In $(2+1)$ dimensions it is related to the solution of Abel's equation [83]. These exact solutions are isolated as they have no free parameters. Variational approximations are then found to the nematicon solution using sech, sech^2 and Gaussian trial functions. These approximations are then compared with numerically calculated nematicons obtained using the imaginary time evolution method (ITEM) [68]. It will be shown that the hyperbolic secant trial functions give the best agreement with numerical solutions for parameter values which lie within the experimental range. The Gaussian trial function shows significant disagreement with numerical solutions, even though this is the predicted nematicon profile for very large nonlocality [59]. The reasons for this will be discussed. Moreover, solutions of the nematicon equations can exhibit the same

solitary wave profile in different operating regimes of the NLC sample, introducing a novel form of bistability. The implications of this type of bistability will be discussed. Finally, it will be shown that there is a minimum power at which a nematicon can form, with good agreement between numerical and variational minimum values.

This Chapter is based on the publication in reference [84].

3.2 Governing Equations

We consider, as before, the propagation of a coherent polarised beam of light inside and along a planar cell filled with nematic liquid crystals (NLC), fluid dielectrics with optical birefringence and long range orientational order [36]. The setup and equations are presented here again for completeness. The propagation direction is taken to be z and the x direction is taken as the direction of linear polarisation of the electric field of the input light. The y coordinate completes the orthogonal coordinate triad. The NLC optic axis (or molecular director) is initially orthogonal to the electric field of the beam. To eliminate the resulting reorientation threshold, the optical Freédericksz transition [36], a low frequency electric field (voltage) is externally applied in the x direction in order to pre-tilt the NLC molecules at a finite angle θ_0 to the z direction in the (x, z) plane [15]. The electric field of the optical beam can then rotate the light-induced molecular dipoles (nematic molecules) by an extra angle θ, so that the molecular director makes a total angle $\theta_0 + \theta$ to the direction of the beam wavevector (taken collinear with z). In this manner, milliwatt power (squared L^2 norm of the electric field) light beams can generate an optical solitary wave, a nematicon [15,18,19], by increasing the extraordinary refractive index n_e [4] of the uniaxial according to

$$n_e = \left(\frac{\cos^2(\theta_0 + \theta)}{n_\perp^2} + \frac{\sin^2(\theta_0 + \theta)}{n_\parallel^2} \right)^{-1/2}, \tag{3.1}$$

where $n_\parallel$ and $n_\perp$ are the refractive indices for electric fields parallel and normal to the director, respectively. Assuming $\theta_0 \approx \pi/4$ in order to enhance the reorientational response [85], the non-dimensional equations governing the propagation of the beam through the NLC cell in the SVEA, are [14, 18, 19, 86]

$$i\frac{\partial u}{\partial z} + \frac{1}{2}\nabla^2 u + u \sin 2\theta = 0, \tag{3.2}$$

$$\nu\nabla^2\theta - q \sin 2\theta = -2|u|^2 \cos 2\theta. \tag{3.3}$$

Here u is the complex valued envelope of the electric field of the light. The Laplacian is in the transverse (x, y) plane. The constant ν measures the elastic response of the NLC and is large, $O(100)$, in the usual experimental regimes [17, 18, 77]. The parameter q is proportional to the square of the pre-tilting electric field [14, 15].

As explored thoroughly in the previous Chapter, while the system of equations (3.2) and (3.3) has been introduced in the context of light propagation through nematic liquid crystals, they also govern optical propagation in general media for which nonlinearity is accompanied by some diffusive phenomenon [87].

For the milliwatt (mW), or even sub-mW, power levels used in experiments [15, 18], the reorientation of the director due to the optical beam is small, so that $|\theta| \ll \theta_0$. In that case, the director orientation terms in the full nematicon equations (3.2) and (3.3) can be approximated by the first terms in their Taylor series, resulting in the linearised, or simply, the nematicon equations

$$i\frac{\partial u}{\partial z} + \frac{1}{2}\nabla^2 u + 2\theta u = 0, \tag{3.4}$$

$$\nu\nabla^2\theta - 2q\theta = -2|u|^2. \tag{3.5}$$

To study the nematicon equations (3.4) and (3.5) variationally, we will need the Lagrangian representation

$$L = i\left(u^* u_z - u u_z^*\right) - |\nabla u|^2 + 4\theta|u|^2 - \nu|\nabla\theta|^2 - 2q\theta^2, \tag{3.6}$$

where the superscript * denotes the complex conjugate.

3.3 Exact nematicon solutions

The first novel contribution of this thesis is the discovery of an exact nematicon solution. As mentioned in the basic aspects section of Chapter 2, the nematicon equations are known to admit at least one solitary wave solution [33]. However, no exact solitary wave (nematicon) solutions have been found to date, with all studies of these solitary waves relying on numerical, approximate or variational solutions [14, 18, 19, 39, 52, 88]. We shall now derive two isolated, exact nematicon solutions of the nematicon equations (3.4) and (3.5) in both one and two transverse dimensions.

3.3.1 One space dimension

Let us first consider the nematicon equations in one transverse spatial dimension and seek an exact solitary wave solution. While the evolution of an optical beam in a liquid crystal cell is two dimensional in the plane transverse to the propagation direction, it has been found that an adequate approximation is to reduce the transverse dependence to the one dimensional case [89]. We then seek a solitary wave solution of the linearised nematicon equations (3.4) and (3.5)

$$u = f(x)e^{i\sigma z}, \quad \theta = \theta(x). \tag{3.7}$$

The solitary wave profile f is therefore the solution of

$$\frac{d^2 f}{dx^2} - 2\sigma f + 4\theta f = 0, \quad \frac{d^2\theta}{dx^2} - \frac{2q}{\nu}\theta + \frac{2}{\nu}f^2 = 0. \tag{3.8}$$

The simple, however non-obvious, insight is that these ordinary differential equations are identical if $\theta = f/(\sqrt{2\nu})$ and $\sigma = q/\nu$. An exact $(1+1)$ dimensional solitary wave, or nematicon, solution is then

$$u = \frac{3q}{2\sqrt{2\nu}}\,\mathrm{sech}^2\left(\sqrt{\frac{q}{2\nu}}\,x\right)\, e^{iqz/\nu}, \quad \theta = \frac{3q}{4\nu}\,\mathrm{sech}^2\left(\sqrt{\frac{q}{2\nu}}\,x\right). \tag{3.9}$$

It should be noted that this is not a general solitary wave solution as it has a fixed amplitude and width and so lacks the one free parameter as with the NLS-type solitary wave [4]. This limits its usefulness in terms of being employed by a perturbative or variational method. For example, had we known the exact solitary wave solution for an arbitrary σ, one not fixed by q and ν, then the search for the optimal trial function would be over. However, there are some interesting aspects of this solution offering insights into the questions asked in the Introduction. The first is that the functional form of this nematicon is the same as that of the soliton solution of the Korteweg-de Vries equation and is not the sech profile of the NLS soliton [4]. This is important as it suggests an additional possibility in terms of an ansatz used for a variational method and was the grounds for searching for nematicon bistability. The second thing that should be noted is the widths of the beam and the director are exactly the same *regardless of the degree of nonlocality*, a fact bringing into question the very interpretation of the word and explored in more detail in Section 3.3.3. It should be noted that, after the discovery

of this solution, an isolated solitary wave solution was found independently for solitary waves in χ^2 media [90, 91]. However, the connection to nematic liquid crystals and its consequences have so far been unreported. Furthermore, the construction by setting the two equations equal rather than by trial and error substitution, is novel and allows us to derive solutions for the (2+1) dimensional case as well.

3.3.2 Two space dimensions

Let us now derive the $(2+1)$ dimensional equivalent of the $(1+1)$ dimensional exact nematicon solution (3.9). To do so, we make some further simplifications. Let us assume that there is no external low-frequency electric field, so that $q = 0$ in the director equation (3.5) [92]. In this case, the nematicon equations (3.4) and (3.5) also govern light beams in nonlinear, self-focusing thermo-optic media [41, 43]. We look for circularly symmetric solutions

$$u = f(r)e^{i\sigma z} \quad \text{and} \quad \theta = \frac{1}{\sqrt{2\nu}} f(r) + \frac{\sigma}{2}, \tag{3.10}$$

where $r^2 = x^2 + y^2$. Note in particular for a decaying $f(r)$, θ approaches a constant. One possible physical manifestation of this is a non-zero angle of the director well outside of the influence of the electric field. As before, the nematicon equations reduce to the single equation for f

$$f_{rr} + \frac{f_r}{r} + \frac{2\sqrt{2}}{\sqrt{\nu}} f^2 = 0. \tag{3.11}$$

Remarkably, this is the Lane-Emden equation of the second kind for a cylindrically symmetric self-gravitating fluid of index two governed by Newtonian gravitation, arising in astrophysics [47], another notorious non-integrable system. The general cylindrically symmetric Lane-Emden equation of the second kind is

$$\frac{d^2 f}{dr^2} + \frac{1}{r}\frac{df}{dr} + \alpha f^m = 0, \tag{3.12}$$

with m termed the index [47]. To date there are no known exact solutions of this equation for $m = 2$. Using the change of variable

$$f(r) = \frac{\phi(\ln(r))}{r^2} \tag{3.13}$$

and denoting $t = \ln(r)$, the differential equation (3.11) for the nematicon profile becomes

$$\frac{d^2\phi}{dt^2} - 4\frac{d\phi}{dt} + 4\phi + \frac{2\sqrt{2}}{\sqrt{\nu}}\phi^2 = 0. \tag{3.14}$$

This equation also governs travelling reaction-diffusion front solutions of speed 4 of Fisher's equation, which arises in mathematical biology [23]. These front solutions transform to solitary wave solutions on using $t = \ln r$. Therefore, the differential equation governing the profile of a $(2+1)$ dimensional solitary wave in NLC is general as it arises in areas as diverse as nonlinear optics, astrophysics and reaction-diffusion processes. The final substitution $\phi' = \rho(\phi)$ results in Abel's equation of the second kind [83]

$$\rho\frac{d\rho}{d\phi} - 4\rho + 4\phi + \frac{2\sqrt{2}}{\sqrt{\nu}}\phi^2 = 0, \tag{3.15}$$

for which the nematicon profile ϕ now appears as the dependent variable. Recently, an exact solution of Abel's equation of the second kind has been derived [93, 94], so that, in principle, solutions of Fisher's equation [23] and the Lane-Emden equation [47] can also be found. The solution as found by Panaytounakos [94] is given as follows. Let us set

$$f(\phi) = -\phi - \frac{\sqrt{2}}{2\sqrt{\nu}}\phi^2. \tag{3.16}$$

Then the solution of Abel's equation (3.15) is

$$\rho = (2\phi + \lambda)\Big[\bar{N}(4\phi) + \frac{1}{3}\Big], \tag{3.17}$$

where $\bar{N}(\xi)$ are the real roots of the cubic equation

$$\bar{N}^3(\xi) + p\bar{N}^2(\xi) + q = 0, \tag{3.18}$$

with p, q and ξ as

$$\xi = \ln|4\phi + 2\lambda|, \tag{3.19}$$

$$p = -\frac{a^2}{3} + b, \quad q = 2\left(\frac{a}{3}\right)^3 - \frac{ab}{3} + c, \tag{3.20}$$

$$a = -4, \quad b = 3 + 4[G(\xi) + f(\xi)]e^{-\xi}, \quad c = -4[G(\xi) + 2f(\xi)]e^{-\xi}, \tag{3.21}$$

$$G(\xi) = \frac{1}{16}\frac{\Big[(\xi\sin\xi + \cos\xi)\,\mathrm{Ci}(\xi) + \cos^2\xi\Big]\Big[4\xi\mathrm{Ci}(\xi) + \cos\xi\Big]}{[\xi\mathrm{Ci}(\xi)]^3}e^{-\xi} - 2f(\xi). \tag{3.22}$$

The constant of integration arises as λ and $\mathrm{Ci}(\xi)$ is the cosine integral

$$\mathrm{Ci}(\xi) = \gamma_{EM} + \ln \xi + \int_0^{\xi} \frac{\cos t - 1}{t} dt, \tag{3.23}$$

with γ_{EM} the Euler-Mascheroni constant. While the Abel's equation solution (3.17) gives, in principle, an exact (2+1) dimensional nematicon solution and exact solutions of the Lane-Emden equation and Fisher's equation, as well as this solution being extremely involved, to determine the actual nematicon solution the integral given by $\phi' = \rho(\phi)$ needs to be evaluated. So, while elegant, the $(2+1)$ dimensional nematicon solution is not of practical use.

3.3.3 Nonlocality

It can be seen that for the $(1+1)$ and $(2+1)$ dimensional nematicon solutions (3.9) and (3.10) the solitary wave and director distribution have the same width. This raises a question regarding the interpretation of nonlocality. In the physics literature, nonlocality is used in the sense that the medium response extends much further than the forcing optical field [14, 18, 19, 59]. This in contrast to a local medium for which the medium response has a similar width to the optical forcing. The interpretation of nonlocality in the physics literature means that for a nonlocal medium, the parameter γ given by

$$\gamma = \frac{w_{1/2}^{\theta}}{w_{1/2}^{|u|}} \tag{3.24}$$

is large, where $w_{1/2}^{\theta}$ is the full width at half the maximum amplitude of the medium response and $w_{1/2}^{|u|}$ is the same quantity for the optical field. The heuristic argument for this interpretation is as follows. The director equation (3.5) can in principle be solved using Fourier transforms. Denoting the Fourier transform by $\mathcal{F}$, this yields

$$\theta = \mathcal{F}^{-1}\left(\frac{2/\nu}{|\mathbf{k}|^2 + 2q/\nu} \mathcal{F}(|u|^2(\mathbf{k})) \right). \tag{3.25}$$

The Green's function for the director equation (3.5) is then

$$G(\frac{x}{\sqrt{\nu}}) = \mathcal{F}^{-1}\Big(\frac{2/\nu}{|\mathbf{k}|^2 + 2q/\nu} \Big). \tag{3.26}$$

This Green's function is slowly varying relative to the electric field for the large values of ν used in experiments. Thus the relative width ratio $\gamma \gg 1$ interpretation of nonlocality is a consequence of $\nu \gg 1$, suggesting that the limit ν large be termed "the nonlocal limit," as in the literature [14, 18, 19]. This idea can be carried further. The distinguishing physical feature of nonlocal optical solitary waves is their stability, in contrast to those governed by the $(2+1)$ dimensional NLS equation [11]. Solitary wave solutions of (local) NLS equations in more than one spatial dimension are unstable [11]. Above a power threshold, they blow up (catastrophic collapse) in finite z. Below the threshold, they diffract and spread into radiation. In contrast, nematicons exist [33] and are stable above a certain power threshold [14, 18, 19]. As the convolution nonlinearity of the nematicon system mathematically distinguishes the nematicon equations from higher dimensional NLS equations, the width ratio $\gamma \gg 1$ property following from the $\nu \gg 1$ argument has been used to explain the stability of higher dimensional nonlocal solitary waves [14, 18, 19].

However, this identification of large nondimensional elasticity $\nu \gg 1$ with nonlocality in the sense that $\gamma \gg 1$ neglects the detailed dependence of u on ν, or $u(\mathbf{x}) = u(\mathbf{x}; \nu)$ over the entire range of nematicon amplitudes and widths, as demonstrated by both exact solutions (3.9) and (3.10). For these exact solutions, the medium response varies on the same scale as the electric field, that is $\gamma = 1$ for all values of ν. The argument that the width ratio $\gamma \gg 1$ follows from large non-dimensional elasticity $\nu \gg 1$ is therefore not always valid. The stability of these exact solutions is confirmed by the ITEM method used in Section 3.5, as this numerical method only converges to linearly stable solutions. Thus, the stability of $(2+1)$ dimensional nematicons is not due to the width ratio being large, $\gamma \gg 1$. This suggests that the two limits, $\nu \gg 1$ and $\gamma \gg 1$, should be distinguished. The former will be termed the limit of large non-dimensional elasticity (elasticity for brevity) of the NLC and the latter the physical nonlocal limit or nonlocal assumption. In contrast to the physical idea of nonlocality, the mathematical concept of nonlocality is related to the medium response being governed by an elliptic partial differential equation, so that the solution at a point depends on the solution in the entire domain [95]. In the present chapter the term nonlocal in nonlocal optical solitary waves will be used in this mathematical sense.

The exact solutions (3.9) and (3.10) have small amplitude for high elasticity ν and, thus, it is possible they may not be observable in experiments. In general, the nonlocal assumption in the sense that the response of the director to the optical beam

far exceeds the optical forcing has been proven to be a useful analytical assumption in perturbative and variational studies of nematicons of $O(1)$ amplitude for ν large [14, 18, 19, 43, 59, 85, 96]. The validity of this assumption will be commented on and examined in more detail in the following sections.

3.4 Variational approximate solutions

The exact solutions (3.9) and (3.10) are not general nematicon solutions, but isolated ones since they do not have a free parameter. In the absence of general exact solutions, variational approximations have proved to be useful to analyse the propagation of optical solitary waves [56] since their first introduction by Anderson [57]. In the context of nonlinear optical beam propagation in nematic liquid crystals, such methods have been found to give solutions in good agreement with numerical solutions [39, 50, 51, 52, 53, 54, 55] and experimental results [77, 97, 98, 99]. Variational solutions for steady nematicons in one and two transverse dimensions will now be compared with numerical steady nematicon solutions obtained using the imaginary time method (ITEM) [68]. The variational approximate solutions will be based on a number of different, widely used trial functions in order to determine their absolute and relative accuracies. The details of these variational solutions have been given elsewhere [39, 100], so they will only be summarised here. The three trial functions to be used are a hyperbolic secant [39], as this is the profile of the soliton solution of the $(1 + 1)$-D NLS equation, a Gaussian [56, 59, 100] and a hyperbolic secant squared, the last based on the exact solution (3.9). The hyperbolic secant squared profile has not been used before.

3.4.1 One spatial dimension

In $(1 + 1)$ dimensions the trial functions to be used are of the form

$$u = af\left(\frac{x}{w}\right)e^{i\sigma(z)} \quad \text{and} \quad \theta = \alpha g\left(\frac{x}{\beta}\right). \tag{3.27}$$

To be valid approximations to the nematicon and director (or refractive index) profiles, f and g must be symmetric about $x = 0$ and monotonically decreasing to 0 as $|x| \to \infty$. For convenience, f and g are chosen to have amplitude one. The three trial functions

used are the hyperbolic secant

$$f(x) = \operatorname{sech} x, \quad g(x) = \operatorname{sech}^2 x, \tag{3.28}$$

the hyperbolic secant squared

$$f(x) = \operatorname{sech}^2 x, \quad g(x) = \operatorname{sech}^2 x, \tag{3.29}$$

and the Gaussian

$$f(x) = e^{-x^2}, \quad g(x) = e^{-x^2}. \tag{3.30}$$

The general idea, as outlined in Chapter 2 is that the trial functions are now substituted into the Lagrangian (3.6), which is then "averaged" by integrating in x from $-\infty$ to ∞ [4]. This yields an averaged Lagrangian $\mathcal{L}$ which depends on z only. Variations of this averaged Lagrangian then result in variational, or modulation, equations which give a variational approximation to the steady nematicon.

The only difficulty in calculating the averaged Lagrangian is that the integral of the cross term $4\theta|u|^2$ in the Lagrangian (3.6) cannot be evaluated exactly for the two hyperbolic secant trial functions. To overcome this obstacle, the idea of "equivalent functions" was developed [86], which involves replacing the trial functions in this cross integral by the "equivalent" Gaussians $f \sim e^{-x^2/(Cw)^2}$ and $g \sim e^{-x^2/(A\beta)^2}$. In this case, the cross integral can be evaluated exactly as

$$\int_{-\infty}^{\infty} gf^2 \, dx = \frac{\sqrt{\pi} w \beta A C}{\sqrt{w^2 C^2 + 2A^2\beta^2}}. \tag{3.31}$$

The constants A and C are then found by matching the first two orders of the Taylor series of

$$\int_{-\infty}^{\infty} f(x/w) g(x/\beta) \, dx \tag{3.32}$$

under the assumption $\beta \gg w$ using the original trial functions in the expression (3.31). Of course, for the Gaussian trial function $C = A = 1$. The "equivalent Gaussian" approximation is useful as when calculating an averaged Lagrangian the key quantities are the values of integrals, not the specific form of the integrands [86].

The fourth and final trial function is taken in direct analogy with the $(1+1)$-D

exact solution (3.9)

$$u = a\,\mathrm{sech}^2\left(\frac{x}{w}\right)e^{i\sigma(z)}, \quad \theta = \alpha\,\mathrm{sech}^2\left(\frac{x}{w}\right), \tag{3.33}$$

with the widths of the nematicon light beam and director distribution being the same. This trial function will then be termed the narrow director in the sense that the beam and the director have the same widths, in contrast to the other three previously discussed, which are termed wide director as it was assumed that $\beta \gg w$, $\gamma \gg 1$ (3.24). As the nematicon and director distribution have the same width for this trial function, the "equivalent Gaussian" approximation discussed above does not need to be used as all the integrals can be evaluated explicitly.

Substituting the general wide director trial function (3.27) into the Lagrangian (3.6) and averaging by integrating in x from $-\infty$ to ∞ gives the averaged Lagrangian

$$\mathcal{L} = -2\sigma' a^2 w c_1 - \frac{a^2}{w}c_2 + \frac{4\sqrt{\pi}\alpha a^2 ACw\beta}{\sqrt{C^2w^2 + 2A^2\beta^2}} - \frac{\nu\alpha^2}{\beta}c_3 - 2q\alpha^2\beta c_4, \tag{3.34}$$

where the c_i are constants whose values depend on the specific trial function. They are given by

$$c_1 = \int_{-\infty}^{\infty} f(\rho)\,d\rho, \quad c_2 = \int_{-\infty}^{\infty} \left(f'(\rho)\right)^2 d\rho, \quad c_3 = \int_{-\infty}^{\infty} \left(g'(\rho)\right)^2 d\rho, \quad c_4 = \int_{-\infty}^{\infty} g(\rho)\,d\rho. \tag{3.35}$$

Taking variations of this averaged Lagrangian with respect to the parameters σ, a, w, α, β give the variational, or modulation, equations determining the variational approximation to the steady nematicon as

$$\begin{aligned}
\frac{d}{dz}\left(a^2 w\right) &= 0,\\
2\sigma' w c_1 + \frac{c_2}{w} - \frac{4\sqrt{\pi}\alpha ACw\beta}{\sqrt{C^2w^2 + 2A^2\beta^2}} &= 0,\\
2\sigma' c_1 - \frac{c_2}{w^2} - \frac{8\sqrt{\pi}\alpha A^3 C\beta^3}{(C^2w^2 + 2A^2\beta^2)^{3/2}} &= 0,\\
\frac{2\sqrt{\pi}a^2 ACw\beta}{\sqrt{C^2w^2 + 2A^2\beta^2}} - \alpha\left(\frac{\nu c_3}{\beta} + 2q\beta c_4\right) &= 0,\\
\frac{4\sqrt{\pi}AC^3w^3}{(C^2w^2 + 2A^2\beta^2)^{3/2}} - \alpha\left(2qc_4 - \frac{\nu c_3}{\beta^2}\right) &= 0.
\end{aligned} \tag{3.36}$$

It can be seen that the nematicon phase σ is linear in z, as expected [11]. The director amplitude α can be eliminated between the last two of the modulation equations (3.36),

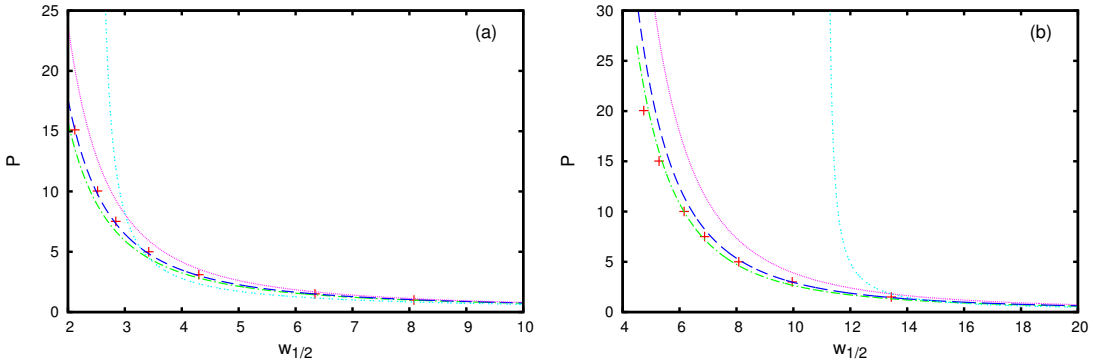

Figure 3.1: Comparison of power P versus half width $w_{1/2}$ of $(1+1)$ dimensional steady nematicon as given by full numerical and modulation solutions for $q = 2$. Full numerical solution: red crosses; sech trial functions (3.28): green (dot dash) line; sech^2 trial functions (3.29): blue (dashed) line; Gaussian trial functions (3.30): pink (dotted) line; narrow director trial functions (3.33): light blue (dotted with gaps) line. (a) $\nu = 10$ (b) $\nu = 200$.

resulting in the width β of the director distribution being given by

$$\beta^2 = \frac{1}{qA^2c_4}\left[qw^2C^2c_4 + \nu c_3A^2 + \sqrt{(qw^2C^2c_4 + \nu c_3A^2)^2 + 12q\nu A^2C^2w^2c_3c_4}\right]. \quad (3.37)$$

The equivalent Gaussian constants A and C are given in Appendix A.1, as are the integrals c_i, $i = 1, \ldots, 4$, for the various trial functions. The optical power P of the nematicon is then

$$P = \int_{-\infty}^{\infty} |u|^2\, dx = \frac{c_1c_2(2qc_4 - \nu c_3)(C^2w^2 + 2A^2\beta^2)^3}{8\pi A^2C^6w^6\beta^3}. \quad (3.38)$$

The averaged Lagrangian and modulation equations for the steady nematicon can similarly be found for the narrow director trial function (3.33). The averaged Lagrangian is

$$\frac{3}{8}\mathcal{L} = -wa^2\sigma' - \frac{2a^2}{5w} + \frac{8\alpha a^2 w}{5} - \frac{2\nu\alpha^2}{5w} - q\alpha^2 w \quad (3.39)$$

and the modulation equations are

$$\begin{aligned} \frac{d}{dz}\left(a^2w\right) &= 0, \\ \sigma' &= \frac{8\alpha}{5} - \frac{2}{5w^2}, \\ a^2\sigma' - \frac{8\alpha a^2}{5} + a\alpha^2 - \frac{1}{w^2}\left(\frac{2a^2}{5} + \frac{2\nu\alpha^2}{5}\right) &= 0, \\ \frac{8a^2w}{10\alpha} &= \frac{2\nu}{5w} + qw. \end{aligned} \quad (3.40)$$

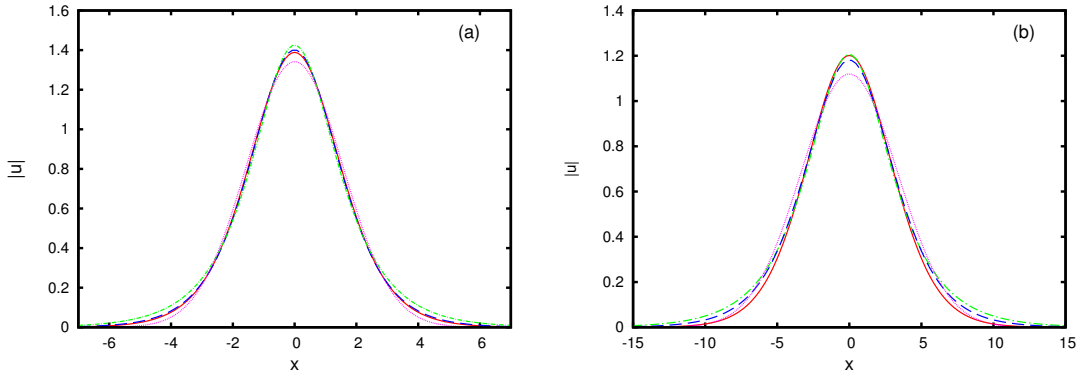

Figure 3.2: (1+1) dimensional nematicon profiles $|u|$ for $q = 2$. Full numerical solution: red (solid) line; sech trial functions (3.28): green (dot dash) line; sech^2 trial functions (3.29): blue (dashed) line; Gaussian trial functions (3.30): pink (dotted) line (a) $P = 5$, $\nu = 10$, (b) $P = 7.5$, $\nu = 200$.

The optical power (3.38) is then

$$P = \frac{4}{3}a^2 w = \frac{w}{15}\Big(\frac{2\nu}{5w^2} + 5q\Big)^2\Big(q - \frac{2\nu}{5w^2}\Big)^{-1}, \tag{3.41}$$

with the requirement that $w > \sqrt{2\nu/(5q)}$. There is then a minimum width requirement for the trial function (3.33) to be a valid approximation to the actual nematicon profile. This approximate variational solution reduces to the exact solution (3.9) when $w = \sqrt{2\nu/q}$, as required.

3.4.2 Two spatial dimensions

Similar variational approximations to the steady $(2+1)$ dimensional nematicon can be derived as for the $(1+1)$ dimensional case of the previous subsection. However, it will be found in the Results section 3.5 that the narrow director trial function (3.33) yields poor comparisons with numerical solutions. Hence, this trial function will not be used in the present $(2+1)$ dimensional case. We then only consider the three wide director trial functions, sech, sech^2 and a Gaussian. As the nematicon in $(2+1)$ dimensions is radially symmetric, the Lagrangian (3.6) is set in polar coordinates as

$$L = ir(u^* u_z - u u_z^*) - r|u_r|^2 + 4r\theta|u|^2 - \nu r\theta_r^2 - 2qr\theta^2. \tag{3.42}$$

The wide director trial functions are the radially symmetric equivalents of the (1+1)-

D trial functions (3.27)

$$u = af\left(\frac{r}{w}\right)e^{i\sigma(z)} \quad \text{and} \quad \theta = \alpha g\left(\frac{r}{\beta}\right), \tag{3.43}$$

where f and g are given by the forms (3.28), (3.29) and (3.30) of the previous subsection. Substituting the trial functions (3.43) into the Lagrangian (3.42) and integrating in r from 0 to ∞ results in the averaged Lagrangian

$$\mathcal{L} = -2a^2w^2\sigma' D_1 - a^2 D_2 + \frac{2\alpha a^2 w^2 C^2 \beta^2}{w^2C^2 + 2A^2\beta^2} - \alpha^2 \nu D_3 - 2q\alpha^2\beta^2 D_4, \tag{3.44}$$

where the constants D_i, $i = 1, \ldots, 4$, are given by the following integrals of the trial functions

$$\begin{aligned} &D_1 = \int_0^\infty \rho f(\rho)\, d\rho, \quad D_2 = \int_0^\infty \rho\big(f'(\rho)\big)^2\, d\rho, \quad D_3 = \int_0^\infty \rho\big(g'(\rho)\big)^2\, d\rho, \\ &D_4 = \int_0^\infty \rho g(\rho)\, d\rho. \end{aligned} \tag{3.45}$$

The constants A and C are due to using the "equivalent Gaussian" approximation to evaluate the integral of θu, as described in the previous subsection, with their values given in Appendix A.2, along with the values of the integrals D_i, $i = 1, \ldots, 4$, for the various trial functions. Taking variations with respect to σ, a, w, α and β of the averaged Lagrangian (3.44) results in the modulation equations

$$\begin{aligned} &\frac{d}{dz}\left(a^2w^2\right) = 0, \\ &2w^2\sigma' D_1 + D_2 - \frac{2\alpha w^2 C^2 \beta^2 A^2}{w^2C^2 + 2A^2\beta^2} = 0, \\ &\sigma' = \frac{2\alpha C^2\beta^4 A^4}{D_1(w^2C^2 + 2A^2\beta^2)^2}, \\ &\alpha = \frac{a^2 w^2 C^2 A^2 \beta^2}{(\nu D_3 + 2q\beta^2 D_4)(w^2C^2 + 2A^2\beta^2)}, \\ &\alpha = \frac{a^2 w^4 C^4 A^2}{qD_4(w^2C^2 + 2A^2\beta^2)^2}. \end{aligned} \tag{3.46}$$

Again, α can be eliminated between the last two of these modulation equations to give the width β of the director distribution as

$$\beta^2 = \frac{w^2C^2 + \sqrt{w^4C^4 + 8A^2C^2w^2D_3\nu/(qD_4)}}{4A^2}. \tag{3.47}$$

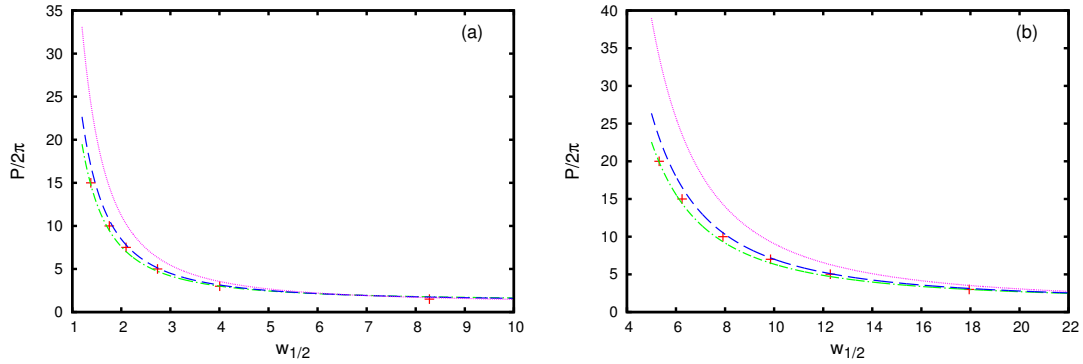

Figure 3.3: Comparison of power P versus half width $w_{1/2}$ of $(2+1)$ dimensional steady nematicon as given by full numerical and modulation solutions for $q = 2$. Full numerical solution: red crosses; sech trial functions (3.28): green (dot dash) line; sech^2 trial functions (3.29): blue (dashed) line; Gaussian trial functions (3.30): pink (dotted) line. (a) $\nu = 10$ (b) $\nu = 200$.

The $(2+1)$ dimension optical power P is

$$\frac{1}{2\pi}P = \frac{1}{2\pi}\int_{-\infty}^{\infty}\int_{-\infty}^{\infty}|u|^2\,dxdy = \frac{qD_1D_2D_4(w^2C^2+2A^2\beta^2)^4}{2C^8A^4w^6\beta^2}. \tag{3.48}$$

3.5 Results

The modulation theory results of the previous section for the steady nematicon in $(1+1)$ and $(2+1)$ dimensions will now be compared with numerical solutions for a steady nematicon obtained using the imaginary time evolution method [68], described in detail in B. It should be noted that the ITEM method will only converge to linearly stable solutions [68], which verifies the linear stability of the steady nematicons in both $(1+1)$ and $(2+1)$ dimensions, both when the director deformation is much wider and when it has the same width as the optical beam.

3.5.1 One space dimension

Solutions of the modulation equations (3.36) and (3.40) for a steady $(1+1)$ dimensional nematicon will now be compared with full numerical solutions of the nematicon equations (3.4) and (3.5) for the steady nematicon. Fig. 3.1 shows a comparison for the power P of a steady nematicon,

$$P = \int_{-\infty}^{\infty}|u|^2\,dx, \tag{3.49}$$

as given by the full numerical solution and as given by modulation theory based on the sech (3.28), sech^2 (3.29), Gaussian (3.30) and narrow director (3.33) trial functions for a moderate value of elasticity, $\nu = 10$, and a high value, $\nu = 200$, which is a typical experimental value [17, 18, 77]. It can be seen that both the sech and sech^2 trial functions give excellent agreement with the numerical power, with the sech^2 trial function being slightly better for the smaller elasticity ν and the sech trial function being slightly better for the higher elasticity. However, the Gaussian trial function, while in reasonably good agreement with the numerical solution, performs significantly worse than the hyperbolic secant trial functions, particularly for narrow nematicons. This is in contrast to the widespread use of a Gaussian in variational approximations, particularly in optics [56, 57]. In the infinite elasticity limit $\nu \to \infty$, the approximation that the director deformation is much wider than the optical beam has been used and it was then found that the nematicon profile becomes a Gaussian [14, 59], which explains its widespread use for approximating nematicons [19]. The results of the present work show that, while the nematicon theoretically has a Gaussian profile for infinite elasticity, for experimentally relevant ranges it is better approximated by the sech profile of an NLS soliton [19]. Figure 3.1 also shows that the narrow director trial function (3.33), based on the $(1+1)$ dimensional exact solution (3.9), performs poorly, except for wide nematicons which have low amplitudes. This poor agreement for high amplitudes and good agreement for low amplitudes is somewhat expected as the exact solution (3.9) has low amplitude for large ν.

Figure 3.2 compares the nematicon profiles $|u|$ for $\nu = 10$ and $\nu = 200$ as given by the numerical solution and the sech (3.28), sech^2 (3.29) and Gaussian (3.30) trial functions. These comparisons show similar conclusions to those drawn from the power comparisons of Fig. 3.1. The sech and sech^2 trial function profiles are in excellent agreement with the numerical profiles, with sech slightly worse for the lower elasticity $\nu = 10$ and slightly better for the higher $\nu = 200$. The Gaussian trial function shows significant disagreement around the peak. However, it can be seen that the Gaussian profile is in excellent agreement with the tails of the numerical nematicon profile for $\nu = 200$. This is in accord with the theoretical result that the soliton profile is a Gaussian in the limit $\nu \to \infty$ [59].

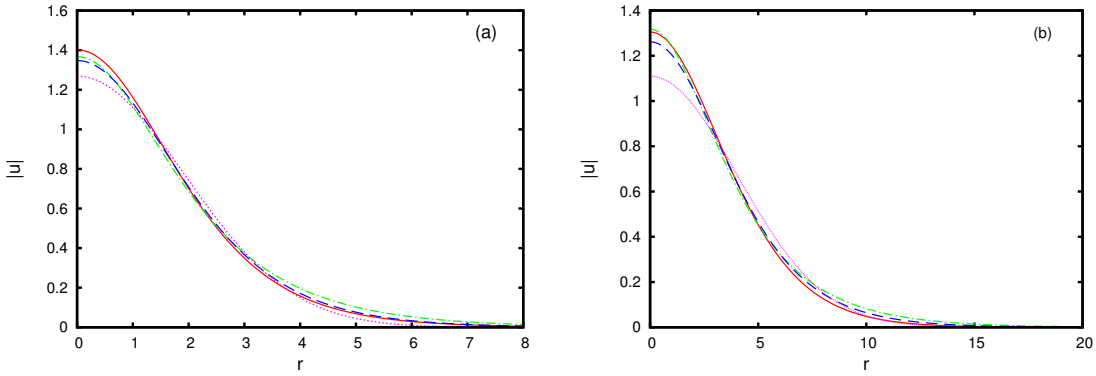

Figure 3.4: (2+1) dimensional nematicon profiles $|u|$ for $q = 2$. Full numerical solution: red (solid) line; sech trial functions (3.28): green (dot dash) line; sech^2 trial functions (3.29): blue (dashed) line; Gaussian trial functions (3.30): pink (dotted) line. (a) $P = 3$, $\nu = 10$, (b) $P = 10$, $\nu = 200$.

3.5.2 Two space dimensions

Let us now consider similar power and profile comparisons for $(2 + 1)$ dimensional nematicons. The nematicon power in $(2 + 1)$ dimensions is

$$P = 2\pi \int_0^\infty r|u|^2 \, dr. \tag{3.50}$$

The only difference in the comparisons to those for $(1 + 1)$ dimensions is that there are no narrow director trial function comparisons due to the poor agreement of the narrow director trial function in $(1 + 1)$ dimensions.

The nematicon power comparisons of Fig. 3.3 for $\nu = 10$ and $\nu = 200$ lead to the same broad conclusions as those of Fig. 3.1 for $(1 + 1)$ dimensions. The sech (3.28) and sech^2 (3.29) trial functions give significantly better agreement than the Gaussian trial function (3.30). The main difference in $(2 + 1)$ dimensions is that the sech trial function is better than the sech^2 trial function for both values of ν.

Figure 3.4 compares the numerical nematicon profile and those given by the sech (3.28), sech^2 (3.29) and Gaussian (3.30) trial functions, similar to the $(1 + 1)$ dimensional comparisons of Fig. 3.2. These comparisons again reinforce the conclusions of the power comparisons. The hyperbolic secant trial functions give excellent profile comparisons, with the sech^2 slightly worse. The Gaussian again shows significant differences around the peak, but is in excellent agreement with the numerical profile in the tails, as expected from the limit $\nu \to \infty$ [59].

It should be again noted that the steady nematicons in both $(1 + 1)$ and $(2 + 1)$

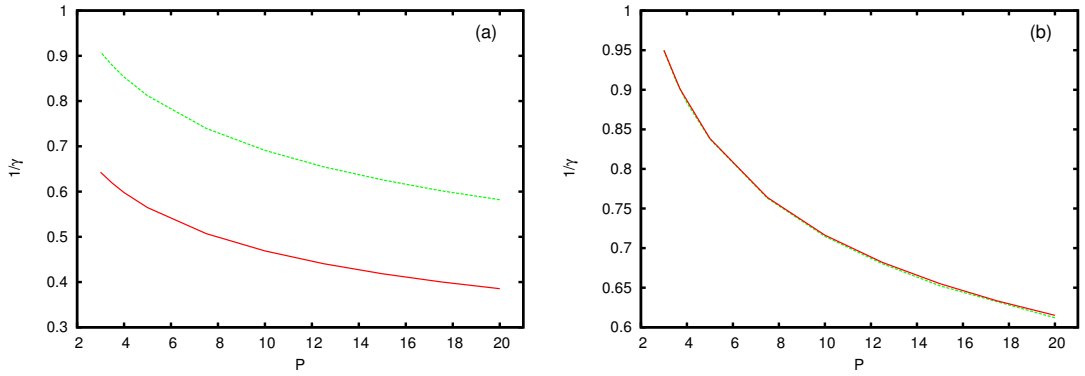

Figure 3.5: Inverse width ratio $\gamma^{-1} = w_{1/2}^{|u|}/w_{1/2}^{\theta}$ as a function of power P for $q = 2$. Red (solid) line: $\nu = 200$, green (dashed) line: $\nu = 10$. (a) $(1+1)$ dimensions, (b) $(2+1)$ dimensions.

dimensions are linearly stable as the ITEM will only converge to linearly stable solutions [68].

Figure 3.5 further explores the relationship between the value of the nonlocality parameter ν and the relative width γ of the director response to the nematicon width. It can be seen that, as discussed above, high values of ν do not guarantee that the director response is always much wider than the optical beam. As was deduced from Figures 3.1 and 3.3, low power values result in the director width being similar to the optical beam width, while high values result in the director response being wider than the optical beam. Surprisingly, the width ratio shows little dependence on the nonlocality ν in $(2+1)$ dimensions, in contrast to $(1+1)$ dimensions.

3.5.3 Minimum nematicon power

An additional feature of the variational solution of Section 3.4 is the prediction of a minimum power for solitary waves to exist for the cylindrically symmetric, $(2+1)$ dimensional, linearized nematicon equations (3.4) and (3.5). A minimum power for a $(2+1)$ dimensional solitary wave on an infinite domain was proven in the recent work by Panayotaros and Marchant [33]. However, obtaining accurate numerical approximations of this power threshold poses a challenge. Computationally, common and efficient methods for computing solitary waves on an infinite domain suitably truncate the domain such that the support of the solitary wave is well contained within the artificial boundaries [101]. In this case, imposing Dirichlet boundary conditions can then be considered admissible as outlined in Lord *et al* [102] and serves as a strong approximation to the original problem. However, in the small power or low amplitude

regime, Panayotaros and Marchant note a subtle difficulty with this approach. The continuous Dirichlet problem on a truncated domain contains ground states of arbitrarily low power, suggesting a suitable soliton solution can always be found in the numerical framework and thus the power threshold cannot be found from numerical solutions. We shall now further investigate the consequences of this numerical domain truncation and find, in fact, that the low power regime is a region of rich numerical behaviour.

One illustration of the effects of Dirichlet conditions affecting the power threshold computation is a steep increase in the computation time of the ITEM as the imposed power decreases. For example, for the parameter values $\nu = 10$ and $q = 2$, the ITEM took $\sim$ 6 minutes to converge for a power of 3 and $\sim$ 3.5–4 hours to converge for a power of 1.2. As the computation time becomes prohibitive in a regime for which boundary effects become significant, the behaviour of the ITEM in low power situations was investigated further by monitoring the energy, or Hamiltonian, given by

$$H(u) = \int_0^\infty \left(\frac{1}{4}|\nabla u|^2 - \theta|u|^2\right) r dr, \tag{3.51}$$

as the ITEM progressed. In addition, to compute solitary wave profiles in regimes for which the ITEM can be prohibitively slow, a Newton iteration, whose usefulness for solitary wave computations was detailed by Yang [69], was used (see details in Appendix B). We note that in all computations, the Newton iteration is orders of magnitude more efficient than the ITEM and is capable of computing solutions for which the ITEM would otherwise fail, mirroring previous studies [69, 71].

In addition to the slow computation of the ITEM for low power solitary waves, we observed other interesting numerical behaviour. The first was the evolution of the Hamiltonian as the ITEM progressed. As found in Ref. [33], solitary wave solutions of the system (3.4) and (3.5) have negative, non-zero Hamiltonians. Using an initial guess whose Hamiltonian is strictly positive, the number of iterations for the ITEM to a return a negative Hamiltonian value is orders of magnitude larger for a smaller power than it is for a larger one. This is illustrated in Fig. 3.6(a) and is comparable to the qualitative behaviour observed by Bao in the computation of Bose-Einstein condensates. While this is possibly a consequence of the renormalization step arresting the ITEM from converging to the zero solution, we found in a similar power regime setting ($P = 0.94$, $q = 2$, $\nu = 10$) that the Newton iteration produces a solution which

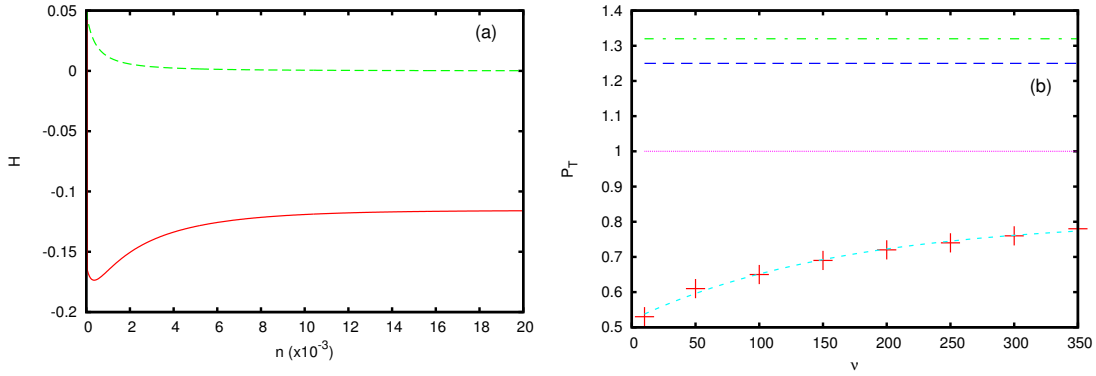

Figure 3.6: (a) Hamiltonian dependence as the ITEM progresses. $P = 2$: solid red line; $P = 0.5$: green dashed line. (b) Power thresholds P_T as a function of ν. Full numerical solution: red pluses; best fit curve: light blue (short dash) line; sech trial functions (3.28): green (dot dash) line; sech^2 trial functions (3.29): blue (dashed) line; Gaussian trial functions (3.30): pink (dotted) line.

does not decay exponentially at the boundaries, as illustrated in Fig. 3.7. This suggests that the influence of the Dirichlet conditions at the boundaries is detrimentally affecting the computation of solitary waves. This solution was found to be stable to radially symmetric perturbations in a simulation which solved the cylindrically symmetric dynamic problem (3.4) and (3.5), using the z-dependent numerical method from Chapter 2. Using the Newton iteration further, σ was varied so as to explore solutions with powers lower than the state illustrated in Fig. 3.7. Qualitatively, we found, in general, as σ decreases, the power decreases, agreeing with previous studies of similar systems [33, 71]. However, for particular low values of σ, depending on the domain size and the point in (q, ν) space, convergence can not only be erratic when using a low power, based on a sufficiently decaying solitary wave ($O(10^{-8})$ at $r = 180$ with $R_{max} = 200$) as an iterative starting point, but in some cases oscillatory solutions can found, as in Fig. 3.8, which illustrates $f(r)$, where $u = f(r)e^{i\sigma z}$. This confirms the possibility of a bifurcation as predicted by Panayotaros and Marchant [33], whereby the artificial Dirichlet conditions give rise to a system admitting multiple solutions depending on σ. This also offers a partial explanation for the difficulties experienced by the ITEM, whose convergence is linked to linearized stability and, thus, is uncertain when presented with multiple solution branches.

In general, the accuracy of criteria for finite domain numerical approximations of infinite domain power thresholds appears to depend not only on a suitable domain truncation, but also on the choice of the algorithm used and appropriately designed

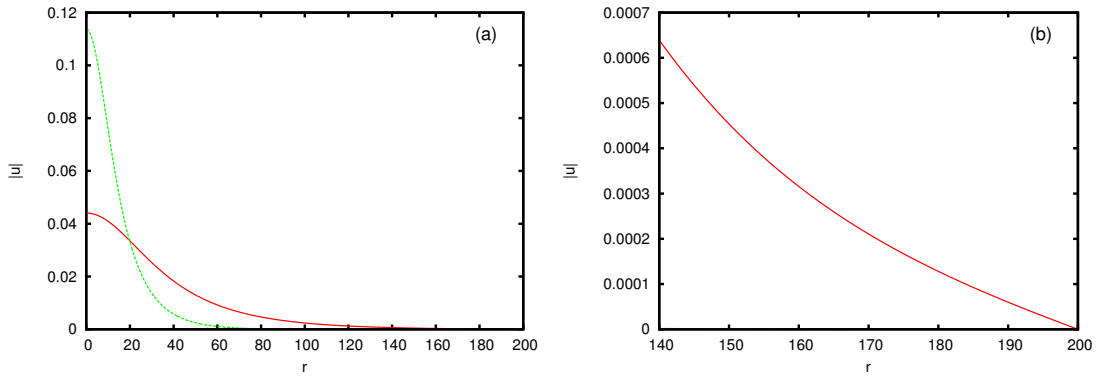

Figure 3.7: Low power solitary wave computed using Newton iteration for $P = 0.94$, $q = 2$, $\nu = 200$ and $\sigma = 0.0004$. Solid red line: computed profile, dashed green line: initial guess. (a) Full profiles, (b) zoomed profiles near the boundary. Note the initial guess is less than $O(10^{-6})$ over the $r = 140 \sim 200$ range.

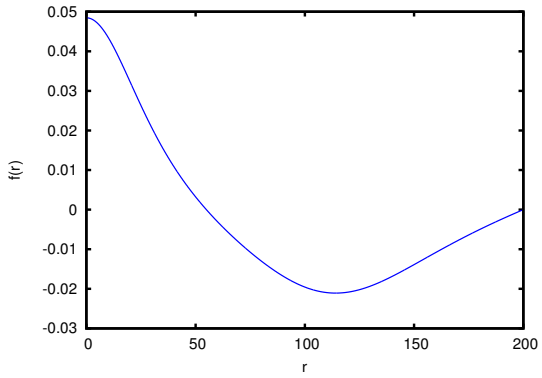

Figure 3.8: Oscillatory solution obtained from Newton iteration with $\sigma = 0.00008$. Note the amplitude and σ value and compare with Fig. 3.7 (a).

boundary conditions, as well as a thorough bifurcation analysis. This is an analysis of fundamental interest for nonlinear waves that deserves a thorough study. Such a study would be extensive and so is beyond the scope of the present thesis. It is thus left to future study.

While the difficulties of power threshold computation are now more clearly understood, we would still like to determine the relative performance of the different ansätze used in modulation theory. To this end, we use a simple threshold approximation. Using the ITEM, iterations tending to a negligible Hamiltonian ($O(10^{-5})$) were considered approximately below a power threshold as this is the order of the numerical error in the ITEM. Iterations tending to a non-negligible, negative value of the Hamiltonian were considered as converging to a solution approximately above the power threshold. This criterion determines the approximate region in which numerical methods begin to fail, providing sufficient insight for our qualitative comparison.

Figure 3.6(b) shows a comparison of the power threshold P_T for a solitary wave to exist as a function of the nonlocaility ν as given by the ITEM solution of the full equations (3.4) and (3.5) and the variational approximations based on the sech, sech^2 and Gaussian trial functions. In addition, the ITEM power threshold results have been fitted with $f(\nu) = a - b\, e^{-c\nu}$, giving $a = 0.807712$, $b = 0.286894$ and $c = 6.0672 \times 10^{-3}$. It is clear that the Gaussian trial function gives the best prediction for the numerical power threshold, which asymptotes to 0.807712 for large elasticity ν. All the trial functions give a constant minimum power. This can be seen from the variational solution of Section 3.4. Near the power threshold, the nematicon becomes low and wide. The solution (3.47) for the director β gives that $\beta \sim Cw/(\sqrt{2}A)$ as w becomes large. The expression (3.48) for the nematicon power then shows that it is independent of ν as w becomes large.

While giving poorer agreement than the Gaussian trial function, the hyperbolic secant trial functions give better agreement as the nonlocality ν increases as for these trial functions the averaged Lagrangian (3.44) was obtained in the limit ν large, so that the thresholds as predicted by these trial functions become better as ν increases. In addition, "equivalent Gaussians" were used to evaluate the mixed integral (3.31) for these trial functions, which assumed that $\gamma \gg 1$, $\beta \gg w$. As discussed in the previous section, this wide director approximation is poor for low power solutions as the beam and director have increasingly similar widths as the power decreases. The Gaussian variational solution, on the other hand, is free from these approximations as all the integrals for it were evaluated explicitly for all ν, explaining its better performance in approximating the power threshold. It should also be noted that the asymptotic error for large ν in the power threshold as given by the Gaussian variational solution is of the order of 20%, which is similar to the error for the amplitude threshold for an NLS soliton to exist for the initial condition $a\,\text{sech}\,x$ as given by the same variational approximation used here as compared with the result of the inverse scattering solution of the NLS equation [60]. In general, variational approximations only give general agreement for thresholds as these thresholds depend on fine details which are not captured by variational approximations.

3.5.4 Limits of Linearisation

The linearised nematicon equations (3.4) and (3.5) were obtained from the full equations (3.2) and (3.3) on the assumption that the extra rotation θ of the nematic molecules from their pre-tilt state was small. This assumption was necessary in order to derive the exact solutions of Section 3.3 and the variational approximations of Section 3.4. The effect and accuracy of this small deviation assumption will now be examined using numerical solutions for both sets of nematicon equations.

Figure 3.9 shows the amplitudes of $(1+1)$ and $(2+1)$ dimensional nematicons for $\nu = 200$ as a function of the pre-tilt parameter q. The differences between the nematicon amplitudes as given by both sets of equations show similar trends in both dimensions. The amplitudes as given by the full and linearised equations are the same for high values of q, but differ for low values of q. This is because as q decreases, the light induced reorientation θ increases, so that approximating the trigonometric functions in the full equations (3.2) and (3.3) by the first terms in their Taylor series becomes increasingly inaccurate. This will be further explored below. In addition, for low q (q corresponds to the external electric field applied to pre-tilt the molecular director in the (x, z) plane), two stable nematicons of equal amplitudes are supported by the full nematicon equations for two different values of q. The term optical bistability normally refers to the existence of two distinct stable states for a given excitation of the local [81] or nonlocal system [103, 104], as has been found to occur for solitary waves in saturable Kerr-like media [82, 105, 106]. That is, two different solitary waves exist for the same wave number σ, however, with differing powers, leading to a possible all-optical switching mechanism. Here, the NLC samples exhibit optical bistability in the sense that two nematicons of the same amplitude exist for two different pre-tilts of the molecular director, i.e. samples with dissimilar inhomogeneous distributions of the optic axis.

Figure 3.10 displays the nematicon profile $|u|$ and the director distribution θ for cases in $(1+1)$ and $(2+1)$ dimensions for which different biasing fields, different q, lead to nematicons of the same amplitude. The solutions displayed are solutions of the full nematicon equations (3.2) and (3.3). It can be seen that, as well as having the same amplitude, the nematicon profiles are identical to within graphical accuracy, with the director distributions being markedly different. As discussed above, the smaller q lead to director distributions θ of higher amplitude. So approximating the trigonometric

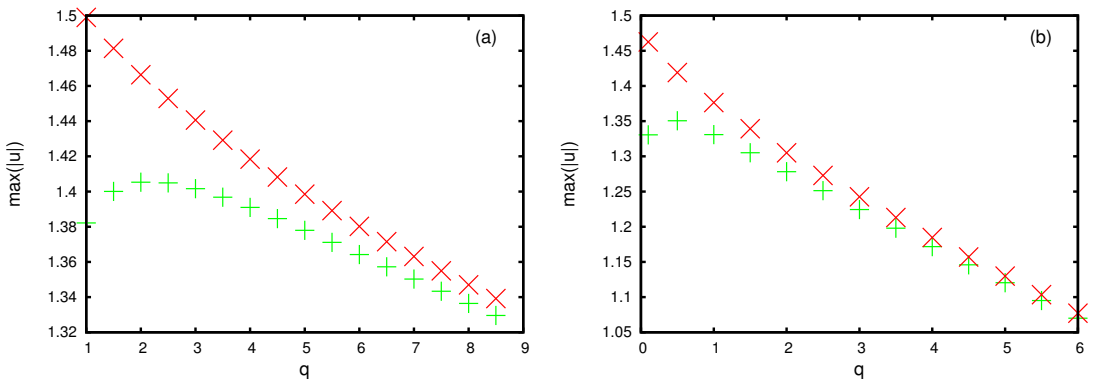

Figure 3.9: Nematicon amplitude as a function of q for $\nu = 200$. Red cross: numerical solution of linearised nematicon equations (3.4) and (3.5); green plus: numerical solution of full nematicon equations (3.2) and (3.3). (a) $(1+1)$ dimensions, (b) $(2+1)$ dimensions.

functions in the full equations (3.2) and (3.3) by the first terms in their Taylor series becomes less valid as q decreases.

It can also be seen from Fig. 3.10 that the bistable nematicon solutions for high and low q are supported by widely different director distributions. These solutions relate to the concept of nonlocality discussed in the Introduction and Exact Solutions sections. The exact solutions (3.9) and (3.10) in $(1+1)$ and $(2+1)$ dimensions and the theoretical work of Panayotaros and Marchant [33] show that for all values of ν there exist solutions of the linearized nematicon equations (3.4) and (3.5) that have narrow directors, $\gamma \sim 1$ or $\gamma \leq 1$. These solutions are restricted to low amplitudes for high values of the elasticity ν and, as mentioned, it is possible that these low amplitude, narrow director solutions may not be experimentally observable. The solutions of Fig. 3.10, however, show that narrow director nematicons of order one amplitude exist in the highly elastic regime $\nu \gg 1$. So both wide director, $\gamma \gg 1$, solutions, which are termed nonlocal in the physics literature [18, 19], and narrow director solutions, $\gamma = O(1)$, which are termed local in the physics literature [18,19], can exist in the high elasticity limit $\nu \gg 1$. Since, nonlocality is more generally ascribed to and described by the elliptic nature of the equation governing the medium response, this reinforces the earlier conclusion that the stability of $(2+1)$ dimensional nematicons cannot be solely attributed to the "nonlocal" assumption $\gamma \gg 1$ [18].

While optical solitary waves in highly elastic media are not necessarily nonlocal in the physical sense, the optical bistability of NLC samples suggests that one can find a region in the (q, ν) parameter space in which the highly elastic limit does imply that the

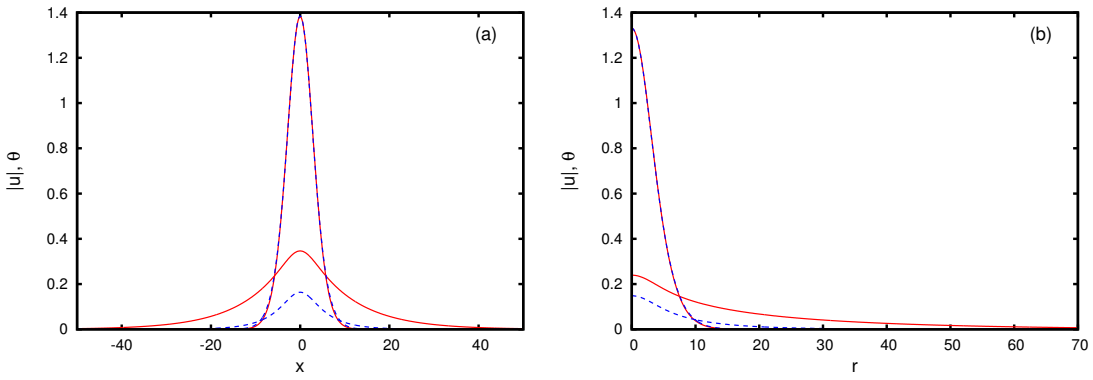

Figure 3.10: Numerical steady nematicons for full nematicon equations (3.2) and (3.3) for $\nu = 200$. $|u|$: upper two curves; θ: lower two curves. (a) $(1+1)$ dimensions, $q_1 = 1.0$: red (solid) line; $q_2 = 4.5$: blue (dashed) line, (b) $(2+1)$ dimensions, $q_1 = 0.1$: red (solid) line; $q_2 = 1.0$: blue (dashed) line.

medium response is much wider than the optical beam. Defining this region requires the more precise mathematical criterion for nonlocality, as discussed above.

3.6 Conclusions

Steady solitary wave, nematicon, solutions of the coupled system of equations governing the propagation of nonlinear optical beams in reorientational nematic liquid crystals have been studied. This system of equations consists of an NLS-type equation for the electric field of the light beam and an elliptic Poisson equation for the rotation of the optic axis or director of the medium. In both $(1+1)$ and $(2+1)$ dimensions, isolated exact nematicon solutions were found, without a free parameter, at variance with usual solitary wave solutions [4]. These exact solutions also showed that the standard explanation for the stability of nematicons in (2+1) dimensions, that the director distribution is much wider than the soliton profile [14], is not complete inasmuch as stability is associated with the director distribution being governed by an an elliptic equation whose solution at a point depends on the whole domain [95]. These exact solutions also illustrate the connections between the models governing optical solitary waves in optical media with those ruling reaction-diffusion fronts, Fisher's equation [23], the equation governing a self-gravitating gas in astrophysics, the Lane-Emden equation [47], and the Schrödinger-Newton equations of quantum gravity [46]. The present work has derived a new cylindrically symmetric solution of the Lane-Emden equation in terms of the recent solution of Abel's equation [93, 94].

Due to the lack of a general, exact solitary wave solution of the nematicon equations,

variational approximations to this nematicon solution were derived, based on three forms of trial function for the solitary wave profile, these being a sech, as for the NLS soliton, a sech^2, as for the exact $(1+1)$ dimensional exact nematicon, and a Gaussian, which is a widely used trial function [56]. The hyperbolic secant trial functions gave excellent agreement with the numerical nematicon solution, with the sech being slightly better in the experimental $(2+1)$ dimensional case. This is in contrast to the usual employment of a Gaussian profile in variational nematicon studies, as in the limit $\nu \to \infty$ the nematicon profile has been shown to be Gaussian [14]. It was found that in $(2+1)$ dimensions there is a power threshold for a solitary wave solution of the nematicon equations to exist. To obtain this threshold using the ITEM numerical method requires a careful examination of exactly what the method is converging to. Finally, it was also found that the full nematicon equations, prior to linearisation for small optically induced reorientation of the nematic director, possess a type of optical bistability in that there exists the same nematicon with different director (or refractive index) distributions corresponding to distinct values of the external biasing field, that is q.

Chapter 4

Heuristic Asymptotic Solutions of Nonlinear, Highly Nonlocal Solitary Waves

4.1 Motivation

In addition to the question of the appropriate ansatz for the variational approximation addressed in the previous Chapter, a more glaring question one may ask is how would one approximate nematicons solutions *asymptotically*. The presence of a small parameter $\varepsilon = \frac{1}{\nu}$ in the high elasticity regime suggests that we may be able to do this. This, however, is an old and non-trivial problem. The first attempt to the author's knowledge was in 1977 where Simenog [107] studied the Hartree equation and used the Taylor series approach later employed by Snyder and Mitchell in the context of optical solitary waves [59]. In that work, the lens thought experiment described in Chapter 2 was also used to find this approximation. However, no discussion of error or comparison with numerical solutions was done. This is similar to the Snyder-Mitchell case and it had been found consistently that there is no physically realistic system in which their approximation produces quantitatively reliable results [18,19,61]. Since their work, the nonlinear optics community has looked to preserve the possibility of finding simple expressions for nonlocal solitons using various asymptotic arguments, such as the further perturbative approaches discussed in Chapter 2. However, each idea has either been applied to a non-physical system in order to avoid Green's function singularities [19], only applies to the (1+1) dimensional case [63], quickly loses sight of simplicity or does

not offer extensible arguments to other systems [32]. The variational method, while impressively robust, can also have difficulties coping with equations in which integrals can be difficult to evaluate.

There are, perhaps more than ever, excellent reasons to abandon these standard approaches in favour of a novel perspective. The first is the number of connections the nematicon system shares with other, relevant physical systems [18, 20, 44]. The importance of this is in the experimental realm. For instance, those interested in studying solitary waves in fluid mechanics are looking at building or purchasing a tank that can be a great cost, both financially and time-wise. Experiments are also delicate and the amount of clean, reliable data is relatively slim. Optics, however, produces exceptionally clean experimental results that are relatively cheap to produce and can be done on a table top [15]. One can see how exploiting this analogy between optics and other areas is beneficial not only to fluid mechanics, but to astrophysics, mathematical biology or plasma physics. In particular, as mentioned, the nematicon equations are formally equivalent to the Schrödinger-Newton system from quantum gravity. This allows optical experiments to investigate quantum gravitational phenomena that may otherwise be simply unobservable [21]. Thus simple, accessible solitons are a nice theoretical idea, but the experimental possibilities of nematicons and their relatives suggests that we focus our attention on developing robust analytic tools to, if possible, asymptotically approximate them.

In this Chapter we develop a rather general, heuristic asymptotic method for approximating general solitary wave solutions of nonlinear, nonlocal Schrödinger type equations. We consider nematicons as well as those arising in thermal media, and two other straight forward, but previously intractable extensions. The ideas are simple to implement, relying only on a Taylor series, and can apply to systems of arbitrary dimension, extend simply and clearly to other systems and perform exceptionally well when compared with numerical solutions. As another point of interest, in most cases the solitary wave solutions are explicit, without the need to resort to quadrature. As a caveat, these are not rigorously asymptotic, that is, the solutions cannot be proven to approach the true solution in the limit $\varepsilon \to 0$. Thus we use the term heuristic.

This Chapter has not appeared in any publication aside from this thesis.

4.2 Governing Equations

The system of equations we consider is the same as those considered in Chapter's 2 and 3 with a slight renaming of the variables. Hence we consider,

$$i\partial_z u + \frac{1}{2}\nabla^2 u + 2\theta u = 0, \tag{4.1}$$

$$\nabla^2\theta - \kappa\varepsilon\theta + 2\varepsilon|u|^2 = 0. \tag{4.2}$$

Here we have taken $\kappa = 2q$ and $\varepsilon = \frac{1}{\nu}$ to simplify future expressions. The above system arises from coupling Maxwell equations to the continuum model for NLC's under the slowly-varying envelope assumption and with considerable, yet reasonable, restrictions on the NLC's movement [14]. The slowly varying envelope of the beam is given by u, the orientation of the NLC, as measured from its initial bias, is given by θ. The parameter κ is linked to the initial orientational bias and the small parameter, ε is related to the resistance of the NLC to reorientation. We are concerned with solitary waves solutions of the form $u = \tilde{u}(\mathbf{x})e^{i\sigma z}$ and $\theta = \tilde{\theta}(\mathbf{x})$, under the assumption that $\tilde{u}$ and $\tilde{\theta}$ are real. Substituting this ansatz into (4.1) and (4.2) dropping the tildes the system becomes

$$\frac{1}{2}\nabla^2 u - \sigma u + 2\theta u = 0, \tag{4.3}$$

$$\nabla^2\theta - \kappa\varepsilon\theta + 2\varepsilon u^2 = 0. \tag{4.4}$$

Here, it is now convenient to consider two distinct cases. The two cases of interest are $\kappa > 0$ and $\kappa = 0$. The case $\kappa = 0$ corresponds to an NLC with no initial bias and is also a model for solitary waves in nonlinear thermal media (one can imagine this arising from the steady-state heat equation) [41, 42] and thus we will henceforth call these solitary waves thermal solitary waves. The thermal problem is posed on a finite domain with zero boundary conditions whereas the nematic problem is posed on an infinite domain and we require sufficient decay for $|\mathbf{x}| \to \infty$. The difference in domains is so that a Green's function can be found for θ. It is possible that the Green's function arising when considering the thermal problem on the infinite domain ($G(r, s) = \frac{1}{4\pi}\ln(r - s)$), convoluted with a solitary wave converges but this is not pursued in this thesis. In each case, the derivation from Chapter 2 applies.

4.3 Analysis

4.3.1 Finite Domain Approximate Solutions

An interesting example to begin with is (4.1) and (4.2) with $\kappa = 0$ in the cylindrically symmetric case as the solitary wave solution has not been satisfactorily approximated and the analysis is relatively simple. Furthermore, the extension to other models follows immediately. We look for a non-trivial solution to the nonlinear eigenvalue problem (4.3) and (4.4) for a fixed $\sigma > 0$, such that u and θ have continuous second derivatives for all $r = \sqrt{x^2 + y^2} \in [0, L)$ (typical values of L being $15 \sim 20$), achieve their maximum at $r = 0$, and both decay monotonically to zero as $r \to L$. In general, we assume the existence of such a family of solutions, parameterized by either the amplitude of u or σ, as to the author's knowledge there is no conclusive proof of this assumption. However, there is substantial numerical evidence, in addition to rigorous proofs for the more analytically difficult case $\kappa \neq 0$ and in other nonlocal settings of the existence of such solutions, making this assumption a safe one [33, 71].

The first consideration in the analysis is that of scaling. Of physical interest are those envelopes u that remain $\mathcal{O}(1)$ in amplitude. Therefore, setting $u = U(R)$, $\theta = \varepsilon^{\frac{1}{2}}\Theta(R)$ and $\sigma = \varepsilon^{\frac{1}{2}}\mu$, for $R = \varepsilon^{\frac{1}{4}}r$, we find

$$\frac{1}{2}\nabla_R^2 U - \mu U + 2\Phi U = 0, \tag{4.5}$$

$$\nabla_R^2 \Phi + 2U^2 = 0, \tag{4.6}$$

which is perfectly scaled. Thus finding U, Θ and μ amounts to finding the exact solitary wave solution of the original equations (4.3) and (4.4). This leads to the natural assumption that we can take a small amplitude expansion in θ, provided Θ in the perfectly scaled regime remains $\mathcal{O}(1)$. Furthermore, we have run into a fundamental problem with scaling arguments as nonlocality, parameterized by ε, is no longer available. This is discussed shortly.

Continuing with scaling, we need to show that for U remaining $\mathcal{O}(1)$, then the same holds for Θ. This is indeed the case, as can be seen from the following justification. From the assumption Θ obtains its maximum at the origin, solving explicitly gives

$$\Theta = 2\int_0^L G(R, S)U^2 dS, \tag{4.7}$$

where the Green's function is that for $-\nabla_R^2$ which we will be referencing frequently and is given by

$$G(R,S) = \begin{cases} \big(\ln(L) - \ln(R)\big)S & 0 \le S \le R \le L, \\ \big(\ln(L) - \ln(S)\big)S & 0 \le R \le S \le L. \end{cases} \tag{4.8}$$

This implies that $\Theta \le \int_0^L (\ln(L) - \ln(S))\, S\ U^2 dS$. As U is of $\mathcal{O}(1)$, Θ then clearly remains $\mathcal{O}(1)$. Note for more general kernels $G(R,S)$ such that $\Theta \le \int_0^L G(0,S)U^2 dS$, this assumption may not hold, as for one-dimensional thermal case. However this is of less physical relevance. Similarly, from equation (4.3) for U, at the maximum at $R = 0$, $\nabla^2 U < 0$, leading to the inequality

$$(-\mu + 2\Theta(0))\, U(0) > 0, \tag{4.9}$$

implying $\mu < 2\Theta(0)$ and therefore μ is $\mathcal{O}(1)$, making σ at most $\mathcal{O}(\sqrt{\varepsilon})$.

Having a more detailed understanding of the relative scales, we formally adopt the multiple scales expansion

$$u = \sum_{i=0}^{N} \varepsilon^{\frac{i}{4}} u_i(r,R), \quad \theta = \varepsilon^{\frac{1}{2}} \sum_{i=0}^{N} \varepsilon^{\frac{i}{4}} \phi_i(r,R), \tag{4.10}$$

with $R = \varepsilon^{\frac{1}{4}} r$. The eigenvalues are similarly expanded as

$$\sigma = \varepsilon^{\frac{1}{2}} \sum_{i=0}^{N} \varepsilon^{\frac{i}{4}} \sigma_i. \tag{4.11}$$

We then have from (4.3)

$$\mathcal{O}(1) \qquad \frac{1}{2}\nabla_r^2 u_0 = 0, \tag{4.12}$$

$$\mathcal{O}(\varepsilon^{\frac{1}{4}}) \qquad \frac{1}{2}\nabla_r^2 u_1 + \frac{\partial^2}{\partial r \partial R} u_0 = 0, \tag{4.13}$$

$$\mathcal{O}(\varepsilon^{\frac{1}{2}}) \qquad \frac{1}{2}\nabla_r^2 u_2 + \frac{\partial^2}{\partial r \partial R} u_1 + \frac{1}{2}\nabla_R^2 u_0 - \sigma_0 u_0 + 2\phi_0 u_0 = 0,$$

and from equation (4.4)

$$\mathcal{O}(\varepsilon^{\frac{1}{2}}) \qquad \nabla_r^2\phi_0 = 0, \tag{4.14}$$

$$\mathcal{O}(\varepsilon^{\frac{3}{4}}) \qquad \nabla_r^2\phi_1 + 2\frac{\partial^2}{\partial r\partial R}\phi_0 = 0, \tag{4.15}$$

$$\mathcal{O}(\varepsilon) \qquad \nabla_r^2\phi_2 + 2\frac{\partial^2}{\partial r\partial R}\phi_1 + \nabla_R^2\phi_0 + 2u_0^2 = 0. \tag{4.16}$$

We have used the shorthand $\nabla_r^2 = \frac{\partial^2}{\partial r^2} + \frac{1}{r}\frac{\partial}{\partial r}$, and similarly for ∇_R^2, for the cylindrically symmetric Laplacian. Solving at leading order for u_0 gives

$$u_0 = A(R)\ln(r) + B(R). \tag{4.17}$$

To avoid the singularity at the origin, the simplest choice is to take $A(R) = 0$. We then look for a $B(R)$ which satisfies, at least approximately, the leading order boundary conditions. Denoting $B(R) = U_0(R)$ we progress to the next order, where we find similarly $u_1(r, R) = U_1(R)$. Simple analysis shows that θ behaves similarly at leading order, and therefore we have $\phi_0(r, R) = \Phi_0(R)$ and $\phi_1(r, R) = \Phi_1(R)$. Then the equations for u_2 and ϕ_2 become, respectively,

$$\frac{1}{2}\nabla_r^2 u_2 = -\Big\{\frac{1}{2}\nabla_R^2 U_0 - \sigma_0 U_0 + 2\Phi_0 U_0\Big\}, \tag{4.18}$$

$$\nabla_r^2\phi_2 = -\Big\{\nabla_R^2\Phi_0 + 2U_0^2\Big\}, \tag{4.19}$$

We enforce

$$\frac{1}{2}\nabla_R^2 U_0 - \sigma_0 U_0 + 2\Phi_0 U_0 = 0, \tag{4.20}$$

$$\nabla_R^2\Phi_0 + 2U_0^2 = 0 \tag{4.21}$$

to remove secularity in r. This is precisely the re-scaled system discussed before (4.5) and (4.6). Therefore, finding Φ_0, σ_0 and U_0 is equivalent to solving the system exactly and the expansion can be truncated immediately. In the absence of an explicit solution of (4.20) and (4.21) as well as, after rescaling, a small parameter, we must rely on a heuristic approach to approximate solutions of (4.3) and (4.4).

In particular, it appears we have made the problem more difficult by this perturbation expansion. However, equations (4.20) and (4.21) are informative, particularly about errors arising from previous methods, which we shall now detail. The lens idea

of Snyder and Mitchell [59], arguing one only needs the first two terms of a Taylor series, no longer holds in the case of a perfectly balanced system. It is not clear, after scaling, that there is any reason for the response Φ_0 to be much wider than the beam. Similarly, this is the same issue that the Green's function approach developed by Nikolov [63] as found in Chapter 2. Indeed, by assuming the response to be close to the Green's function $\Phi_0 \sim G(R,0)P_u$, one implicitly assumes the beam is a Dirac delta function. This leads to unbounded error for the Φ_0 solution, implying unbounded error for the next order correction ϕ_2. It is possible this is reconcilable in a more general space of functions. However, under our assumptions of a continuous solution (for which there is considerable evidence), this indicates the idea is unreliable.

Furthermore, and critically, the existence of secular growth at this order implies that the best one can hope for is a local approximation. In particular, we see any approximation will induce secular growth for $r \gg \varepsilon^{-1/4}$ and thus only be valid for $R \ll 1$. This suggests, in the absence of an exact solution, one cannot do better than using a local approximation for Φ_0. The break down of previous ideas is then in how this local approximation is constructed. Stricter criteria are needed.

In particular, we would like to retain desirable properties of the previous approaches while faithfully approximating Φ_0 for small R. The simplicity of the Taylor series approach makes this class of equations more "accessible" theoretically, and in general an approximation for small R can be made this way for any ε, and the Green's function approach matches the behaviour of θ for a wider portion of the interval. To retain the benefits of each and improve upon both approaches, we abstract the ideas in a natural way. Each of these previous approximations looks to find a potential, which we denote $\Phi^l(R)$ for reasons that will become apparent, such that $\Phi^l(R) \sim \Phi_0$ for small ε and so that the resulting Schrödinger equation can be solved explicitly. The general method for deriving approximate solutions is as follows.

1. Derive a locally accurate, comparable potential $\Phi^l(R)$ such that

   (a) The equation

   $$\frac{1}{2}\nabla_R^2 U_0 - \sigma_0 U_0 + 2\Phi^l U_0 = 0, \tag{4.22}$$

   can be solved simply and explicitly.

   (b) $\Phi^l \sim \Phi_0$ as $R \to 0$.

   (c) Φ^l is sufficiently differentiable, monotonically decreasing and approaches a

constant $C > 0$ for large R.

2. Solve
$$\frac{1}{2}\nabla_R^2 U_0 - \sigma_0 U_0 + 2\Phi^l U_0 = 0, \tag{4.23}$$
explicitly to get an approximation $U_0 = U^\varepsilon$.

3. Take $\Phi_0 = 2\int_0^L G(R,S)(U^\varepsilon)^2 dS$ to remove secularities at $\mathcal{O}(\varepsilon)$ in θ.

We can now see how well this idea generalizes previous methods. The locally accurate potential $\Phi^l(R)$, which we formally refer too as a "comparable" potential hereafter, is a natural, but consistent object retaining the properties of the Taylor series and Greens function approaches. These three criteria are inspired by boundary layer theory and the properties of Φ^l they enforce reflects this. The purpose of the first criterion is to enable us to find a closed form approximation, as in any other standard perturbative technique. The second criterion enforces that Φ^l should be locally asymptotic to Φ_0 for small R, so as to capture the essential features of the problem when deriving U^ε. For practical purposes, this can be done by matching the first few terms of the Taylor series. The final criterion forces Φ^l to not only be at least as smooth as Φ_0, but monotonically decreasing, as given both by this assumption and from equation (4.21). Furthermore, and crucially, criterion three enforces that Φ^l approaches some positive constant. This required so as not to neglect, a priori, the possible existence and validity of an outer solution outside of the support of U_0. Note we use the word "support" here to mean the set on which U_0 is non-zero and larger than a very small ϵ, for example machine error $\epsilon = 10^{-16}$. While Φ^l is not unique, the list of comparable candidates becomes rapidly small owing to the requirement that the linear Schrödinger equation is "simply and explicitly" solvable, if not reduced to a single possible potential.

We are now in a position to construct the approximate solutions. Note that, in what follows, we will denote $G(R,S)$ as the Green's function for the earlier operator $-\nabla_R^2$. Choosing the comparable potential

$$\Phi^l(R) = \frac{1}{2}\sigma_0 + \frac{1}{4}pc^2 - \frac{1}{4}pc^2(p+1)\tanh^2(cR) + \frac{1}{4R}pc\tanh(cR),$$

the equation for U_0 can be solved explicitly to obtain

$$U^\varepsilon = U_M \operatorname{sech}^p(cR). \tag{4.24}$$

To force $\Phi^l(R) \sim \Phi_0$ as $R \to 0$, we match the first couple terms of the Taylor series near $R = 0$. There are, of course, other means of forcing $\Phi^l(R)$ to be as close as possible to Φ_0, and in general this lies in approximation theory. However, one can show that matching the Taylor series automatically fufils the requirements of matching Padé approximants (rational approximations). More accurate techniques, such as expansion by an orthonormal basis, are more global in nature and make solving for coefficients a bit more involved. It is possible this makes a better asymptotic solution, however, this is not explored here as simplicity and accessibility is the goal. Also the results are sufficiently strong so that it is not warranted. Expanding $\Phi^l(R)$ we find

$$\Phi^l(R) \sim \frac{1}{2}\sigma_0 + \frac{1}{2}pc^2 - \frac{pc^4}{4}(p+\frac{4}{3})R^2 + \frac{pc^6}{6}(p+\frac{6}{5})R^4 + \mathcal{O}(R^6). \tag{4.25}$$

Doing the same for Φ_0 by substituting a power series into (4.21) we obtain

$$\Phi_0(R) \sim \Phi_M - \frac{\left(U_M\right)^2}{2}R^2 + \frac{c^2 p}{8}U_M^2 R^4 + \mathcal{O}(R^6). \tag{4.26}$$

Φ_M is given explicitly by

$$\Phi_M = 2\int_0^L G(0,S)\ U^2(S)dS. \tag{4.27}$$

Equating each order of R leads to the system

$$\frac{1}{2}\sigma_0 + \frac{1}{2}pc^2 = \Phi_M, \quad \frac{pc^4}{4}(p+\frac{4}{3}) = \frac{U_M^2}{2},$$
$$\frac{pc^6}{6}(p+\frac{6}{5}) = \frac{c^2 p}{8}U_M^2,$$

which can be solved exactly upon substituting the expression for U^ε. The resulting constants are given by

$$p = \frac{2}{3} + \frac{2}{15}\sqrt{205}, \quad c = \left(\frac{2(U_M)^2}{p(p+\frac{4}{3})}\right)^{\frac{1}{4}}, \tag{4.28}$$

$$\frac{1}{2}\sigma_0 = \Phi_M - \frac{1}{2}pc^2, \tag{4.29}$$

which now explicitly depend on U_M as a parameter. The closed form approximate

solution is then given as

$$u = U_M \operatorname{sech}^p(cR), \quad \theta = 2\varepsilon^{\frac{1}{2}} \int_0^L G(R,S)(u)^2 dS. \tag{4.30}$$

4.3.2 Some Simple Extensions

One principal advantage of this technique over previous methods is its clear extensibility. It appears that, under our strict assumptions of monotonicity and high nonlocality, one can construct an approximate solution provided the first three terms of the Taylor series are available. Naturally this should be checked extensively with numerical solutions, and that is something we do in this Chapter. This idea, however, clearly has broad impact, applying to systems of solitary wave equations and equations more general nonlinearities. In this thesis, we restrict our focus to generalized nonlinearities. We consider two toy models, which could plausibly arise in optics, but as of writing have not been linked to a physical system. These illustrate the method's flexibility, as well as situations in which it can fail.

The first is a more general nonlinearity, which could arise for instance, if the reorientational nonlinearity were proportional to a power law nonlinearity other rather intensity. Consider

$$\frac{1}{2}\nabla^2 u - \sigma u + 2\theta u = 0, \tag{4.31}$$

$$\nabla^2 \theta + 2\varepsilon |u|^\gamma = 0. \tag{4.32}$$

Then we can find an approximation using the comparable potential method. Omitting the details, it is

$$u = U_M \operatorname{sech}^p(cR), \tag{4.33}$$

$$\theta = 2\varepsilon^{\frac{1}{2}} \int_0^L G(R,S)(u)^\gamma dS, \tag{4.34}$$

$$p = \frac{-(\gamma/2-2) + \sqrt{(\gamma/2-2)^2 + 18\gamma/5}}{3\gamma/8}, \tag{4.35}$$

$$c = \left(\frac{2U_M^\gamma}{p(p+4/3)}\right)^{1/4}, \ \frac{1}{2}\sigma_0 = \Phi_M - \frac{1}{2}pc^2. \tag{4.36}$$

Note, U_M, the amplitude of the solitary wave, is a free parameter and Φ_M is the amplitude of the response which can be found as before. Similar to the generalized

nonlinearity, and an interesting example to consider is that of competing nonlinearities [108,109,110]. These are commonly found in phenomenological nonlinear optics models from Taylor series expansions of the permittivity. In the context of nonlocal nonlinear optics, competing nonlinearities is usually understood in the sense of different nonlocal kernels G_1+G_2, which, is phenomenologically derived as well. In this paper, we consider competing power nonlinearities and leave competing kernels to future work. One aspect of studying the competing power nonlinearities is the possibility of creating a system where our approximation breaks down and illustrates the limits of local analysis. We now consider the system

$$\frac{1}{2}\nabla^2 u - \sigma u + 2\theta u = 0, \tag{4.37}$$

$$\nabla^2\theta + 2\varepsilon(|u|^{\gamma_1} + \alpha|u|^{\gamma_2}) = 0. \tag{4.38}$$

Again, omitting the details, an approximate solution is given by

$$u = U_M \operatorname{sech}^p(cR), \tag{4.39}$$

$$\theta = 2\varepsilon^{\frac{1}{2}} \int_0^L G(R,S)\left(|u|^{\gamma_1} + \alpha|u|^{\gamma_2}\right). \tag{4.40}$$

$$c = \left(\frac{2(U_M^{\gamma_1} + \alpha U_M^{\gamma_2})}{p(p+4/3)}\right)^{1/4} \tag{4.41}$$

$$\frac{1}{2}\sigma_0 = \Phi_M - \frac{1}{2}pc^2, \tag{4.42}$$

where p now solves a slightly more involved quadratic than before, given by

$$r_1 p^2 + (4r_1/3 - r_2)p - 6r_2/5 = 0, \tag{4.43}$$

$$r_1 = 3\gamma/8\left(U_M^{\gamma_1} + \alpha\gamma_2/\gamma_1 U_M^{\gamma_2}\right), \tag{4.44}$$

$$r_2 = 2\left(U_M^{\gamma_1} + \alpha U_M^{\gamma_2}\right). \tag{4.45}$$

The positive quadratic solution is taken for p. In this case, the competing nonlinearities now create a type of potential, at some critical points of which the solution will break down. In particular, choosing the case $\alpha < 0$ indicates that at some amplitude either $\frac{d^2}{dr^2}\theta = 0$ or $\frac{d^4}{dr^4}\theta = 0$. Numerical solutions indicate that solitary waves exist when $\gamma_1 = 2.0$, $\gamma_2 = 4.0$ and $\alpha = -0.5$ (see Fig 4.1) for amplitudes larger than the critical $U_M = 1.0$, whereas the asymptotic approximation gives the constant solution. This breakdown is essentially due to local nature of our approximation, which is incapable

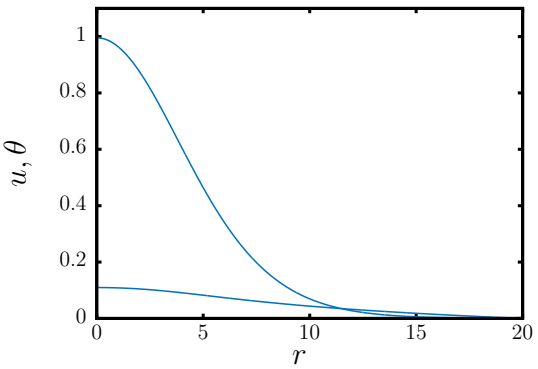

Figure 4.1: Profile of numerically computed mixed solitary wave of Amplitude approximately one. Note the asymptotic approximation only returns a constant solution in this case.

of handling more intricate competing nonlinearities. We point this out as a limitation and are leave its resolution to future research.

4.3.3 Infinite Domain Approximate Solutions

Returning to the original system (4.3) and (4.4), we now consider the nematicon case, corresponding to $\kappa > 0$.

In the (2+1)D cylindrically symmetric case, we proceed in the same way as for the thermal analysis. The scaling and comparable potential remain the same, as we choose to retain the $\kappa\varepsilon^{1/2}$ term. Omitting the details, the resulting system for the coefficients is

$$\Phi_M = \frac{U_M^2}{\sqrt{\kappa\varepsilon^{\frac{1}{2}}}} \int_0^\infty K_0\left(\sqrt{\kappa\varepsilon^{\frac{1}{2}}} S\right) \operatorname{sech}^{2p}(cS) S dS, \tag{4.46}$$

$$\frac{c^4}{3}\left(p+\frac{6}{5}\right) + \kappa\varepsilon^{\frac{1}{2}}\left\{\frac{c^2}{2}\left(p+\frac{4}{3}\right)\right\} - \frac{U_M^2}{4} = 0, \tag{4.47}$$

$$pc^4\left(p+\frac{4}{3}\right) - \left(2U_M^2 - \kappa\varepsilon^{\frac{1}{2}}\Phi_M\right) = 0, \tag{4.48}$$

$$\frac{1}{2}\sigma_0 = \Phi_M - \frac{1}{2}pc^2. \tag{4.49}$$

In general, however, this system is not simple to solve analytically. However, for ε small, we recover *the same* electric beam profile u as we did in the *thermal, finite domain case*. That is, locally, a nematicon is close to a thermal solitary wave. In this respect, we can take the electric field of a nematicon to be, at leading order, *the same as that of the thermal solitary wave*. For the material response, we still take the solution to be the Green's function for a nematicon convolved with the thermal solitary wave. The final

solution is then

$$u = U_M \operatorname{sech}^p(cR), \tag{4.50}$$

$$\theta = 2\varepsilon^{\frac{1}{2}} \int_0^\infty G_\kappa(R,S) u^2(S) dS = \varepsilon^{\frac{1}{2}} \Phi_0(R), \tag{4.51}$$

$$\sigma = \varepsilon^{\frac{1}{2}} \sigma_0 \tag{4.52}$$

where c and p are given in (4.39) and $G_\kappa(R,S)$ is now the Green's function for $-\nabla_R^2 + \kappa\varepsilon^{\frac{1}{2}}$, given by

$$G_\kappa(R,S) = \begin{cases} \frac{1}{\sqrt{\kappa\varepsilon^{\frac{1}{2}}}} S I_0\left(\sqrt{\kappa\varepsilon^{\frac{1}{2}}} S\right) K_0\left(\sqrt{\kappa\varepsilon^{\frac{1}{2}}} R\right) & 0 \le S \le R < \infty, \\ \frac{1}{\sqrt{\kappa\varepsilon^{\frac{1}{2}}}} S I_0\left(\sqrt{\kappa\varepsilon^{\frac{1}{2}}} R\right) K_0\left(\sqrt{\kappa\varepsilon^{\frac{1}{2}}} S\right) & 0 \le R \le S < \infty. \end{cases} \tag{4.53}$$

4.4 Results and Discussion

In this section we compare the results of the approximate solutions obtained with numerical solutions. In general, due to the heuristic nature of our solution derivation, it is too much to ask that the approximation U^ε be ε^γ away from some exact solution u in the sense of a norm i.e. we cannot expect there exists some exact solution u_e (after solving for θ) such that

$$||u_e(R) - U^\varepsilon(R)|| \le C\varepsilon^{C_2} \tag{4.54}$$

for C_1 and C_2 independent of ε and a norm $||\cdot||$, which is generally determined during the analysis. This is due to the fact that all quantities in the rescaled equations (4.20) and (4.21) are $\mathcal{O}(1)$. While, in general, it looks as if $\mathcal{O}(1)$ error bounds can be determined, more detailed information regarding the error can be gleaned from comparing with numerical results. Of particular interest are moderately small values of ε, around $\mathcal{O}(10^{-2})$ as these arise naturally from the Biot number for thermal optical solitary waves and are typical elasticity constants in the NLC case [71].

For all values we found the asymptotic solution to be sufficiently close to the numerical solution, that using a modified Newton iteration [76] (detailed in the Appendix C) was a very efficient means of computing numerical solitary waves, in most cases under $1sec$ per solution. The error was measured as follows. Taking our approximate solution to be the vector $\mathbf{u}^\varepsilon = (u^\varepsilon, \theta^\varepsilon)^T$ and the numerical ("exact") solution, written as $\mathbf{u}_e = (u_e, \theta_e)^T$, the error was taken to be $||e||_\infty = \max_{r\in[0,L)} |\mathbf{u}_e - \mathbf{u}^\varepsilon|$. This error

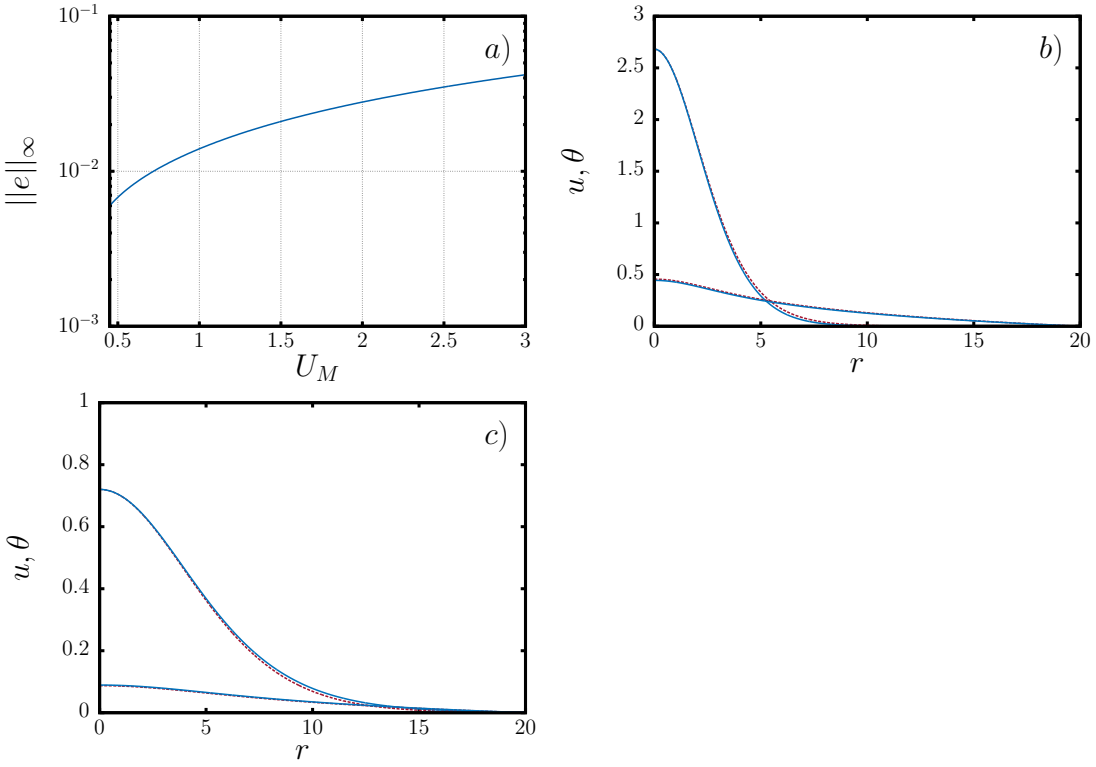

Figure 4.2: Error analysis and profile comparisons for thermal optical solitary waves. a) Error as a function of amplitude, b) Profile comparisons for a large amplitude solitary wave, blue (solid) is the numerical solution, red (dashed) is the analytic approximation, upper curves are the beam envelope u, lower curves are the reorientational response θ, c) Smaller amplitude profile comparisons, colors and styles are the same as before.

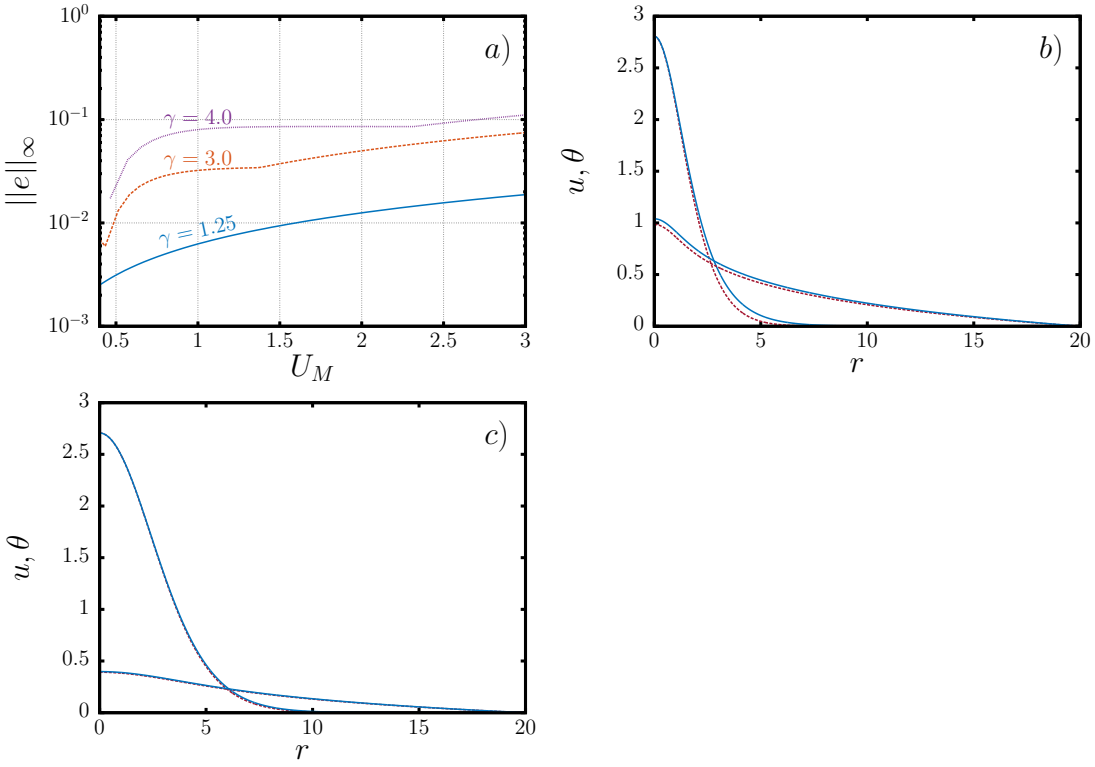

Figure 4.3: Error analysis and profile comparisons for generalized thermal optical solitary waves. a) Error as a function of amplitude b) Profile comparisons for a large amplitude solitary wave with $\gamma = 4.0$, blue (solid) is the numerical solution, red (dashed) is the analytic approximation, upper curves are the beam envelope u, lower curves are the reorientational response θ, c) Large amplitude profile for $\gamma = 1.25$.

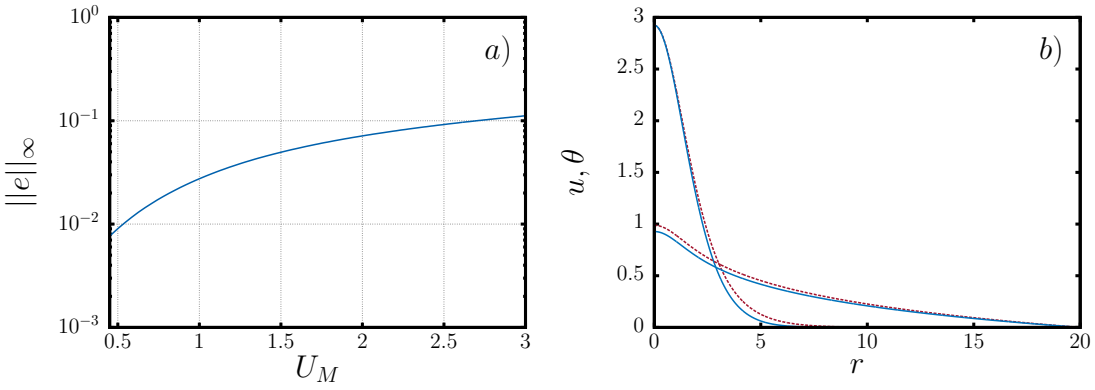

Figure 4.4: Error analysis and profile comparisons for optical solitary waves with a competing nonlinearity. a) Error as a function of amplitude b) Profile comparisons for a large amplitude solitary wave, blue (solid) is the numerical solution, red (dashed) is the analytic approximation, upper curves are the beam envelope u, lower curves are the reorientational response θ.

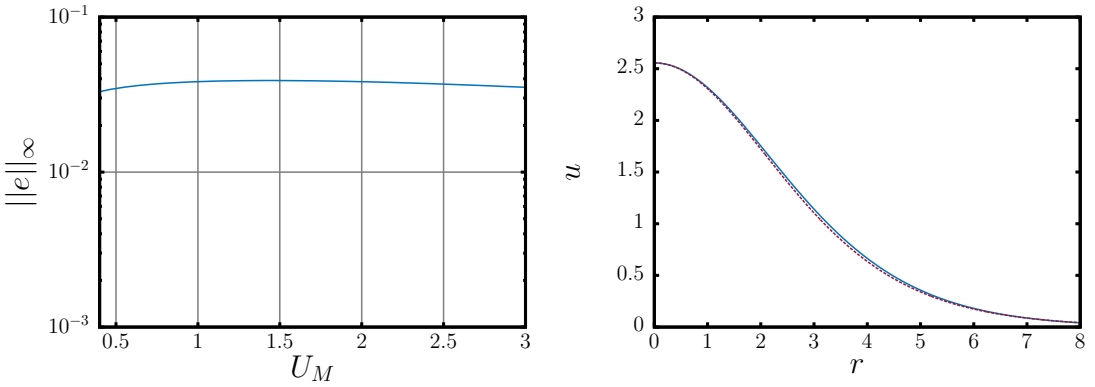

Figure 4.5: Error analysis and profile comparisons for (2+1) dimensional nematicons. a) Error as a function of amplitude. Blue (solid) is the solution error from (4.50) and (4.51). b) Profile comparisons for a large amplitude solitary wave. Blue (solid) is the numerical solution, red (long dashed) is the analytic full nematicon solution.

estimation gives a representative picture of errors that occur in the tails of the solitary waves, which is where the majority of our error occurs.

The error for the solutions of classical thermal media, equations (4.1) and (4.1) with $\kappa = 0$, is shown in Figure 4.2 (a) and comparisons with numerical profiles are given in Figure 4.2 (b) and Figure 4.2 (c) respectively. In general we observe excellent agreement, the solution only perceptibly detaching from the numerical solution in the tails, which is expected from our local argument. Furthermore, we find that the solution tends to break down at a value of roughly $r \sim \mathcal{O}\left(\varepsilon^{-1/4}\right)$, precisely the value predicted by the multiple scales analysis, albeit further out for smaller solitary waves.

For the generalized nonlinearity we still observe excellent agreement between the analytically derived solutions and numerical ones. These are shown in Figure 4.3. Of

particular note, we find that for smaller values of γ the approximate solutions are nearly indistinguishable from the numerical solutions up to graphical error. An example of this is seen in Figure 4.3 (c), where a taller solitary wave is shown with a γ value of 1.25. In general, we find higher amplitude solitary waves are indistinguishable from their numerical counterparts. As the value of γ increases, however, accuracy is lost. This loss of accuracy manifests itself in a larger, relatively speaking, mismatch in the tails of the solitary waves. An example of this is shown in Figure 4.3 b) where now $\gamma = 4.0$. While still an excellent result for an amplitude in the range of higher error, the analytic solution fails to capture the asymptotic behaviour of the solitary wave as it approaches the boundary. This, once again, could be expected from our analysis based on local arguments.

For the competing nonlinearities, we once again find excellent agreement for the strictly positive nonlinearity where $\alpha = 0.5,\ \gamma_1 = 2.0,\ \gamma = 4.0$. The results are shown in Figure 4.4. In general, we notice there is poorer matching with the tails for larger amplitude solutions, as in the generalized nonlinearity case. However, the results are still generally excellent.

The results for the (2+1) dimensional analytical solution for the nematicon are shown in Figure 4.5. In general, we find the best agreement of all cases thus far considered. The majority of the profiles are essentially indistinguishable from the numerical ones up to graphical accuracy. In addition to studying how well the full analytical solution performed for the nematicon case, that is, for the analytical approximation given by (4.50) and (4.51), it is equally interesting to study how well the analytical solution for the thermal solitary wave, given by (4.30), whose parameters can be expressed explicitly, performs in this case. Remarkably, the expression for the thermal solitary wave does exceptionally well. In a zoomed in plot comparing profiles, Figure 4.5 (b), it is difficult to distinguish between the full nematicon analytic solution, the thermal approximation and the numerical one. This indicates that, for $\kappa \sim \mathcal{O}(1)$ and $\varepsilon \ll 1$, the $\kappa\varepsilon^{\frac{1}{2}}\theta$ term in equation (**??**) is negligible in a local approximation. Fortunately, this can simplify nematicon approximations in the future and draws an important, but previously undiscovered, connection between the two systems.

4.5 Conclusion

We have analysed approximate solutions for a broad class of nonlinear, highly nonlocal solitary waves. A heuristic asymptotic method was developed which is capable of approximately solving, with excellent comparison to numerical solutions, for the solitary wave solution of a broad class of equations describing beam propagation in nonlocal nonlinear optical media, resolving an old problem. The idea can now be applied to other applications of nematicon equations, namely the Schrödinger-Newton equations in three dimensions [46], as well as other physically relevant optical systems. Of particular note is how well the explicit, thermal solitary wave solution compares with the nematicon solution, connecting intimately two previously separately treated systems.

Chapter 5

Diffraction Induced Instability of Coupled Dark Solitons

For our final study we turn our attention to the much less studied and understood defocussing solitary waves. Remarkably, for a coupled, defocussing nonlinear Schrödinger equation system, we have found that for a broad and reasonable set of conditions a steady state solitary wave *cannot* exist, being unstable in a non-trivial way to perturbations. As a word of background, dark solitary waves are those arising in defocussing media. There are only two essential differences mathematically from bright solitary waves. The first is the nonlinearity of the governing NLS equation is now negative. The second is that the solitary wave solutions approach non-zero constants at infinity. Physically, dark solitary waves are not as robust as their bright solitary wave counterparts and furthermore, technological applications are much less understood. Therefore, in general, most studies have been on bright solitary waves. However, dark solitary waves have unique challenges. In particular, as we show in this chapter, it is unlikely one can observe localized, coupled dark solitary waves. This is due to a novel form of a nonlinear instability which, to the authors knowledge, is reported and analyzed here for the first time.

Wave instabilities arising from nonlinear wave models are among the most intriguing of physical phenomena. In particular, the discovery of modulational instability (MI) by Benjamin and Fier [4, 111, 112] was a hallmark result in nonlinear wave theory. The governing equation in that work was the nonlinear Schrödinger (NLS) equation. This work demonstrated a remarkable instability mechanism that has no analog in linear systems. The NLS equation is a standard, ubiquitous equation in nonlinear wave theory

as it describes weakly nonlinear wave packets with a narrow spectrum arising in many physical phenomena, as discussed in Chapter 1 [4,10], including instabilities and solitary waves in nonlinear optics [4, 11], as well as fluid mechanics [4, 112] and biology [113]. In addition to systems governed by the NLS equation, MI and other instabilities have been discovered for a wide array of generally applicable integrable and non-integrable equations [4], including systems applicable to nonlocal, saturable, dissipative and higher order nonlinear optics [11, 19]. Collectively, the broad application of these integrable and non-integrable wave equations makes the study of their associated instabilities one of fundamental importance in optics, and in physics in general.

The focusing NLS equation

$$i\partial_z u + \frac{1}{2}\partial_x^2 u + |u|^2 u = 0 \tag{5.1}$$

models beam self-focusing and has bright soliton solutions, i.e. humps on a zero background. The defocusing NLS equation

$$i\partial_z u + \frac{1}{2}\partial_x^2 u - |u|^2 u = 0 \tag{5.2}$$

models beam self-defocusing and supports dark soliton solutions, i.e. dips (notches) in a non-zero background of constant amplitude, with a π phase change of u on axis [11, 114]. Several demonstrations of individual and coupled dark solitary waves have been reported in various media [115], including semiconductors [116], soft matter [26, 117, 118, 119] and photovoltaic photorefractive crystals [120, 121]. Here, we deal with vector solitary wave solutions of two coupled defocusing NLS equations, as, for example, governing the incoherent interaction of two dark optical beams in a generic nonlinear dielectric with a Kerr nonlinearity [11]. Previous work has shown that stable vector dark solitary wave solutions of such equations exist if the diffraction coefficients are equal [11, 12, 122]. Similarly, the only rigorous results for stability have been found for equal diffraction coefficients in the bright case [123]. However, substantive empirical, numerical evidence suggests for non-equal diffraction coefficients, the bright vector solitary waves are stable [50].

In the present work, we find a novel instability, driven by a difference in diffraction coefficients, of defocussing vector solitary waves. If the diffraction of the two components (dark beams) is different, for example for beams of different wavelengths [16] or

polarizations, the coupled vector solitary wave is unstable to radiation. One of the wavepackets collapses into radiation, leaving a single dark solitary wave in the other mode. We investigate this novel radiation induced instability using perturbation theory and numerical solutions.

This Chapter is based on the publication in reference [124]. Material original to this thesis is the exact asymptotic behaviour for dark and bright solitary waves in Section 5.2.1, as well as the power curve for the bright solitary wave in Section 5.2.1, appear here for the first time.

5.1 Governing Equations

We are going to consider a familiar setup. The co-propagation of two collimated, collinear beams in a Kerr medium with a self-defocusing optical response. This is an example still underneath the umbrella of nematic liquid crystals (and, more generally, nonlocal solitary waves), whose nonlinear response can be tailored to include local nonlinearities so that the nemaitcon equations (1.12) and (1.13) are indistinguishable from the nonlinear Schödinger equations. This is done by adjusting the cell configuration [125]. Each of the two dark modes consists of a notch on a constant background, with a zero electric field on axis, and the modes are based on beams of distinct wavelengths, so each beam has a different group velocity and experiences different diffraction. The coupled, defocusing NLS equations governing these two dark beams with coupled envelopes u and v are then

$$\begin{aligned} i\frac{\partial u}{\partial z} + \frac{D_u}{2}\frac{\partial^2 u}{\partial x^2} - \left(|u|^2 + |v|^2\right) u &= 0, \\ i\frac{\partial v}{\partial z} + \frac{D_v}{2}\frac{\partial^2 v}{\partial x^2} - \left(|u|^2 + |v|^2\right) v &= 0, \end{aligned} \tag{5.3}$$

with D_u and D_v the diffraction coefficients for modes u and v, respectively. Such equations arise in various areas of nonlinear optics in general [11] and nonlinear two colour beam propagation in, e.g., reorientational soft-matter [12, 16, 26] and photorefractive crystals [43, 120].

Crucially, in the scenario of $D_u = D_v$, herein called the "symmetric case", the equations are equal. In fact, the initial value problem is uniquely solvable using the inverse scattering transform as discovered by Manakov [126]. Thus this system is also called the "Manakov system". In this work, we consider initial conditions of the form

$v = C_1 u$. In the symmetric case then, we can consider, without loss of generality, the single NLS equation for u, as described in the Introduction. What this illustrates is that for no perturbations in the diffraction coefficients, solitons and instabilities of the coupled NLS equations can be reduced to the study of the NLS equation and so all the instability mechanisms for this equation apply. It is when the diffraction coefficients are *not* equal, which we call the *non-symmetric* case, that is $D_u \neq D_v$, that the instability arises.

5.2 Perturbative Analysis

To understand the evolution of the coupled dark solitary waves governed by the non-symmetric equations (5.3), we consider the limit of the diffraction coefficients differing by a small amount, so that $D_v = D_u + \epsilon$, where $|\epsilon| \ll D_u$. This case usefully demonstrates that the instability of the two coupled dark solitary waves is due to the rise of secular terms in a regular perturbation expansion. In general, we would like to show that the perturbation grows in z. However, from numerical experiments, we also have growth in x. We are able to combine both these perturbation and numerical approaches to show the novelty of this instability. We further confine our scope to dark solitons that have the same constant background level $U_0 = V_0$, which is of more physical interest as it corresponds to beams of equal power.

The steady dark soliton solutions in the modes u and v can then be expanded as

$$u = u_0 + \epsilon u_1 + \epsilon^2 u_2 + \ldots, \quad v = v_0 + \epsilon v_1 + \epsilon^2 v_2 + \ldots \tag{5.4}$$

At first order the dark soliton solution is [11]

$$u_0 = v_0 = U_0 \tanh(\gamma x)\ e^{-2iU_0^2 z}, \tag{5.5}$$

with $\gamma = \sqrt{2}U_0/\sqrt{D_u}$. At second order, $O(\epsilon)$, the corrections to this steady dark soliton are determined by

$$i\frac{\partial u_1}{\partial z} + \frac{D_u}{2}\frac{\partial^2 u_1}{\partial x^2} - |u_0|^2(3u_1 + v_1) - u_0^2(u_1^* + v_1^*) = 0, \tag{5.6}$$

$$i\frac{\partial v_1}{\partial z} + \frac{D_u}{2}\frac{\partial^2 v_1}{\partial x^2} - |u_0|^2(3v_1 + u_1) - u_0^2(u_1^* + v_1^*) = -\frac{1}{2}\frac{\partial^2 u_0}{\partial x^2}, \tag{5.7}$$

where the superscript * denotes the complex conjugate. Subtracting these equations

gives that the difference $\theta = u_1 - v_1$ is governed by the forced Schrödinger equation

$$i\frac{\partial\theta}{\partial z} + \frac{D_u}{2}\frac{\partial^2\theta}{\partial x^2} - 2|u_0|^2\theta = \frac{1}{2}\frac{\partial^2 u_0}{\partial x^2}. \tag{5.8}$$

This is a convenient equation to study as now all secular behaviour can be studied in the context of the Schrödinger equation with the Pöschl-Teller potential we encountered in the previous chapter. In particular, we can now see the first indication of secularity. The $\partial^2 u_0/\partial x^2$ forcing term of the Schrödinger equation (5.8) is secular in x as it is proportional to $\operatorname{sech}^2\gamma x \tanh\gamma x = \tanh\gamma x - \tanh^3\gamma x$, with $\tanh\gamma x$ being a solution of the homogeneous equation. However, it is not clear how the growth manifests for large x or even that it should. This has not been found for the bright case and is not clear why one the dark case exhibits growth and the bright case does not. The same question applies to secular growth in z. There is no obvious reason it should happen in the dark case and not the bright.

To answer these questions we proceed in two steps. First, we study the bounded stationary states, showing conclusively one does not exist for the dark equation (5.8). In fact, the exact stationary state θ_s can be found and is given by

$$\theta_s = \tanh(\gamma x)\ln(\operatorname{sech}^2(\gamma x)) \sim \tanh(\gamma x)\left\{\ln(4) - 2\gamma x - \ln\left(\frac{1}{(1+\exp(-2\gamma x))^2}\right)\right\} \tag{5.9}$$

where the asymptotic behaviour is for $x \to \infty$. This unbounded behaviour for large x does not occur in the bright case, agreeing with previous studies [50,52], but this is non-trivial to demonstrate. Furthermore, secularity is found in z in the form $||\theta||_{L^2(\mathbb{R})} \sim Cz^{\frac{3}{2}}$ which is explained in detail below. Numerical results show this growth in z does not occur for the bright solitary wave. The analysis is detailed in the following subsections.

5.2.1 Stationary Solutions

Dark Stationary Solutions

We begin by seeking solitary wave solutions as before. The ansatz for those whose intensity remains constant in z are of the form

$$\theta = \Theta(x)e^{-2iU_0^2 z}, \tag{5.10}$$

with Θ real. The forced Schrödinger equation (5.8) then becomes

$$\frac{D_u}{2}\Theta'' + 2U_0^2 \operatorname{sech}^2(\gamma x)\Theta = -\gamma^2 U_0 \operatorname{sech}^2(\gamma x)\tanh(\gamma x). \tag{5.11}$$

We can then find the general solution of this equation as follows. Using the change of variable $\Theta(x) = \tilde{\Theta}(y)$ for $y = \tanh(\gamma x)$, we arrive at the following equation (after dropping the tildes)

$$(1-y^2)\Theta''(y) - 2y\Theta' + 2\Theta = -\frac{2U_0}{D_u}y. \tag{5.12}$$

This is a forced Legendre's equation. In particular, solvability for the boundary value problem with $\Theta(-1) = \Theta(1) = 0$, i.e. $\theta \to 0$ as $x \to \pm\infty$ clearly fails. To see this we write the equation as $\mathcal{L}\Theta = f$ on $y \in [-1, 1]$. Note that the y interval is the result of taking $|x| \to \infty$. Thus the boundary conditions are imposed as a limit. This is done in the setting of the Hilbert space $\mathcal{H} = L^2([-1, 1])$ with the standard inner product $< f, g >= \int_{-1}^{1} f\bar{g}dx$. As $\mathcal{L}$ is self-adjoint, multiplying (5.12) by an arbitrary homogeneous solution Θ_h and integrating over the interval we find the requirement

$$< f, \Theta_h >= 0, \tag{5.13}$$

which plainly fails for $\Theta_h = y$. Solving explicitly we have [127]

$$\Theta = c_1 y + c_2\left(-1 + \frac{y}{2}\ln\left(\frac{1+y}{1-y}\right)\right) + \frac{U_0 y}{3D_u}\left(\ln\left((1-y)(1+y)\right)\right). \tag{5.14}$$

In the original variables, after taking $c_1 = c_2 = 0$ and so studying the particular solution, this reduces to the remarkably compact expression

$$\theta = u_1 - v_1 = \frac{U_0 \tanh(\gamma x)}{3D_u}\ln\left(\operatorname{sech}^2(\gamma x)\right)e^{-2iU_0^2 z}. \tag{5.15}$$

Using the definition of $\operatorname{sech}(x)$ we can find the asymptotic behaviour as $x \to \infty$ of this particular solution as

$$\begin{aligned}\Theta =& \frac{U_0 \tanh(\gamma x)}{3D_u}\ln\left(\frac{4e^{-2\gamma x}}{(1+e^{-\gamma x})^2}\right) \\ =& \frac{U_0 \tanh(\gamma x)}{3D_u}\left[\ln(4) - 2\gamma x - \ln\left(\frac{1}{(1+e^{-\gamma x})^2}\right)\right].\end{aligned} \tag{5.16}$$

Higher order terms can then be computed using the Taylor series for small ξ

$$\frac{1}{(1+\xi)^2} = \sum_{n=0}^{\infty}(-1)^n(n+1)\xi^n, \tag{5.17}$$

and

$$\ln(1+\xi) = \sum_{n=0}^{\infty}(-1)^{n+1}\frac{\xi^n}{n}, \tag{5.18}$$

applied to the final logarithmic term for x sufficiently large. The perturbation expansion then breaks down at $O(\varepsilon)$ and there are no localized vector dark solitary waves of the coupled defocusing NLS equations (5.3).

Bright Solitary Wave Solutions

In contrast to the dark solitary wave case, this spatial resonance does not appear in the bright solitary wave case, that is, with a positive sign in the nonlinearity of the system (5.3). In this case, the corresponding equation for Θ_b for bright solitary waves $u_0 = v_0 = a\,\mathrm{sech}\,\tilde{\gamma}x\, e^{ia^2z}$ (subscript "b" for "bright"), which is defined by its relation to the next order correction, θ, by

$$\theta = u_1 - v_1 = \Theta_b e^{ia^2z/2}, \tag{5.19}$$

is given by

$$\frac{D_u}{2}\Theta_b'' + a^2\left(2\,\mathrm{sech}^2\,\tilde{\gamma}x - 1\right)\Theta_b = \frac{a\tilde{\gamma}^2}{2}\left(\mathrm{sech}\,\tilde{\gamma}x - 2\,\mathrm{sech}^3\,\tilde{\gamma}x\right), \tag{5.20}$$

with $\tilde{\gamma} = \sqrt{2}a/\sqrt{D_u}$. It appears there is still a resonant forcing term $\mathrm{sech}\,\tilde{\gamma}x$ and yet an instability of this type has not been reported for bright solitary waves. In contrast to the previous analysis for dark solitary waves we no longer have an explicit solution available for Θ_b. In particular, a simple expansion in terms of $\exp(-\tilde{\gamma}x)$ for large x does not appear to show the resonance as this does not recover the previous growing behaviour of the dark solitary wave case. This is essentially due to the fact that the leading order behaviour of the RHS in (5.20) in terms of $\exp(-\tilde{\gamma}x)$ for large x is no longer a homogeneous solution, so that the resonance is lost. An alternative approach is needed.

We begin by re-scaling. Changing variables by taking $\Theta_b = \tilde{\Theta}_b(X)$, where $X = \tilde{\gamma}x$,

we obtain after dropping the tildes

$$\Theta_b'' + (2\,\mathrm{sech}^2(X) - 1)\Theta_b = \frac{a}{D_u}\left(\mathrm{sech}(X) - 2\,\mathrm{sech}^3(X)\right). \tag{5.21}$$

We now base our analysis on the previous asymptotic form of the leading order dark solution. Notice that to leading order in X, the dark behaviour is $X\tanh(X)$, or a homogeneous solution multiplied by X. One possible avenue is using a similar ansatz $X\,\mathrm{sech}(X)$ for (5.21) and see how close this is to the exact solution Θ_b. As it turns out, this is possible using classical theory for integral equations [128]. In particular, we study the rate that the difference

$$|\Theta_b^c| = |\Theta_b - \Theta_b^a|, \tag{5.22}$$

approaches zero. Here we have decomposed the exact solution, denoted Θ_b, into our approximation

$$\Theta_b^a = \alpha X\,\mathrm{sech}(X), \tag{5.23}$$

where α is to be determined, and the remaining correction, denoted by Θ_b^c. In particular, we find $|\Theta_b^c|$ approaches zero rapidly for an ansatz of the form (5.23) and the rate can be given explicitly. Furthermore, and crucially, this reproduces the previous behaviour of X multiplied by a homogeneous solution from the dark case.

To show that Θ_b^c is small for large X, we proceed in the following steps.

1. Determine α by minimizing the residual for large X.
2. Derive an integral equation for Θ_b^c.
3. Solve the integral equation for Θ_b^{c+}, the restriction of Θ_b^c, to the domain $x \in (R, \infty)$.
4. Determine leading order asymptotic behaviour of Θ_b^{c+}.

Note this is equivalent to determining the leading order behaviour for large X provided we choose R sufficiently large. In general, the analysis relies on a proof similar to Banach's fixed point theorem. We therefore skip preliminaries.

We begin by determining α. Writing equation (5.21) in the more compact notation

$$\mathcal{L}_b\Theta_b = f_b, \tag{5.24}$$

where

$$\mathcal{L}_b = \frac{d^2}{dx^2} + (2\,\mathrm{sech}^2(X) - 1), \quad f_b = \frac{a}{D_u}\left(\mathrm{sech}(X) - 2\,\mathrm{sech}^3(X)\right). \tag{5.25}$$

We define the residual of the approximation Θ_b^a as

$$\mathcal{R}_{\Theta_b^a} = f_b - \mathcal{L}_b\Theta_b. \tag{5.26}$$

After substituting $\Theta_b = \Theta_b^a + \Theta_b^c = \alpha X\,\mathrm{sech}(X) + \Theta_b^c$, we see that Θ_b^c satisfies

$$\mathcal{L}_b\Theta_b^c = \mathcal{R}_{\Theta_b^a}. \tag{5.27}$$

The explicit expression for $\mathcal{R}_{\Theta_b^a}$ is

$$\begin{aligned}\mathcal{R}_{\Theta_b^a} &= f_b - \mathcal{L}_b\Theta_b^a \\ &= \frac{a}{D_u}\left(\mathrm{sech}(X) - 2\,\mathrm{sech}^3(X)\right) + 2\alpha\,\mathrm{sech}(X)\tanh(X).\end{aligned} \tag{5.28}$$

Choosing

$$\alpha = -\frac{a}{2D_u} \tag{5.29}$$

minimizes the residual $\mathcal{R}_{\Theta_b^a}$ as $X \to \infty$, and thus we have our particular, asymptotic solution. What remains is to determine the amplitude of $|\Theta_b^c|$ as $X \to \infty$. To do this we use the integral form of (5.27) in operator notation

$$\Theta_b^c + \mathcal{K}\Theta_b^c = \tilde{\mathcal{R}}_{\Theta_b^a}. \tag{5.30}$$

Here $\mathcal{K}$ is the linear operator defined by

$$\mathcal{K}\phi = \int_{-\infty}^{\infty} \exp(-|X - X'|)\,\mathrm{sech}^2(X)\phi(X')dX' \tag{5.31}$$

and $\tilde{\mathcal{R}}_{\Theta_b^a}$ is the modified RHS of (5.27) given by

$$\tilde{\mathcal{R}}_{\Theta_b^a} = \frac{1}{2}\int_{-\infty}^{\infty} \exp(-|X - X'|)\mathcal{R}_{\Theta_b^a}(X')dX' \tag{5.32}$$

for $\mathcal{R}_{\Theta_b^a}$ as above. Furthermore, we decompose the solution Θ_b^c into a partition

$$\Theta_b^{c-} = \Theta_b^c \text{ for } x \in (-\infty, -R), \tag{5.33}$$

$$\Theta_b^{cM} = \Theta_b^c \text{ for } x \in [-R, R], \tag{5.34}$$

$$\Theta_b^{c+} = \Theta_b^c \text{ for } x \in (R, \infty). \tag{5.35}$$

To avoid confusion, we use the variable y as the restriction of x to (R, ∞). Restricting ourselves to solving for Θ_b^+ as the analysis for Θ_b^- is identical by symmetry, we now study the modified integral equation

$$\Theta_b^+ + \int_y^\infty \exp(-|y-y'|)\operatorname{sech}^2(y')\Theta_b^+(y')dy' = \frac{1}{2}\int_y^\infty \exp(-|y-y'|)\mathcal{R}_{\Theta_b^a}(y')dy'. \tag{5.36}$$

Rewritten in operator notation, this is

$$\Theta_b^+ + \mathcal{K}^+\Theta_b^+ = \tilde{\mathcal{R}}^+_{\Theta_b^a}. \tag{5.37}$$

Then, provided we choose R large enough such that $\mathcal{K}^+$ is a contraction, that is $||\mathcal{K}^+|| < 1$, we can write the explicit Neumann series for the solution Θ_b^+ [128]. Note this is also precisely the perturbation method known as the "Born series" in quantum and classical scattering theory [129]. As the kernel of $\mathcal{K}^+$ is continuous, it follows as a standard result that $\mathcal{K}$ is a compact operator on the Banach space of the set of continuous functions on the line $\mathfrak{B} = C(\mathbb{R})$ endowed with the standard supremum norm [128] denoted by

$$||f||_\infty = \sup_{x\in\mathbb{R}} |f(x)|. \tag{5.38}$$

In this setting the operator norm is given by

$$||\mathcal{K}^+|| = \sup_{||\phi||_\infty=1} ||\mathcal{K}^+\phi||_\infty, \tag{5.39}$$

which we can show is a contraction using simple inequalities. Taking $|\mathcal{K}^+\phi|$ we obtain

$$\begin{aligned}|\mathcal{K}^+\phi| &\leq \int_y^\infty |\exp(-|y-y'|)\operatorname{sech}^2(y')\phi(y')|dy' \\ &\leq \int_y^\infty \operatorname{sech}^2(y')dy'||\phi||_\infty \\ &= (1-\tanh(y))||\phi||_\infty \\ &\leq (1-\tanh(R))||\phi||_\infty. \end{aligned} \tag{5.40}$$

Choosing R such that $(1-\tanh(R)) < 1$, which gives just $R > 0$, and taking the supremum over $\phi \in \mathfrak{B}$ such that $||\phi||_\infty = 1$, we have

$$||\mathcal{K}^+|| < 1. \tag{5.41}$$

Accordingly, the explicit solution of (5.36) is given by [128]

$$\Theta_b^{c+} = \sum_{n=0}^{\infty}(-1)^n(\mathcal{K}^+)^n(\tilde{\mathcal{R}}^+_{\Theta_b^a}), \tag{5.42}$$

where the iterated operator $(\mathcal{K}^+)^n$ is given by

$$(\mathcal{K}^+)^n(\phi) = \int_y^\infty \dots \int_{y_n}^\infty \exp\left(-\sum_{m=0}^{n}|y_m - y'_m|\right)\operatorname{sech}^2(y')\dots\operatorname{sech}^2(y'_n)\phi(y'_n)dy'_n\dots dy'. \tag{5.43}$$

Note, the same result arises from using Banach's fixed point theorem. We can now summarize with asymptotic behaviour of the solution Θ_b^+. In particular, we have the following estimate

$$|(\mathcal{K}^+)^n(\tilde{\mathcal{R}}^+_{\Theta_b^a})| \leq (1-\tanh(R))^n||\tilde{\mathcal{R}}^+_{\Theta_b^a}||_\infty. \tag{5.44}$$

This implies that, upon using the definition $\Theta_b^+ - \Theta_b^{a+} = \Theta_b^{c+}$,

$$\begin{aligned}
|\Theta_b^+ - \Theta_b^{a+}| &\leq \sum_{n=0}^{\infty} |(\mathcal{K}^+)^n(\tilde{\mathcal{R}}^+_{\Theta_b^a})| \\
&\leq \sum_{n=0}^{\infty} (1-\tanh(R))^n ||\tilde{\mathcal{R}}^+_{\Theta_b^a}||_\infty \\
&= \frac{||\tilde{\mathcal{R}}^+_{\Theta_b^a}||_\infty}{1-(1-\tanh(R))} \\
&\leq \frac{\frac{a}{D_u}(1-\tanh(R))\,\mathrm{sech}(R)}{1-(1-\tanh(R))},
\end{aligned} \tag{5.45}$$

where we have used the estimate $||\tilde{\mathcal{R}}^+_{\Theta_b^a}||_\infty \leq \frac{a}{D_u}(1-\tanh(R))\,\mathrm{sech}(R)$. This is derived as follows

$$\begin{aligned}
|\tilde{\mathcal{R}}^+_{\Theta_b^a}| &= \frac{1}{2}\Big| \int_y^\infty \exp(-|y-y'|)\mathcal{R}_{\Theta_b^a}(y')dy'\Big|, \\
&\leq \frac{1}{2}\int_y^\infty |\mathcal{R}_{\Theta_b^a}(y')|dy', \\
&= \frac{a}{2D_u}\int_y^\infty |(1-\tanh(y'))\,\mathrm{sech}(y') - 2\,\mathrm{sech}^3(y')|dy', \\
&= \frac{a}{2D_u}(1-\tanh(y))\,\mathrm{sech}(y), \\
&\leq \frac{a}{2D_u}(1-\tanh(R))\,\mathrm{sech}(R).
\end{aligned} \tag{5.46}$$

Note that this usefully proves a couple of points. First, as hoped, there is no secular growth in X for the bright solitary wave case. This is something we would expect as there is no report, to the author's knowledge, of an instability of this type in any other solitary wave system, particularly those governed by focussing nonlinear Schrödinger equations. Second, and nicely, our choice of ansatz becomes exponentially accurate for large R, as for the dark case. Having established the asymptotic behaviour for large X, we now turn our attention to the growth in z.

5.2.2 z-dependent behaviour

The asymptotic results in terms of growth in z are, in general, more challenging than for the asymptotic behaviour for large x and so general behaviour from numerical solutions of the next order correction is required. In particular, we observe numerically a growth in the power of the solution for θ satisfying the first order dark perturbation equation

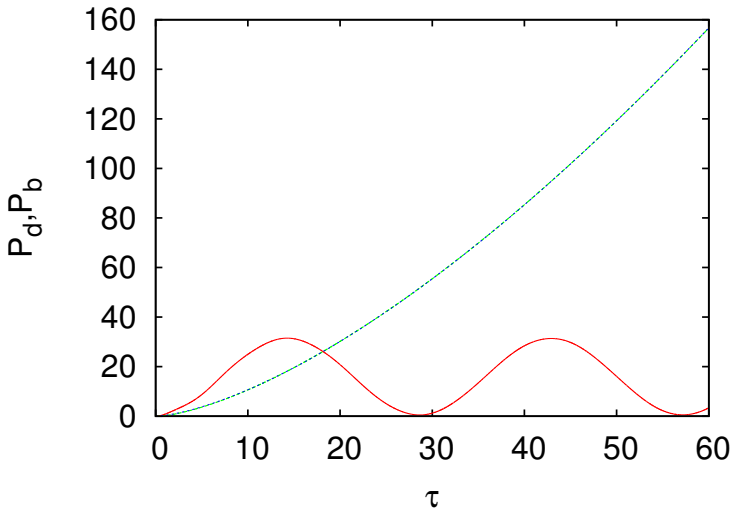

Figure 5.1: Power P of the difference $\tilde{\theta} = u(\tilde{x}, \tau) - v(\tilde{x}, \tau)$ in both the bright and the dark case. $\tilde{\theta} = 0$ at $z = 0$ in both cases. Red (solid) line: numerically calculated power for the bright case (denoted P_b); blue (dashed) line: numerically calculated power for the bright case (denoted P_d); green (dotted) line: fitted dark power curve $f(\tau) = 0.366\tau^{\frac{3}{2}}$. Note, the dark power curve and its fit coincide.

(5.8), governed by

$$i\frac{\partial\theta}{\partial z} + \frac{D_u}{2}\frac{\partial^2\theta}{\partial x^2} + 2U_0^2\,\mathrm{sech}^2(\gamma x)\theta = -\gamma^2\,\mathrm{sech}^2(\gamma x)\tanh(\gamma x), \tag{5.47}$$

and not in the case of the bright solitary wave correction, governed by

$$i\frac{\partial\theta_b}{\partial z} + \frac{D_u}{2}\frac{\partial^2\theta_b}{\partial x^2} + a^2(2\,\mathrm{sech}^2(\tilde{\gamma}x) - 1)\theta_b = \frac{a\tilde{\gamma}^2}{D_u}\left(\mathrm{sech}(\tilde{\gamma}x) - 2\,\mathrm{sech}^3(\tilde{\gamma}x)\right). \tag{5.48}$$

We recall that θ is the difference between the two corrections $\theta = u_1 - v_1$ for both the bright and dark case. In the dark case, this can be argued using dispersive estimates for linear Schrödinger operators with a decaying potential [130]. Such a result is not available in the bright case.

Computational Study

We study secular growth using full numerical simulation of equation (5.8). These numerical solutions also show that the asymptotic result for the non-existence of coupled dark solitary waves carries over to a finite difference in diffraction coefficients. In addition, they show in detail the dynamic collapse of the coupled state. The forced Schrödinger equation (5.8) was solved numerically using a 4th-order Runge-Kutta

scheme (RK4) (see Chapter 2) in the normalized unit $\tau = U_0^2 z$ and centered finite differences in $\tilde{x} = \gamma x$, with $\theta(x, z) = \tilde{\theta}(\tilde{x}, \tau)$. The domain was taken to be large ($L \sim 1000$) and artificial homogeneous Neumann conditions were applied at the boundaries. Fig. 5.1 illustrates clear, substantial growth in the power P of $\tilde{\theta}$, defined as the integral of $|\tilde{\theta}|^2$ (obtained numerically), demonstrating secular growth is not solely confined to the spatial dimension, but occurs for the evolution variable as well. These numerical results were fitted with the curve $f(\tau) = 0.366\tau^{\frac{3}{2}}$. This power growth can be obtained from an asymptotic analysis of (5.8) for large z. Using Duhamel's principle [131] we can write

$$\theta = i \int_0^z \Phi(\tilde{x}, \tilde{s}) d\tilde{s}\, e^{-2iU_0^2 z}, \tag{5.49}$$

provided Φ satisfies the initial value problem

$$i\frac{\partial \Phi}{\partial \tilde{z}} + \frac{\partial^2 \Phi}{\partial \tilde{x}^2} + 2\,\mathrm{sech}^2\,\tilde{x}\,\Phi = 0,\ \Phi(x, 0) = \gamma^2\,\mathrm{sech}^2\,\tilde{x}\tanh\tilde{x}. \tag{5.50}$$

For the above initial value problem we have the dispersive estimate [130]

$$||\Phi||_{L^\infty(\mathbb{R})} \leq Cz^{-1/2}, \tag{5.51}$$

where the constant C can be sharp and therefore for z large enough,

$$||\Phi||_{L^\infty(\mathbb{R})} \sim Cz^{-1/2} \tag{5.52}$$

Note, crucially, this estimate applies because the potential for Φ, $\mathrm{sech}^2(X)$, decays at infinity and has a constant C such that $\mathrm{sech}(X)^2 \leq C(1 + X^2)^{-1}$. Furthermore, the projection of the initial condition, $\gamma^2\,\mathrm{sech}^2\,\tilde{x}\tanh\tilde{x}$, onto the discrete spectrum, in this case just $\mathrm{sech}(\tilde{x})$, is zero and thus the estimate holds as the only remaining solution is the projection onto the continuous spectrum [132]. This does not apply in the bright case, for which the potential is not bounded and the projection of the initial condition onto the discrete spectrum is non-zero. Furthermore, it can be shown that (5.8) has a similarity solution of the form $f(x/\sqrt{z})e^{-2iU_0^2 z}$. Thus the solution is widening at a rate proportional to $\sqrt{z}$. Heuristically then, taking the power to be approximately the width of the solution multiplied by the square of the amplitude, we arrive at

$$\int_{-\infty}^{\infty} |\theta|^2 dx \sim \tilde{C} z^{\frac{3}{2}}, \tag{5.53}$$

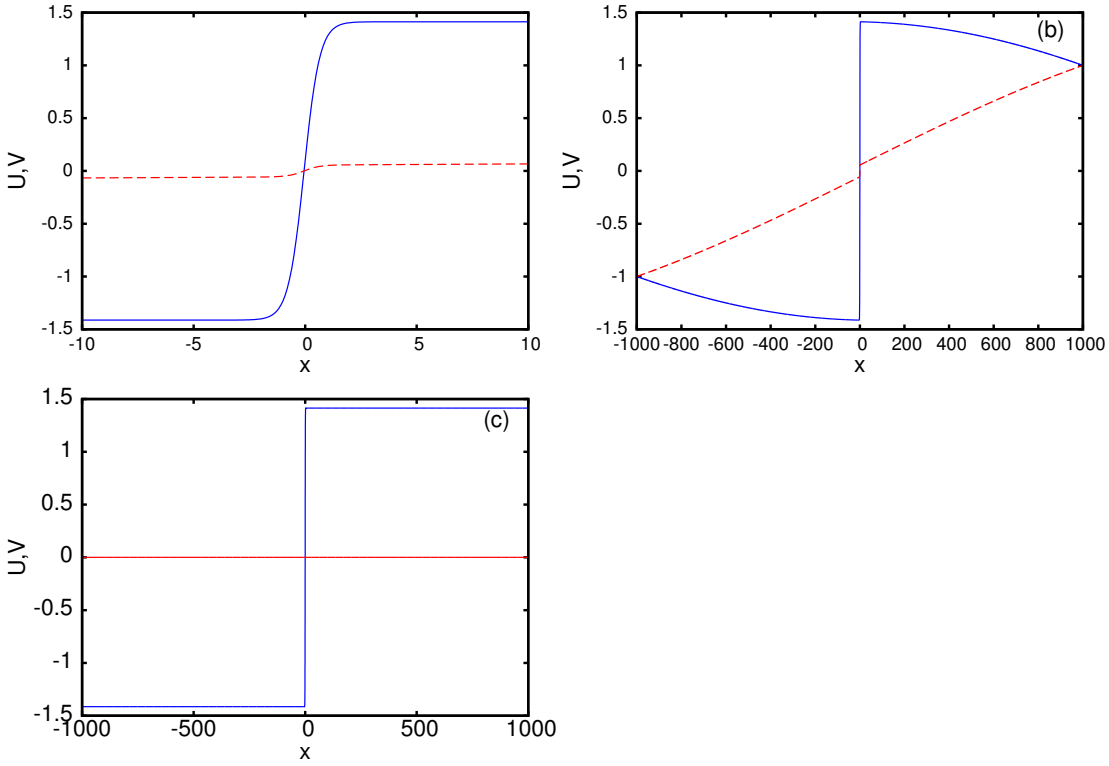

Figure 5.2: Numerically computed coupled dark solitary waves. a) and b) show results for artificial Dirichlet conditions, c) shows the result for artificial Neumann conditions. u mode: blue (solid) line; v mode: red (dotted) line. The diffraction parameters are $D_u = 1.0$ and $D_v = 1.02$. a) Local view, b) expanded view.

giving the secular growth in z as desired.

5.3 Full Numerical Solutions

The lack of a steady, coupled, localized state was confirmed by full numerical solutions. We first integrated the governing equations (5.3) using the same RK4 z-stepping and centered differences for the x derivatives as used in numerically integrating (5.8). The domain was taken very large ($L \sim 2000$) to avoid boundary effects such as radiation reflection. In each simulation, the quantities $u\exp(-i(U_0^2 + V_0^2)z)$ and $v\exp(-i(U_0^2 + V_0^2)z)$ were found to be purely real for arbitrary stopping "times" z. We therefore sought numerical solutions for steady coupled solitary waves $u = U(x)e^{-i\sigma z}$ and $v = V(x)e^{-i\sigma z}$, so that

$$\begin{aligned} \frac{D_u}{2}\frac{\partial^2 U}{\partial x^2} + \sigma U - \left(U^2 + V^2\right) U &= 0, \\ \frac{D_v}{2}\frac{\partial^2 V}{\partial x^2} + \sigma V - \left(U^2 + V^2\right) V &= 0 \end{aligned} \tag{5.54}$$

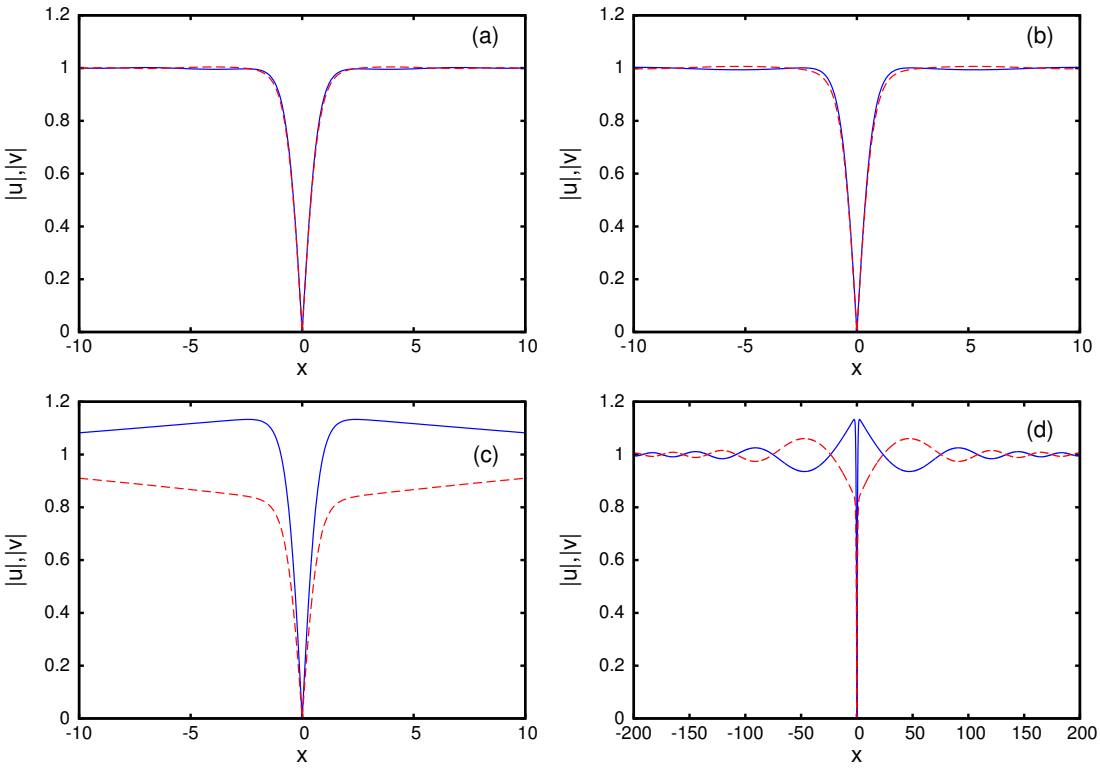

Figure 5.3: Evolution of the instability for a small difference in the diffraction coefficients. u beam: blue (solid) line; v beam: red (dotted) line. (a) Profiles at $z = 3$, (b) profiles at $z = 10$, (c) solution around $x = 0$ at $z = 700$, (d) expanded solution at $z = 700$. $U_0 = V_0 = 1$ and the diffraction parameters are $D_u = 1.0$ and $D_v = 1.02$.

for real U and V. The system (5.54) was solved using a Newton iteration scheme (see Chapter 2 and [69] for details) with the exact solution for $D_u = D_v$ as an initial guess and continuing, without loss of generality, the D_v parameter so that it became larger than D_u. Both fixed boundary conditions, so that $U(L) = U_0$ and $U(-L) = -U_0$ and similarly for V with $\sigma = U_0^2 + V_0^2$, and zero flux boundary conditions, so that $\partial_x U(\pm L) = \partial_x V(\pm L) = 0$, were applied to determine whether the choice of boundary condition made any difference to the stability. A representative example for solutions found with the fixed boundary conditions is shown in Fig. 5.2. Fig. 5.2(a) shows that locally, around $x = 0$, the v dark beam is the trivial solution, while the u mode corresponds to the exact solitary wave with $\sigma = \sqrt{2}U_0$. Fig. 5.2(b) shows that, away from $x = 0$, the dark modes approach the original background levels. This is due to the fixed boundary conditions at $x = \pm L$. This figure clearly shows qualitatively that the difference $U - V$ matches the linear growth behaviour predicted by the asymptotic result (5.16) and is a behaviour found in full numerical simulations, discussed later. In the case of zero flux boundary conditions, the scheme converged to the steady state corresponding to the exact dark NLS soliton solution with $v = 0$ and $\sigma = \sqrt{2}U_0$, as shown in Fig. 5.2 (c), in agreement with the fixed boundary condition result. These numerical results indicate that a stable localized steady state consists solely of a single mode, as opposed to the coupled modes found in the focussing NLS case.

Full numerical solutions of equations (5.3) confirm the results found from the study of the steady states. Figure 5.3 illustrates full numerical solutions of the coupled defocusing NLS equations (5.3) for a small difference in diffraction coefficients, $D_u = 1.0$ and $D_v = 1.02$, as for the perturbation solution discussed previously. The initial conditions used were

$$u = v = U_0 \tanh(\gamma x), \tag{5.55}$$

with $\gamma = \sqrt{2}U_0/\sqrt{D_u}$. Clearly the u beam is settling down to a local dark solitary wave, while the v beam is spreading out and decaying in a way that approaches, locally, the steady solutions found with the fixed boundary conditions. This instability is driven by the difference in the diffraction coefficients and occurs via a non-standard process. The larger diffraction D_v of the v mode makes it initially diffract more than the u dark beam. Such widening of the v notch relative to the u mode causes the u dark beam to deform, which reinforces the widening of v. The latter is accompanied by the shedding of diffractive radiation of growing amplitude, with the v mode progressively decaying

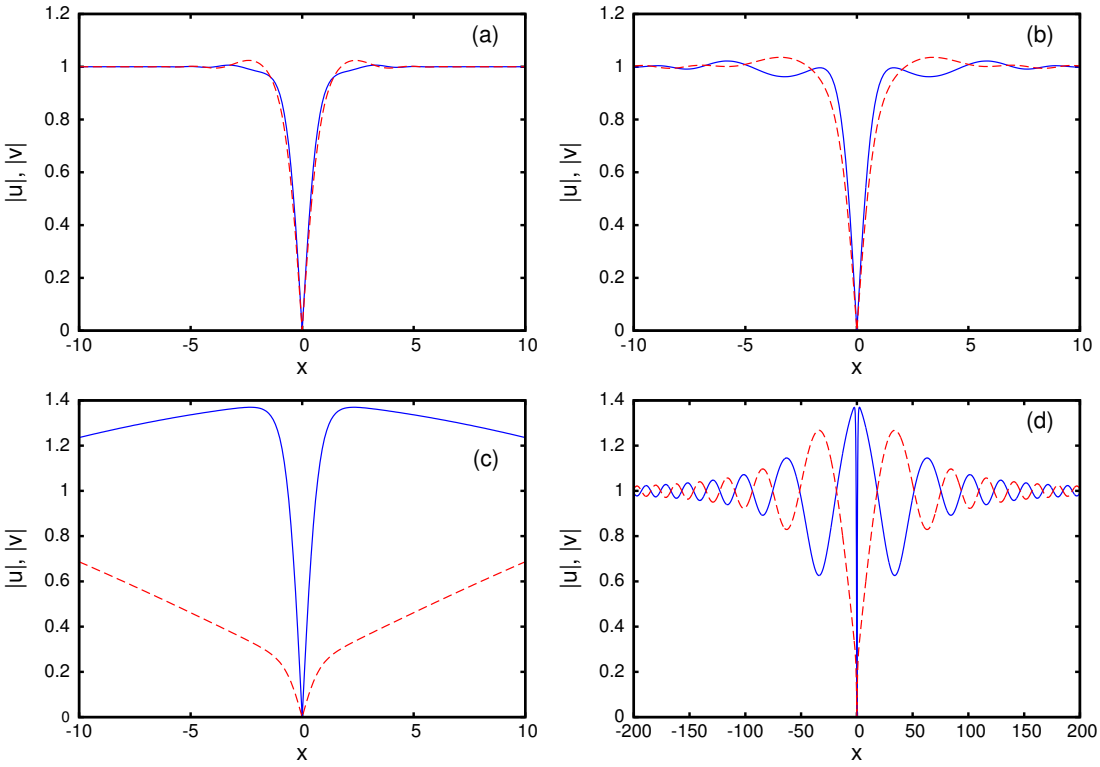

Figure 5.4: Evolution of the instability for a larger difference in the diffraction coefficients. u beam: blue (solid) line; v beam: red (dotted) line. (a) Profiles at $z = 1$, (b) profiles at $z = 3$, (c) solution around $x = 0$ at $z = 500$, (d) expanded solution at $z = 500$. $U_0 = V_0 = 1$ and the diffraction constants are $D_u = 1.0$ and $D_v = 1.25$.

to zero, as shown in Fig. 5.3(c) in the vicinity of $x = 0$ and in Fig. 5.3(d) over a larger region around $x = 0$ in order to emphasise the shed diffractive radiation. The decay of v to 0 is accompanied by the growth of shed radiation as both the u and v modes individually conserve power, i.e. "mass" in the sense of invariances of the Lagrangian of the coupled system (5.3); the power

$$P_u = \int_{-\infty}^{\infty} \left(|U_0|^2 - |u|^2 \right) \, dx \tag{5.56}$$

of the u mode and the power

$$P_v = \int_{-\infty}^{\infty} \left(|V_0|^2 - |v|^2 \right) \, dx \tag{5.57}$$

of the v mode are individually conserved. To conserve P_v, however, the v mode can only decay by shedding radiation rising above $v = V_0$ and so balance the decay to 0 in a region expanding from $x = 0$. Therefore, the released diffractive radiation increases in amplitude. Fig. 5.3(c) shows that, locally, the v-component decay is accompanied by the u mode evolving to the new background level $\sqrt{2}U_0$ predicted by the numerical steady state results.

This instability mechanism of two coupled dark solitary waves is considerably more pronounced with an increased difference in the diffraction coefficients of the two modes, as illustrated in Fig. 5.4, for which $D_u = 1.0$ and $D_v = 1.25$. The instability now evolves on a shorter z scale, as expected. Again, Fig. 5.4(c) shows that the v dark beam decays and that the u mode moves to the new background $\sqrt{2}U_0$. This further confirms the lack of a stable localized coupled steady state, the main conclusion of the present work.

5.4 Conclusions

We studied two coupled defocusing NLS equations describing two incoherent dark beams propagating collinearly in a Kerr medium. We found that this system does not possess a stable coupled (vector) solitary wave solution if the two dark components undergo different diffraction, as one mode sheds radiation and progressively decays, while the other settles to a dark soliton. This behaviour is due to a resonant instability induced by the difference in diffraction coefficients. Numerical solutions fully confirm this unstable evolution for arbitrary differences in the diffraction coefficients.

Chapter 6

Conclusions

In this thesis we have studied solitary waves in focussing and defocussing nonlinear, nonlocal optical media. A summary of the research for each chapter, the key contributions and the open questions these raise are given in the following sections.

6.1 Conclusions: Chapter 3

In Chapter 3 we studied exact solitary wave (nematicon) solutions and variational approximations of the nematicon equations. Notably, we constructed the first known explicit solitary wave solution for the model, which arises for a set of parameter values for which the electric field and director equations are identical. This constructive approach is novel as an independent discovery of an equivalent solution was made via trial and error substitution in the case of χ^2 optical media. One consequence of this direct construction is the discovery of previously unknown connections between nematicons and other famous non-integrable equations, which are Fisher's equation from mathematical biology, the Lane-Emden equation from astrophysics and the Schrödinger-Newton equation from quantum gravity. Furthermore, we found solutions in both (1+1) and (2+1) dimensions although the (2+1) dimensional solution relied heavily on a complicated solution of Abel's equation of the first kind. As the exact solutions were restricted to a particular parameter set, we studied more general variational approximations in (1+1) and (2+1) dimensions. Generally it was found that the profiles closest to the NLS type solitary wave and the exact solution profiles were more accurate (compared with numerical solutions) than a Gaussian ansatz, which is more commonly used in optics due to its ease of use, connection with the Snyder-Mitchell approximation, and the fact

lasers give beams with profiles close to a Gaussian. This contributed a much needed, thorough comparison study to the community, as well as the previously undiscovered explicit solution which can now be used as a benchmark.

One feature of the variational method is the prediction of the existence of a power threshold, which was also predicted in the existence proof of Panayotaros [33]. This lead to a subtle question as to how to verify the accuracy approximate solutions as there is a subtle difference between finite domain and infinite domain solitary wave solutions. In particular, it was found in reference [33] that while a power threshold exists for the nematicon equations posed in the infinite domain, one does not exist for the truncated problem on a disk with homogeneous Dirichlet boundary conditions. Indeed, there are non-trivial solutions of arbitrarily small amplitude in the finite, homogeneous Dirichlet case,and not for the infinite domain. This poses a very rich question for solitary waves in nonlocal media in general. As power thresholds are observed in experiment, it suggests the nematicon model is *only* valid if posed on an infinite domain and yet *experimental domains are necessarily finite*. Furthermore, it is an open question on how to *compute* this power threshold. In particular, we observed the beginnings of a bifurcation for lower power solutions with homogeneous Dirichlet boundary conditions. It is not clear if this is an indication of a threshold or not, but suggests a thorough computational study should be undertaken, examining the effects of multiple different boundary conditions (periodic, Robin, Neumann etc.) using numerical continuation techniques and, potentially, the development of novel numerical methods. A similar study should be done for the full nematicon equations to validate the existence of this threshold as a test of the model's validity.

The final finding of the work was the discovery of a novel form of bistability. This was determined numerically by studying the effect of linearizing the pre-tilted nematicon equations to the nematicon equations. This illustrated the suspicion that there are physical phenomena that are lost when studying the linearized nematicon equations. In particular, it seems to broaden our interpretation of bistability as the stable solutions appear restricted to just the director solutions, begging the question of whether or not there is a technological application for this discovery. It also brought into question the notion of "strong nonlocality", which should be discussed at length within the community. Furthermore, it leaves open the critical fundamental question of bistability, which has a direct engineering application as being the theoretical underpinning of an all-optical circuit transistor [81]. This leads to a natural question of whether or

not bistability exists for the full nematicon equations. Work regarding this question is currently underway with promising results.

6.2 Conclusions: Chapter 4

In the fourth Chapter, we described a general and universal method for approximating solitary waves in nonlinear, nonlocal focussing media. The inspiration for such a method was drawn from the Snyder-Mitchell work [59], which stresses the possibility of theoretically accessible solitary waves in a physically realizable system. Our approach adheres to this philosophy, but is considerably more successful. It is the first of its kind in terms of its range of applicability, accuracy, ease of implementation and asymptotic arguments. We derived approximate solutions for solitary waves for four different models, three of which were previously analytically intractable, the fourth being the nematicon equations which was studied in both (1+1) and (2+1) dimensions. These were then extensively compared with numerical solutions and it was found that, in all cases, comparison with numerical solutions was excellent. The multiple scales of the problem, which could not previously be demonstrated analytically, were made clear and a discussion of where error may arise was given. This method is not without its limitations. In particular, we noticed clear failure for a mixed nonlinearity type problem.

This asymptotic method has now opened the possibility of studying analytically a good number of nonlocal, nonlinear systems that were previously intractable. In particular, it looks as if the full nematicon equations, which were previously only accessible numerically, can now be studied analytically in certain circumstances. This would be a long undertaking, as the oscillatory homogeneous solutions of the director equation almost certainly take uniqueness from the problem and allow for a considerably larger and richer set of solitary wave solutions.

One crucial open equation is to determine, if possible, a sharp *a priori* estimate on the approximations. In the absence of a small parameter, we do not necessarily expect these solutions to become better for higher nonlocality. However, such an estimate would be particularly useful when using the approximation to study systems of nonlocal, nonlinear solitary wave equations in higher dimensions, which may be computationally intractable. Then one could then know, *a priori*, the error of the approximation when numerical solutions are not available. Such a computationally intractable problem may

arise when studying, for instance, many non-interacting particles in the presence of a Newtonian gravitational field as described by the Schrödinger-Newton equations.

6.3 Conclusions: Chapter 5

In Chapter 5 we presented the discovery and analysis of a novel instability mechanism for coupled nonlinear dark solitary wave equations in defocussing media. The model under consideration was that of two coupled nonlinear Schrödinger equations with differing diffraction coefficients. We found that, even for a small difference in diffraction coefficients, one of the initially launched solitary waves decayed into radiation. The mechanism underlying this was non-trivial, with the differing diffraction coefficients driving the process. The mode with a higher diffraction coefficient would attempt to do diffract, forcing the hand of the other mode due to conservation of power. This manifested itself analytically in the form of secular terms that arose not only in the stationary case, but in the z dependent case as well. Explicit behaviour was found for large values of x in both the focussing and defocussing case for the limit of close diffraction coefficients. In particular, it turns out for vector dark solitary waves, the instability can be described by secular terms in a forced Schrödinger equation, connecting the phenomena with classical quantum mechanics. In the focussing case, the asymptotic behaviour was found using a Neumann series, which would apply to a broad range of decaying potentials. This explained why the phenomenon does not arise in the case of focussing media, which has gone unreported in the literature. Furthermore, the instability becomes more pronounced as the diffraction coefficient difference becomes larger, which was verified numerically. The main implication of the work is that a vector (meaning both components are non-zero) dark solitary wave is simply unobservable when the beams undergo different diffraction.

Some natural open questions regarding this work are can one study the limit of large diffraction coefficients and if nonlocality could play a role in stabilization. Both of these questions would provide fundamental theory on the underlying dynamics of vector dark solitary waves currently absent from the literature. It appears as if the large diffraction coefficients case is immediately amenable to asymptotic analysis and our own numerical simulations suggest there is rich behaviour to be described as the instability becomes stronger. The nonlocality question is a larger one and open questions remain as to what degree of nonlocality could provide a stable vector dark solitary wave. A first

study would examine the local limit, to see if this is sufficient to dampen secularity at the next order. A second study would look at the effects of large non-locality.

Appendix A

Chapter 3 Constants

A.1 One space dimension constants

For the $(1+1)$ dimensional trial functions (3.27) the integrals c_i, $i = 1, \ldots, 4$, (3.35) in the averaged Lagrangian (3.34) are as follows.

For the sech trial functions (3.28) the equivalent Gaussian constants are

$$C = \frac{2\sqrt{2}}{\sqrt{\pi}}, \quad A^2 = \frac{3C^3\sqrt{2\pi}}{4\pi^2} \tag{A.1}$$

and the integrals are

$$c_1 = 2, \quad c_2 = \frac{2}{3}, \quad c_3 = \frac{16}{15}, \quad c_4 = \frac{4}{3}. \tag{A.2}$$

For the sech^2 trial functions (3.29) the equivalent Gaussian constants are

$$C = \frac{4\sqrt{2}}{3\sqrt{\pi}}, \quad A^2 = \frac{3C^3\sqrt{2\pi}}{8(\frac{\pi^2}{3} - 2)} \tag{A.3}$$

and the integrals are

$$c_1 = c_4 = \frac{4}{3}, \quad c_2 = c_3 = \frac{16}{15}. \tag{A.4}$$

For the Gaussian trial functions (3.30) $A = 1$ and $C = 1$ and

$$c_1 = c_2 = c_3 = c_4 = \sqrt{\frac{\pi}{2}}. \tag{A.5}$$

A.2 Two space dimension constants

For the $(2+1)$ dimensional trial functions (3.43) the integrals D_i, $i = 1, \ldots, 4$, and the equivalent Gaussian constants A and C are as follows.

For the sech trial functions (3.28) the equivalent Gaussian constants are

$$C = 2\sqrt{\ln(2)}, \quad A = \frac{\sqrt{2}\ln(2)}{\sqrt{I_{x32}}}, \quad I_{x32} = \int_0^\infty x^3 \operatorname{sech}^2 x \, dx = 1.352301002\ldots \tag{A.6}$$

and the integrals are

$$D_1 = \ln(2), \quad D_2 = \frac{\ln(2)}{3} + \frac{1}{6}, \quad D_3 = \frac{8\ln(2)}{15} + \frac{1}{15}, \quad D_4 = \frac{2\ln(2)}{3} - \frac{1}{6} \tag{A.7}$$

For the sech^2 trial functions (3.29) the equivalent Gaussian constants are

$$C = 2\sqrt{\frac{2\ln(2)}{3} - \frac{1}{6}}, \quad A = \frac{C^2}{\sqrt{8I_{x34}}}, \quad I_{x42} = \int_0^\infty x^4 \operatorname{sech}^2(x) dx = 0.2082954966\ldots \tag{A.8}$$

and the integrals are

$$D_1 = D_4 = \frac{2\ln(2)}{3} - \frac{1}{6}, \quad D_2 = D_3 = \frac{8\ln(2)}{15} + \frac{1}{15}. \tag{A.9}$$

For the Gaussian trial function $A = 1$ and $C = 1$ and the integrals are

$$D_1 = D_4 = \frac{1}{4}, \quad D_2 = D_3 = \frac{1}{2}. \tag{A.10}$$

Appendix B

Chapter 3 Numerical Methods

For comparison of the results of modulation theory with numerical results we used well-known numerical methods for computing solitary waves, the Imaginary Time Evolution Method or ITEM [68] and a Newton iteration [69]. As Newton iterations are capable of computing unstable solitary waves, the stability of the computed profiles to radially symmetric perturbations was checked using a z dependent numerical method described in Chapter 2.

B.1 Imaginary Time Evolution Method

A well known numerical method for computing solitary waves is the Imaginary Time Evolution Method or ITEM [68]. This method makes the substitution $z \to iz$ in the electric field equation (3.2) or (3.4), converting it to a parabolic, heat-type, equation and integrates this forward in z, while renormalizing the solution at each step in order to have a fixed, given power. If this renormalisation is not done, the solution converges to the trivial one. Otherwise known as a continuous normalized gradient flow, the method is a continuous steepest descent method used to minimize nonlinear Schrödinger functionals [68, 101]. In one dimension, the numerical method was benchmarked to the exact solution derived in Section 2. In the following descriptions, all integrals were evaluated using the trapezoidal rule.

B.1.1 One Dimension

Seeking stationary solutions of the linearised system (3.4) and (3.5) on a finite computational domain $x \in [-L, L]$ (L sufficiently large) with artificial Dirichlet boundary

conditions $u(L) = u(-L) = \theta(-L) = \theta(L) = 0$, we integrate in imaginary time $\tilde{z} = iz$ via the forward Euler method and renormalize at each step. Dropping the tilde on z, in detail the ITEM is the iterative scheme

$$\tilde{v}^n = v^n + dz\left(\frac{1}{2}v^n_{xx} + 2\vartheta^n v^n\right), \tag{B.1}$$

$$v^{n+1} = \sqrt{\frac{P}{||\tilde{v}^n||_{L^2}}}, \tag{B.2}$$

where $\lim_{n\to\infty} v^n$ is the numerical approximation to u and $\lim_{n\to\infty} \vartheta^n$ is the numerical approximation to θ. Here P is the required optical power. The spatial derivatives were approximated using standard, second order finite differences on a uniform grid and the elliptic director equation (3.5) was solved at each iteration using Thomas' algorithm [133].

In the case of the full system (3.2) and (3.3) the ITEM iteration is

$$\tilde{v}^n = v^n + dz\left(\frac{1}{2}v^n_{xx} + \sin(2\vartheta^n)v^n\right), \tag{B.3}$$

$$v^{n+1} = \sqrt{\frac{P}{||\tilde{v}^n||_{L^2}}}. \tag{B.4}$$

To solve the director equation (3.3) we applied a Picard iteration on the equivalent equation

$$\nu\vartheta^n_{xx} - 2q\vartheta^n = q\sin(2\vartheta^n) - 2q\vartheta^n + 2\cos(\vartheta^n)(v^n)^2, \tag{B.5}$$

which was found from numerical experiments to converge much more rapidly than using a straight Picard iteration to solve (3.3) directly. In all computations the values $L = 100$, $dx = 0.1$ and $dz = 0.00125$ were used. Iterations continued until the stopping condition $||\bar{v}^{n+1} - \bar{v}^n||_{l^2} < 10^{-10}$, $\bar{v}^n$ being the spatially discretized approximation of v^n, was satisfied.

B.1.2 Two Dimensions

The only significant numerical differences between the one and two dimensional cases are the formulation of the boundary value problem and the treatment of the singular term in the cylindrically symmetric Laplacian. The method is the same as used in Refs. [33, 68]. We now consider a positive, finite computational domain $r \in [0, R_{max}]$, with R_{max} sufficiently large, and apply the mixed boundary conditions $u_r(0) = \theta_r(0) =$

$u(R_{max}) = \theta(R_{max}) = 0$. Using L'Hôspital's rule, the Laplacian at the origin was approximated by $\nabla^2 \approx 2\partial^2/\partial r^2$. For the linearized nematicon equations (3.4) and (3.5), the ITEM sequence is then the same as in the $(1+1)$ dimensional case, albeit in higher dimensions

$$\tilde{v}^n = v^n + dz\left(\frac{1}{2}\nabla^2 v^n + 2\vartheta^n v^n\right), \tag{B.6}$$

$$v^{n+1} = \sqrt{\frac{P}{||\tilde{v}^n||_{L^2}}}. \tag{B.7}$$

where $\nabla^2 = \partial_r^2 + \frac{1}{r}\partial_r$ and the L^2 norm is given by

$$||f(r)||_{L^2} = \int_0^\infty r f^2(r)\, dr. \tag{B.8}$$

Again, P is the required optical power. The spatial derivatives were again approximated using standard second order finite differences and ϑ^n, given by the director equation (3.5), was found using Thomas' algorithm [133] at each iteration.

In the case of the full equations (3.2) and (3.3) the ITEM iteration is

$$\tilde{v}^n = v^n + dz\Big(\frac{1}{2}\nabla^2 v^n + \sin(2\vartheta^n v^n)\Big), \tag{B.9}$$

$$v^{n+1} = \sqrt{\frac{P}{||\tilde{v}^n||_{L^2}}}. \tag{B.10}$$

The elliptic director equation (3.3) with the mixed boundary conditions was solved, as in one dimension, using the Picard iteration

$$\nu\nabla^2\vartheta^n - 2q\vartheta^n = q\sin(2\vartheta^n) - 2q\vartheta^n + 2\cos(\vartheta^n)(v^n)^2 \tag{B.11}$$

In all computations, the values $R_{max} = 100$, $dx = 0.1$ and $dz = 0.00125$ were used. Iterations continued until the stopping condition $||\bar{v}^{n+1} - \bar{v}^n||_{l^2} < 10^{-10}$, $\bar{v}^n$ being the spatially discretized approximation of v^n, was satisfied.

B.2 Newton Iteration

In addition to the ITEM, a Newton iteration for the two-dimensional problem was used. In contrast to Yang [69], who used a conjugate-gradient or biconjugate gradient method to solve the linear system at each Newton iteration, we use a direct, sparse LU

decomposition. The spatial discretizations, as well as the boundary conditions, are the same as for the ITEM. However, the iteration is now as follows. We define the operator

$$\mathbf{L}(u,\theta) = \begin{pmatrix} \frac{1}{2}\nabla^2 u - \sigma u + 2\theta u \\ \nu\nabla^2\theta - 2q\theta + 2|u|^2 \end{pmatrix} \tag{B.12}$$

and its linearization δu and $\delta\theta$ around given iterates u^n and θ^n

$$\mathbf{L}_{1,n}(\delta u,\delta\theta) = \begin{pmatrix} \frac{1}{2}\nabla^2(\delta u) - \sigma(\delta u) + 2\theta^n(\delta u) + 2u^n(\delta\theta) \\ \nu\nabla^2(\delta\theta) - 2q(\delta\theta) + 4u^n(\delta u) \end{pmatrix}. \tag{B.13}$$

The iteration $\mathbf{L}_{1,n}(\delta u^n,\delta\theta^n) = -\mathbf{L}(u^n,\theta^n)$, where $\delta u^n = u^{n+1} - u^n$, and similarly $\delta\theta^n = \theta^{n+1} - \theta^n$, was continued until $\max_{r\in[0,R_{max}]}\{|\delta u^n|, |\delta\theta^n|\} < 10^{-10}$. As the nematicon equations were solved for a given σ rather than power, solutions for a given σ were found and the power was computed *a posteriori*, which was then used as an input to benchmark with the ITEM.

Appendix C

Chapter 4 Numerical Method

For comparison of the asymptotic approximation with numerical results, a modified Newton iteration was used. We define the operator

$$\mathcal{N}(u,\theta) = \begin{pmatrix} \frac{1}{2}\nabla^2 u - \sigma u + 2\theta u \\ \nabla^2\theta - \kappa\varepsilon\theta + \varepsilon F(u) \end{pmatrix} \tag{C.1}$$

and its linearization around an initial guess u_0, θ_0 applied to $(\delta u, \delta\theta)^T$

$$\mathcal{L}_0(\delta u, \delta\theta) = \begin{pmatrix} \frac{1}{2}\nabla^2 - \sigma + 2\theta_0 & 2u_0 \\ \varepsilon F'(u_0) & \nabla^2 - \kappa\varepsilon \end{pmatrix} \begin{pmatrix} \delta u \\ \delta\theta \end{pmatrix}. \tag{C.2}$$

Then the iteration defined by

$$u^{n+1} = u^n - \mathcal{L}_0^{-1}\mathcal{N}(u^n, \theta^n), \tag{C.3}$$

is the *modified* Newton method and will converge to a solution. In general, the radius of convergence is smaller than Newton's method, as is the order of convergence (from our own testing). However, speed is gained from being able to store the initial factorization rather than re-construct and solve a linear system at each step as in the standard Newton iteration. In two dimensions we used a finite computational domain $r \in [0, L]$ with uniform spacing ($h = 0.01$), where $L = 20$ in the thermal cases and $L = 120$ in the nematicon case. The boundary conditions were taken to be $\frac{d}{dr}u(0) = \frac{d}{dr}\theta(0) = u(L) = \theta(L) = 0$. Standard centered finite differences were used, with the one notable change that ∇^2 was approximated as $2\frac{d^2}{dr^2}$ at the origin, which follows from L'Hôpital's Rule.

Iterations of the modified Newton Method were continued until the L^2 norm,

$$||f||_{L^2} = \int_0^\infty rf(r)dr, \tag{C.4}$$

fell below 10^{-6}. In the (1+1) dimensional nematicon case the only difference is the domain was taken to be $x \in [-L, L]$ with $L = 120$ and h the same. The boundary conditions were $u(L) = u(-L) = \theta(L) = \theta(-L) = 0$ and the iterations continued until the L^2 norm, now given by

$$||f||_{L^2} = \int_{-\infty}^\infty f(x)dx, \tag{C.5}$$

fell below 10^{-6}.

Appendix D

Published Works

In addition to the presentation of this research at numerous conferences, the author of this thesis has also co-authored the following articles

- J. Michael L. MacNeil, Noel F. Smyth and Gaetano Assanto "Exact and approximate solutions for optical solitary waves in nematic liquid crystals." Physica D: Nonlinear Phenomena 284 (2014): 1-15.
- Gaetano Assanto, J. Michael L. MacNeil, and Noel F. Smyth. "Diffraction-induced instability of coupled dark solitary waves." Optics Letters 40.8 (2015): 1771-1774.
- Alessandro Alberucci, Gaetano Assanto, J. Michael L. MacNeil, Noel F. Smyth. "Nematic liquid crystals: An excellent playground for nonlocal nonlinear light localization in soft matter." Journal of Nonlinear Optical Physics and Materials 23.04 (2014): 1450046.
- Gaetano Assanto, J. Michael L. MacNeil, and Noel F. Smyth. "Comments on Nonlinear refractive index induced collision and propagation of nematicons by L. Kavitha, M. Venkatesh, S. Dhamayanthi and D. Gopi." Journal of Molecular Liquids 199 (2014): 481-482.

Bibliography

[1] J. S. Russell, "Report on Waves," *Brit. Assoc. Rep.*, vol. 311, 1844.

[2] J. Boussinesq, "Théorie de lintumescence liquide appelée onde solitaire ou de translation se propageant dans un canal rectangulaire," *Comptes Rendus Acad. Sci (Paris)*, vol. 72, pp. 755–759, 1871.

[3] G. d. V. D. J. Korteweg, "Xli. on the change of form of long waves advancing in a rectangular canal, and on a new type of long stationary waves," *Philosophical Magazine Series 5*, vol. 39, no. 240, pp. 422–443, 1895.

[4] G. Whitham, *Linear and Nonlinear Waves*. Wiley, 1974.

[5] N. J. Zabusky and M. D. Kruskal, "Interaction of "solitons" in a collisionless plasma and the recurrence of initial states," *Physical Review Letters*, vol. 15, no. 6, p. 240, 1965.

[6] C. S. Gardner, J. M. Greene, M. D. Kruskal, and R. M. Miura, "Method for Solving the Korteweg-deVries Equation," *Physical Review Letters*, vol. 19, no. 19, pp. 1095–1097, 1967.

[7] G. Hwang, T. Akylas, and J. Yang, "Gap solitons and their linear stability in one-dimensional periodic media," *Physica D: Nonlinear Phenomena*, vol. 240, no. 12, pp. 1055–1068, 2011.

[8] K. B. Dysthe and K. Trulsen, "Note on breather type solutions of the NLS as models for freak-waves," *Physica Scripta*, vol. 1999, no. T82, pp. 48–52, 1999.

[9] V. Lashkin, "Two-dimensional nonlocal vortices, multipole solitons, and rotating multisolitons in dipolar Bose-Einstein condensates," *Physical Review A*, vol. 75, no. 4, p. 043607, 2007.

[10] A. Newell, *Solitons in Mathematics and Physics*. Society for Industrial and Applied Mathematics, 1985.

[11] Y. Kivshar and G. Agrawal, *Optical Solitons: From Fibers to Photonic Crystals*. Elsevier, 2003.

[12] Y. S. Kivshar and B. Luther-Davies, "Dark optical solitons: physics and applications," *Physics Reports*, vol. 298, no. 2, pp. 81–197, 1998.

[13] A. Shabat and V. Zakharov, "Exact theory of two-dimensional self-focusing and one-dimensional self-modulation of waves in nonlinear media," *Soviet Journal of Experimental and Theoretical Physics*, vol. 34, no. 1, p. 62, 1972.

[14] C. Conti, M. Peccianti, and G. Assanto, "Route to nonlocality and observation of accessible solitons," *Physical Review Letters*, vol. 91, no. 7, p. 073901, 2003.

[15] M. Peccianti, A. De Rossi, G. Assanto, A. De Luca, C. Umeton, and I. Khoo, "Electrically assisted self-confinement and waveguiding in planar nematic liquid crystal cells," *Applied Physics Letters*, vol. 77, no. 1, pp. 7–9, 2000.

[16] A. Alberucci, M. Peccianti, G. Assanto, A. Dyadyusha, and M. Kaczmarek, "Two-color vector solitons in nonlocal media," *Physical Review Letters*, vol. 97, no. 15, p. 153903, 2006.

[17] G. Assanto and M. Peccianti, "Spatial solitons in nematic liquid crystals," *IEEE Journal of Quantum Electronics*, vol. 39, no. 1, pp. 13–21, 2003.

[18] M. Peccianti and G. Assanto, "Nematicons," *Physics Reports*, vol. 516, no. 45, pp. 147 – 208, 2012. Nematicons.

[19] G. Assanto, *Nematicons: Spatial Optical Solitons in Nematic Liquid Crystals*. Wiley Series in Pure and Applied Optics, Wiley, 2012.

[20] P. Tod and I. M. Moroz, "An analytical approach to the Schrödinger-Newton equations," *Nonlinearity*, vol. 12, no. 2, p. 201, 1999.

[21] R. Bekenstein, R. Schley, M. Mutzafi, C. Rotschild, and M. Segev, "Optical simulations of gravitational effects in the Newton-Schrodinger system," *Nature Physics*, 2015.

[22] H. Pecseli and J. J. Rasmussen, "Nonlinear electron waves in strongly magnetized plasmas," *Plasma Physics*, vol. 22, no. 5, p. 421, 1980.

[23] R. A. Fisher, *The genetical theory of natural selection: a complete variorum edition*. Oxford University Press, 1930.

[24] A. Cheskidov, D. D. Holm, E. Olson, and E. S. Titi, "On a Leray–α model of turbulence," *Proceedings of the Royal Society of London A: Mathematical, Physical and Engineering Sciences*, vol. 461, no. 2055, pp. 629–649, 2005.

[25] A. A. Ilyin, E. M. Lunasin, and E. S. Titi, "A modified-Leray-α subgrid scale model of turbulence," *Nonlinearity*, vol. 19, no. 4, p. 879, 2006.

[26] A. Piccardi, A. Alberucci, N. Tabiryan, and G. Assanto, "Dark nematicons," *Optics Letters*, vol. 36, no. 8, pp. 1356–1358, 2011.

[27] M. Peccianti and G. Assanto, "Signal readdressing by steering of spatial solitons in bulk nematic liquid crystals," *Optics Letters*, vol. 26, no. 21, pp. 1690–1692, 2001.

[28] M. Peccianti and G. Assanto, "Nematic liquid crystals: A suitable medium for self-confinement of coherent and incoherent light," *Physical Review E*, vol. 65, no. 3, p. 035603, 2002.

[29] M. Peccianti, C. Conti, G. Assanto, A. De Luca, and C. Umeton, "All-optical switching and logic gating with spatial solitons in liquid crystals," *Applied Physics Letters*, vol. 81, no. 18, pp. 3335–3337, 2002.

[30] A. Pasquazi, A. Alberucci, M. Peccianti, and G. Assanto, "Signal processing by opto-optical interactions between self-localized and free propagating beams in liquid crystals," *Applied Physics Letters*, vol. 87, no. 26, p. 261104, 2005.

[31] S. V. Serak, N. V. Tabiryan, M. Peccianti, and G. Assanto, "Spatial soliton all-optical logic gates," *IEEE Photonics Technology Letters*, vol. 18, no. 12, pp. 1287–1289, 2006.

[32] A. A. Sukhorukov, "Approximate solutions and scaling transformations for quadratic solitons," *Physical Review E*, vol. 61, no. 4, p. 4530, 2000.

[33] P. Panayotaros and T. Marchant, "Solitary waves in nematic liquid crystals," *Physica D: Nonlinear Phenomena*, vol. 268, pp. 106–117, 2014.

[34] D. W. McLaughlin, D. J. Muraki, M. J. Shelley, and X. Wang, "A paraxial model for optical self-focussing in a nematic liquid crystal," *Physica D: Nonlinear Phenomena*, vol. 88, no. 1, pp. 55–81, 1995.

[35] D. Lannes, "High-frequency nonlinear optics: from the nonlinear Schrödinger approximation to ultrashort-pulses equations," *Proceedings of the Royal Society of Edinburgh: Section A Mathematics*, vol. 141, no. 02, pp. 253–286, 2011.

[36] I.-C. Khoo, *Liquid crystals: physical properties and nonlinear optical phenomena*, vol. 64. John Wiley & Sons, 2007.

[37] L. Landau and E. Lifshitz, *Classical mechanics*. Pergamon Press, Oxford, 1960.

[38] J. L. Synge, B. A. Griffith, *et al.*, "Principles of mechanics," *New York*, 1959.

[39] A. A. Minzoni, N. F. Smyth, and A. L. Worthy, "Modulation solutions for nematicon propagation in nonlocal liquid crystals," *Journal of the Optical Society of America B*, vol. 24, no. 7, pp. 1549–1556, 2007.

[40] E. Kuznetsov, A. Rubenchik, and V. Zakharov, "Soliton stability in plasmas and hydrodynamics," *Physics Reports*, vol. 142, no. 3, pp. 103–165, 1986.

[41] F. Dabby and J. Whinnery, "Thermal self-focussing of laser beams in lead glasses.," *Applied Physics Letters*, vol. 13, no. 8, pp. 284–286, 1968.

[42] C. Rotschild, M. Segev, Z. Xu, Y. V. Kartashov, L. Torner, and O. Cohen, "Two-dimensional multipole solitons in nonlocal nonlinear media," *Optics Letters*, vol. 31, no. 22, pp. 3312–3314, 2006.

[43] C. Rotschild, B. Alfassi, O. Cohen, and M. Segev, "Long-range interactions between optical solitons," *Nature Physics*, vol. 2, no. 11, pp. 769–774, 2006.

[44] M. Segev, B. Crosignani, A. Yariv, and B. Fischer, "Spatial solitons in photorefractive media," *Physical Review Letters*, vol. 68, no. 7, p. 923, 1992.

[45] C. Conti and G. Assanto, "Nonlinear optics applications: bright spatial solitons," *Encyclopedia of Modern Optics*, vol. 5, pp. 43–55, 2004.

[46] R. Penrose, "Quantum computation, entanglement and state reduction," *Philosophical Transactions-Royal Society of London Series A Mathematical, Physical and Engineering Sciences*, pp. 1927–1937, 1998.

[47] S. Chandrasekhar, *An introduction to the study of stellar structure*, vol. 2. Courier Corporation, 1957.

[48] T. Tao, *Nonlinear dispersive equations: local and global analysis*, vol. 106. American Mathematical Soc., 2006.

[49] T. Cazenave and P.-L. Lions, "Orbital stability of standing waves for some nonlinear Schrödinger equations," *Communications in Mathematical Physics*, vol. 85, no. 4, pp. 549–561, 1982.

[50] B. D. Skuse and N. F. Smyth, "Interaction of two-color solitary waves in a liquid crystal in the nonlocal regime," *Physical Review A*, vol. 79, no. 6, p. 063806, 2009.

[51] A. A. Minzoni, N. F. Smyth, A. L. Worthy, and Y. S. Kivshar, "Stabilization of vortex solitons in nonlocal nonlinear media," *Physical Review A*, vol. 76, no. 6, p. 063803, 2007.

[52] B. D. Skuse and N. F. Smyth, "Two-color vector-soliton interactions in nematic liquid crystals in the local response regime," *Physical Review A*, vol. 77, no. 1, p. 013817, 2008.

[53] A. A. Minzoni, N. F. Smyth, and Z. Xu, "Stability of an optical vortex in a circular nematic cell," *Physical Review A*, vol. 81, no. 3, p. 033816, 2010.

[54] N. F. Smyth and W. Xia, "Refraction and instability of optical vortices at an interface in a liquid crystal," *Journal of Physics B: Atomic, Molecular and Optical Physics*, vol. 45, no. 16, p. 165403, 2012.

[55] G. Assanto, A. A. Minzoni, N. F. Smyth, and A. L. Worthy, "Refraction of nonlinear beams by localized refractive index changes in nematic liquid crystals," *Physical Review A*, vol. 82, no. 5, p. 053843, 2010.

[56] B. A. Malomed, "Variational methods in nonlinear fiber optics and related fields," *Progress in Optics*, vol. 43, pp. 71–194, 2002.

[57] D. Anderson, "Variational approach to nonlinear pulse propagation in optical fibers," *Physical Review A*, vol. 27, no. 6, p. 3135, 1983.

[58] W. Cheney, *Analysis for applied mathematics*, vol. 208. Springer Science & Business Media, 2013.

[59] A. W. Snyder and D. J. Mitchell, "Accessible solitons," *Science*, vol. 276, no. 5318, pp. 1538–1541, 1997.

[60] W. L. Kath and N. F. Smyth, "Soliton evolution and radiation loss for the nonlinear Schrödinger equation," *Physical Review E*, vol. 51, no. 2, p. 1484, 1995.

[61] A. Alberucci, C. P. Jisha, and G. Assanto, "Accessible solitons in diffusive media," *Optics Letters*, vol. 39, no. 15, pp. 4317–4320, 2014.

[62] Y. Shen, "Solitons made simple," *Science*, pp. 1520–1520, 1997.

[63] N. I. Nikolov, D. Neshev, O. Bang, and W. Z. Królikowski, "Quadratic solitons as nonlocal solitons," *Physical Review E*, vol. 68, no. 3, p. 036614, 2003.

[64] S. Ouyang, Q. Guo, and W. Hu, "Perturbative analysis of generally nonlocal spatial optical solitons," *Physical Review E*, vol. 74, no. 3, p. 036622, 2006.

[65] H. Ren, S. Ouyang, Q. Guo, and L. Wu, "(1+ 2)-dimensional sub-strongly nonlocal spatial optical solitons: Perturbation method," *Optics Communications*, vol. 275, no. 1, pp. 245–251, 2007.

[66] J. P. Boyd, *Chebyshev and Fourier spectral methods*. Courier Corporation, 2001.

[67] T. R. Marchant and N. Smyth, "Nonlocal validity of an asymptotic one-dimensional nematicon solution," *Journal of Physics A: Mathematical and Theoretical*, vol. 41, no. 36, p. 365201, 2008.

[68] J. Yang and T. I. Lakoba, "Accelerated Imaginary-time Evolution Methods for the Computation of Solitary Waves," *Studies in Applied Mathematics*, vol. 120, no. 3, pp. 265–292, 2008.

[69] J. Yang, "Newton-conjugate-gradient methods for solitary wave computations," *Journal of Computational Physics*, vol. 228, no. 18, pp. 7007–7024, 2009.

[70] J. J. García-Ripoll and V. M. Pérez-García, "Optimizing Schrödinger functionals using Sobolev gradients: applications to quantum mechanics and nonlinear optics," *SIAM Journal on Scientific Computing*, vol. 23, no. 4, pp. 1316–1334, 2001.

[71] S. Louis, T. R. Marchant, and N. F. Smyth, "Optical solitary waves in thermal media with non-symmetric boundary conditions," *Journal of Physics A: Mathematical and Theoretical*, vol. 46, no. 5, p. 055201, 2013.

[72] P. G. Ciarlet and C. Mardare, "On the Newton-Kantorovich theorem," *Analysis and Applications*, vol. 10, no. 03, pp. 249–269, 2012.

[73] J. M. Ortega, "The Newton-Kantorovich theorem," *American Mathematical Monthly*, pp. 658–660, 1968.

[74] T. J. Ypma, "Historical development of the Newton-Raphson method," *SIAM Review*, vol. 37, no. 4, pp. 531–551, 1995.

[75] J. P. Boyd, "Why Newtons method is hard for travelling waves: small denominators, KAM theory, Arnolds linear Fourier problem, non-uniqueness, constraints and erratic failure," *Mathematics and Computers in Simulation*, vol. 74, no. 2, pp. 72–81, 2007.

[76] P. Deuflhard, *Newton methods for nonlinear problems: affine invariance and adaptive algorithms*, vol. 35. Springer, 2011.

[77] G. Assanto, A. A. Minzoni, M. Peccianti, and N. F. Smyth, "Optical solitary waves escaping a wide trapping potential in nematic liquid crystals: modulation theory," *Physical Review A*, vol. 79, no. 3, p. 033837, 2009.

[78] W. Królikowski and O. Bang, "Solitons in nonlocal nonlinear media: Exact solutions," *Physical Review E*, vol. 63, no. 1, p. 016610, 2000.

[79] J.-P. Berenger, "A perfectly matched layer for the absorption of electromagnetic waves," *Journal of Computational Physics*, vol. 114, no. 2, pp. 185–200, 1994.

[80] G. I. Stegeman and M. Segev, "Optical spatial solitons and their interactions: universality and diversity," *Science*, vol. 286, no. 5444, pp. 1518–1523, 1999.

[81] H. Gibbs, *Optical bistability: controlling light with light*. Elsevier, 2012.

[82] A. Kaplan, "Bistable solitons," *Physical Review Letters*, vol. 55, no. 12, p. 1291, 1985.

[83] A. D. Polyanin and V. F. Zaitsev, "Handbook of exact solutions for ordinary differential equations," *Boca Raton: CRC Press,— c1995*, vol. 1, 1995.

[84] J. M. L. MacNeil, N. F. Smyth, and G. Assanto, "Exact and approximate solutions for optical solitary waves in nematic liquid crystals," *Physica D: Nonlinear Phenomena*, vol. 284, pp. 1–15, 2014.

[85] M. Peccianti, C. Conti, and G. Assanto, "Interplay between nonlocality and nonlinearity in nematic liquid crystals," *Optics Letters*, vol. 30, no. 4, pp. 415–417, 2005.

[86] C. García Reimbert, A. A. Minzoni, N. F. Smyth, and A. L. Worthy, "Large-amplitude nematicon propagation in a liquid crystal with local response," *Journal of the Optical Society of America B*, vol. 23, no. 12, pp. 2551–2558, 2006.

[87] A. Aceves, J. Moloney, and A. Newell, "Theory of light-beam propagation at nonlinear interfaces. i. equivalent-particle theory for a single interface," *Physical Review A*, vol. 39, no. 4, p. 1809, 1989.

[88] A. Alberucci and G. Assanto, "Modeling nematicon propagation," *Molecular Crystals and Liquid Crystals*, vol. 572, no. 1, pp. 2–12, 2013.

[89] A. Alberucci, A. Piccardi, M. Peccianti, M. Kaczmarek, and G. Assanto, "Propagation of spatial optical solitons in a dielectric with adjustable nonlinearity," *Physical Review A*, vol. 82, no. 2, p. 023806, 2010.

[90] Y. N. Karamzin and A. Sukhorukov, "Nonlinear interaction of diffracted light beams in a medium with quadratic nonlinearity: mutual focusing of beams and limitation on the efficiency of optical frequency converters," *Soviet Journal of Experimental and Theoretical Physics*, vol. 20, no. 11, pp. 339–343, 1974.

[91] Y. N. Karamzin and A. Sukhorukov, "Mutual focusing of high-power light beams in media with quadratic nonlinearity," *Soviet Journal of Experimental and Theoretical Physics*, vol. 41, pp. 414–420, 1976.

[92] M. Peccianti and G. Assanto, "Observation of power-dependent walk-off via modulational instability in nematic liquid crystals," *Optics Letters*, vol. 30, no. 17, p. 2290, 2005.

[93] D. E. Panayotounakos, "Exact analytic solutions of unsolvable classes of first and second order nonlinear ODEs (Part i: Abels equations)," *Applied Mathematics Letters*, vol. 18, no. 2, pp. 155–162, 2005.

[94] D. E. Panayotounakos and N. Sotiropoulos, "Exact analytic solutions of unsolvable classes of first-and second-order nonlinear ODEs (Part ii: Emden–Fowler and relative equations)," *Applied Mathematics Letters*, vol. 18, no. 4, pp. 367–374, 2005.

[95] R. Courant and D. Hilbert, *Methods of Mathematical Physics*, vol. 2. CUP Archive, 1966.

[96] M. Peccianti, K. A. Brzdkiewicz, and G. Assanto, "Nonlocal spatial soliton interactions in nematic liquid crystals," *Optics Letters*, vol. 27, no. 16, pp. 1460–1462, 2002.

[97] G. Assanto, A. A. Minzoni, and N. F. Smyth, "Light self-localization in nematic liquid crystals: modelling solitons in nonlocal reorientational media," *Journal of Nonlinear Optical Physics & Materials*, vol. 18, no. 04, pp. 657–691, 2009.

[98] G. Assanto, N. F. Smyth, and W. Xia, "Modulation analysis of nonlinear beam refraction at an interface in liquid crystals," *Physical Review A*, vol. 84, no. 3, p. 033818, 2011.

[99] G. Assanto, N. F. Smyth, and W. Xia, "Refraction of nonlinear light beams in nematic liquid crystals," *Journal of Nonlinear Optical Physics & Materials*, vol. 21, no. 03, p. 1250033, 2012.

[100] G. Assanto, N. F. Smyth, and A. L. Worthy, "Two-color, nonlocal vector solitary waves with angular momentum in nematic liquid crystals," *Physical Review A*, vol. 78, no. 1, p. 013832, 2008.

[101] W. Bao and Q. Du, "Computing the ground state solution of Bose-Einstein condensates by a normalized gradient flow," *SIAM Journal on Scientific Computing*, vol. 25, no. 5, pp. 1674–1697, 2004.

[102] G. J. Lord, D. Peterhof, B. Sandstede, and A. Scheel, "Numerical computation of solitary waves in infinite cylindrical domains," *SIAM journal on Numerical Analysis*, vol. 37, no. 5, pp. 1420–1454, 2000.

[103] G. Assanto, B. Svensson, D. Kuchibhatla, U. J. Gibson, C. T. Seaton, and G. I. Stegeman, "Prism coupling into ZnS waveguides: a classic example of a nonlinear coupler," *Optics Letters*, vol. 11, no. 10, pp. 644–646, 1986.

[104] G. Stegeman, G. Assanto, R. Zanoni, C. Seaton, E. Garmire, A. Maradudin, R. Reinisch, and G. Vitrant, "Bistability and switching in nonlinear prism coupling," *Applied physics Letters*, vol. 52, no. 11, pp. 869–871, 1988.

[105] R. Enns, S. Rangnekar, and A. Kaplan, "Bistable-soliton pulse propagation: Stability aspects," *Physical Review A*, vol. 36, no. 3, p. 1270, 1987.

[106] S. Gatz and J. Herrmann, "Soliton propagation in materials with saturable nonlinearity," *Journal of the Optical Society of America B*, vol. 8, no. 11, pp. 2296–2302, 1991.

[107] I. Simenog, "Asymptotic solution of stationary nonlinear Hartree equation," *Theoretical and Mathematical Physics*, vol. 30, no. 3, pp. 263–268, 1977.

[108] L. Chen, Q. Wang, M. Shen, H. Zhao, Y.-Y. Lin, C.-C. Jeng, R.-K. Lee, and W. Krolikowski, "Nonlocal dark solitons under competing cubic–quintic nonlinearities," *Optics Letters*, vol. 38, no. 1, pp. 13–15, 2013.

[109] A. S. Reyna, B. A. Malomed, and C. B. de Araújo, "Stability conditions for one-dimensional optical solitons in cubic-quintic-septimal media," *Physical Review A*, vol. 92, no. 3, p. 033810, 2015.

[110] M. Crosta, S. Trillo, and A. Fratalocchi, "The Whitham approach to dispersive shocks in systems with cubic–quintic nonlinearities," *New Journal of Physics*, vol. 14, no. 9, p. 093019, 2012.

[111] T. B. Benjamin and J. Feir, "The disintegration of wave trains on deep water Part 1. Theory," *Journal of Fluid Mechanics*, vol. 27, no. 03, pp. 417–430, 1967.

[112] G. L. Lamb Jr, "Elements of soliton theory," *New York, Wiley-Interscience, 1980. 300 p. 29.95.*, vol. 1, p. 29, 1980.

[113] A. S. Davydov, "Solitons in molecular systems," *Physica Scripta*, vol. 20, no. 3-4, p. 387, 1979.

[114] Y. S. Kivshar, "Dark solitons in nonlinear optics," *IEEE Journal of Quantum Electronics*, vol. 29, no. 1, pp. 250–264, 1993.

[115] G. Swartzlander Jr, D. Andersen, J. Regan, H. Yin, and A. Kaplan, "Spatial dark-soliton stripes and grids in self-defocusing materials," *Physical Review Letters*, vol. 66, no. 12, p. 1583, 1991.

[116] G. Allan, S. Skinner, D. Andersen, and A. L. Smirl, "Observation of fundamental dark spatial solitons in semiconductors using picosecond pulses," *Optics Letters*, vol. 16, no. 3, pp. 156–158, 1991.

[117] B. Luther-Davies and Y. Xiaoping, "Waveguides and Y junctions formed in bulk media by using dark spatial solitons," *Optics Letters*, vol. 17, no. 7, pp. 496–498, 1992.

[118] M. Shalaby and A. J. Barthelemy, "Observation of the self-guided propagation of a dark and bright spatial soliton pair in a focusing nonlinear medium," *IEEE Journal of Quantum Electronics*, vol. 28, no. 12, pp. 2736–2741, 1992.

[119] A. Dreischuh, D. N. Neshev, D. E. Petersen, O. Bang, and W. Krolikowski, "Observation of attraction between dark solitons," *Physical Review Letters*, vol. 96, no. 4, p. 043901, 2006.

[120] M. Taya, M. C. Bashaw, M. Fejer, M. Segev, and G. C. Valley, "Observation of dark photovoltaic spatial solitons," *Physical Review A*, vol. 52, no. 4, p. 3095, 1995.

[121] Z. Chen, M. H. Garrett, G. C. Valley, M. Mitchell, M.-f. Shih, and M. Segev, "Steady-state dark photorefractive screening solitons," *Optics Letters*, vol. 21, no. 9, pp. 629–631, 1996.

[122] Y. S. Kivshar and S. K. Turitsyn, "Vector dark solitons," *Optics Letters*, vol. 18, no. 5, pp. 337–339, 1993.

[123] N. V. Nguyen, "Stability of solitary waves for the vector nonlinear schrdinger equation in higher-order sobolev spaces," *Journal of Mathematical Analysis and Applications*, vol. 409, no. 2, pp. 946 – 962, 2014.

[124] G. Assanto, J. M. L. MacNeil, and N. F. Smyth, "Diffraction-induced instability of coupled dark solitary waves," *Optics letters*, vol. 40, no. 8, pp. 1771–1774, 2015.

[125] A. Fratalocchi and G. Assanto, "Discrete light localization in one-dimensional nonlinear lattices with arbitrary nonlocality," *Physical Review E*, vol. 72, no. 6, p. 066608, 2005.

[126] S. V. Manakov, "On the theory of two-dimensional stationary self-focusing of electromagnetic waves," *Soviet Journal of Experimental and Theoretical Physics*, vol. 38, no. 2, pp. 248–253, 1974.

[127] M. Abramowitz and I. A. Stegun, *Handbook of mathematical functions: with formulas, graphs, and mathematical tables*. No. 55, Courier Corporation, 1964.

[128] R. Kress, V. Maz'ya, and V. Kozlov, *Linear Integral Equations*, vol. 82. Springer, 1989.

[129] M. Born and E. Wolf, *Principles of optics: electromagnetic theory of propagation, interference and diffraction of light*. Cambridge University Press, 1999.

[130] M. Goldberg and W. Schlag, "Dispersive estimates for Schrödinger operators in dimensions one and three," *Communications in mathematical physics*, vol. 251, no. 1, pp. 157–178, 2004.

[131] R. C. McOwen, *Partial Differential Equations: Methods and Applications*. Prentice Hall, 1996.

[132] M. Reed and B. Simon, *Functional Analysis, volume 1 of Methods of Modern Mathematical Physics*. Academic Press, New York, 1972.

[133] W. H. Press, *Numerical recipes 3rd edition: The art of scientific computing*. Cambridge university press, 2007.